INVESTIGATION OF HIGH ENERGY RADIATION FROM A PLASMA FOCUS

FINAL CONTRACTOR REPORT

NASA Grant NGR 43-002-031
February 1969-August 1975

Department of Physics and Astronomy
VANDERBILT UNIVERSITY
Nashville, TN 37235

Department of Physics and Astronomy
Vanderbilt University
Nashville, TN 37235

INVESTIGATION OF HIGH ENERGY RADIATION FROM A PLASMA FOCUS

Final Contractor Report

NASA Grant NGR 43-002-031
February 1969-August 1975

Ja H. Lee, Principal Investigator
Charles E. Roos, and John P. Barach

Dr. Frank Hohl
The NASA Technical Officer
NASA Langley Research Center
Hampton, VA 23665

TABLE OF CONTENTS

I. INTRODUCTION

This report summarizes the results of the investigation of high energy radiation from a plasma focus conducted during the period from February 1969 to August 1975.

In 1964 Filippov of the USSR[1] and in the following year J. Mather of Los Alamos Scientific Laboratory in the USA[2] observed the formation of a highly dense and hot plasma, called a plasma focus, at the end of a coaxial gun when the gun was designed and operated under certain conditions. Since the plasma density and the temperature reaches nuclear fusion conditions it is a copious X-ray and neutron source when deuterium or deuterium-tritium mixture is used as the filling gas.

The investigation of these high energy radiations from the plasma focus is of utmost importance for the determination of plasma properties and the mechanism of the plasma focus formation.

The plasma focus apparatus (PFI) at NASA Langley Research Center, installed in 1967, was used for the early phase of this investigation. Neutrons are studied by means of a time-of-flight method, silver-activation counters and scintillation detectors, while X-rays are investigated by the absorbing foil - pinhole camera system, scintillation detectors and crystal spectrometers. For both neutron and X-ray studies nuclear emulsions were used for their energy analysis. Included in this report are seventeen topics (Chapter II) covering the experimental setup, diagnostics, analyses and various applications of the plasma focus. An invention, a hypocycloidal-pinch apparatus, is also included for it is expected to realize significant improvements in the performance of the plasma focus apparatus.

II. RESULTS AND DISCUSSIONS

A. Dynamics of Plasma-Focus Formation - The plasma focus apparatus has two types of geometry as developed from two different origins. In 1964 Filippov, et al of the USSR found that their metal-wall non-cylindrical Z-pinch device could be operated to form a dense plasma only near the anode. The d-d fusion rates in the plasma was observed to be orders of magnitudes higher than that of a linear Z-pinch device.[1] The following year J. Mather of Los Alamos Scientific Laboratory also found that a dense plasma could be produced in a coaxial gun when it was operated under certain conditions.[2] The d-d fusion rate in the plasma was found to be comparable to that of the non-cylindrical Z-pinch apparatus in the USSR. Figure 1 schematically shows a) Filippov's non-cylindrical Z-pinch and b) Mather's coaxial plasma focus apparatus.

Either of the plasma focus devices is energized by a high voltage, low inductance capacitor bank. The voltages commonly used are 15-50 kV. The switching of the circuit is accomplished by pressurized trigatrons, vacuum switches or dielectric switches which are capable of high Coulomb transfer. After switching, the breakdown occurs along the insulator placed at the base of the electrodes. An inverse pinch configuration is formed and the current sheet is quickly pushed away from the insulator surface by $\vec{J} \times \vec{B}$ force. In Mather type devices the current sheets are continuously accelerated by the increasing $\vec{J} \times \vec{B}$ in the annular channel between the two electrodes. This is called the rundown phase. The rundown phase is well understood by a snow-plow model which is based on magnetohydrodynamics. When the current sheets reach the end of the electrode, the sheets near the center electrode move in radially toward the axis of the device. In Filippov type devices, this radial motion of the current sheets follows immediately after the inverse pinch phase without the rundown phase as in Mather type devices. The NASA Langley plasma-focus apparatus (PFI) is a Mather type consisting of a 5-cm diameter center electrode and 10 cm-diameter outer electrode. The radial implosion of the current sheets produces a high density plasma on the axis. To optimize this implosion the impedance of the circuit is so adjusted that peak current flows at this time. The impedance matching is done mainly by the length of the electrode determined by the following calculations based on the snow-plow model.

Consider unit thickness of the current sheet which "snow-plowed" the mass of gas from the base of the electrodes spacing as shown in Fig. 2. The equation of motion for the mass is

$$\frac{d}{dt}\left[2\pi r\rho_0 z\frac{dz}{dt}\right] = 2\pi r\,\frac{\mu_0}{2}\left(\frac{I}{2\pi r}\right)^2 \qquad \text{MKS ---} \qquad 1$$

where ρ_0 is the density of the filling gas, μ_0 the free space permeability and I the electric current. The left side of Eq. 1 represents the magnetic force $B^2/2\mu_0$ behind the current sheet. With an approximation of $J = I_0 \sin \omega t$, where ω is the ringing frequency of the circuit, and the initial condition $z = 0$ at $t = 0$, we have

$$z^2 = \frac{1}{2}At^2 - \frac{A}{2\omega^2}\sin^2 \omega t$$

where $A \equiv \mu_0 I_0^2/8\pi^2\rho_0 r^2$. Since $I_0 = CEW$, where C is the capacitance and E the charging voltage,

$$z = 1.06 \times 10^{-4}\,\frac{CE}{r}\,\frac{1}{\sqrt{\rho_0}}$$

at $t = \pi/2\omega$ or the end of the quarter period. When deuterium is used as the filling gas,

$$\rho_o = 2.35 \times 10^{-4}\ P_o(\text{Torr})$$

$$Z = 0.69 \times 10^{-2} \cdot \frac{CE}{r} \cdot \frac{1}{\sqrt{\rho_o}}$$

For the Langley PFI apparatus

$$C = 10 \times 12.5 \times 10^{-6} \text{ farads,}$$

$$E = 2 \times 10^{4} \text{ volts}$$

$$r = 3.81 \times 10^{-2} \text{ meters}$$

then

$$Z = 0.69 \times 10^{-2} \cdot \frac{125 \times 10^{-6} \cdot 2 \times 10^{4}}{3.81 \times 10^{-2}} \ \frac{1}{\sqrt{\rho_o}}$$

or

$$Z = 45.3 \ \frac{1}{\sqrt{\rho_o}} \times 10^{-2} \text{ meters}$$

If the initial filling pressure P_o is chosen at 3 Torr, then

$$Z = 26.1 \text{ cm}$$

The length of electrodes of the PFI was selected to be 25 cm so that the midpoint of the current sheet reaches the end of the electrode at the end of the quarter period.

The dense plasma formed on the axis, called a plasma focus, lasts for a period of ∿100 ns and its diameter is ∿2 mm, its length is ∿10 mm when observed with visible or soft X-ray photographs. Fast streak and framing modes of an image converter camera are employed to reveal temporal developments of the plasma. In Figure 3 are examples of streak photographs taken through a slot parallel and perpendicular to the axis of the apparatus. Figure 3(a) shows that the initial collapse of the current sheet occurs from 0.5 cm upward to 1.25 cm above the top of the center electrode. From this region, a very bright feature is observed to move upward with an average velocity of 3×10^7 cm/sec in the z-direction until it reaches a point about 4 cm above the center electrode. The luminous plasma stops at this point and, in many of the pictures obtained, a shock wave originates and propagates upward with a velocity of $>10^7$ cm/sec.

Figure 3(b) is the streak photograph through the slit perpendicular to the axis. The current sheet collapses radially, at a velocity of $\sim 10^7$ cm/sec, to a few millimeters diameter. The collapse to minimum diameter is accompanied by an increased luminosity which is immediately followed by a dark period. The dark period, in turn, is followed by a very intense feature which expands radially outward from the axis at approximately 6×10^4 cm/sec.

Figure 3(c) is a streak photograph obtained through a horizontal slit 4 cm above the end of the center electrode. Figures 2(a) and 2(c) show that a luminous plasma exists 4 cm above the center electrode at the time there is no luminosity at 0.5 cm above the center electrode [Fig. 3(b)]. A comparison of Figs. 3(a) and 3(b) shows that the luminosity following this dark period is due to material coming off the center electrode. The plasma focus is an intense source of neutrons by d-d fusions when deuterium is used as a filling gas as well as copious X-rays with energy up to ∿500 keV. Time correlations among the current sheet dynamics, the neutron detector signal, and the soft X-ray signal are shown in Figure 4. Note that the soft X-rays peak (d) when the current sheet reaches its minimum diameter (b). These appear to come from the plasma and the onset is not intense to enough to be seen by the X-ray screen-fiber optics shown in Figure 4(a). The hard X-rays and neutrons appear to be emitted during the time the plasma (visible) moves up to the 4-cm height (see Figure 4(f)). This burst of hard X-rays also appears to be associated with the plasma, whereas the second burst of soft X-rays is associated with the evaporation of electrode material. The experiment with a hollow center electrode verified this, since, in this configuration, no soft X-rays appeared after the first burst.

Despite extensive studies that have been carried out on the plasma focus, the mechanism of neutron and X-ray production was not well understood when this investigation was launched in 1969. Publications 23, 24, 25, 26 and 28 discuss the problem.

B. Time-of-Flight Neutron Energy Analysis - In principle, measuring neutron energy spectra and neutron fluxes in various directions from the discharge axis, together with the neutron yield, should suffice to select the proper model for neutron production, since the combination of these data have unique characteristics for each of the different mechanisms of neutron production.

Initially, it was assumed that the large neutron yield (10^9-10^{10} per pulse) from a plasma focus could be explained by means of a thermal-plasma model.[3,4] However, subsequent measurements of angular variations in neutron flux and neutron energy showed disagreement with this model.[5,6] A beam-target model, with the ions accelerated linearly by plasma instabilities, is also unsatisfactory because the duration of neutron production, typically 100 nsec, is too long for the attributed magnetohydrodynamic instability, and an unrealistically high ion current (greater than 1 × 10^6 A) must be assumed.[3] Bernstein[6] calculated ion trajectories for crossed electric and magnetic fields in a z-pinch discharge and showed that ion velocities can be randomly oriented without thermalization. This suggests that neutron production can be accounted for by mechanisms other than those assumed in the beam-target and the thermal-plasma models.

Previously, neutron energy spectra have been estimated from time-of-flight measurements that utilized flight paths of less than 10 m.[3] These results are found to deviate strongly from those obtained by using nuclear emulsions.[5,7] Ths discrepancy may be due to the poor resolution inherent in the time-of-flight method when a too short flight path is used.

This report presents the results of time-of-flight neutron spectroscopy in which flight paths as large as 80 m were used to provide better than 10% over-all energy resolution. The shot-to-shot variation of the neutron energy spectrum can be studied by the time-of-flight method since it gives the neutron energy spectrum immediately after each shot of the plasma gun, as opposed to the time-consuming process of scanning nuclear emulsions. The results of this experiment, including some of our preliminary results,[8] are compared with the values predicted by several neutron production models, including a trial model with converging energetic ions.

Time-of-flight measurements of neutron energies were made separately and simultaneously with neutron detectors located in both the axial and the radial directions. Since the axis of the coaxial electrodes was fixed vertically, a 40-m high crane was used for observation in the axial direction. The neutron detectors consisted of NE 102 scintillator-photomultiplier tube combinations. The overall risetime of the detectors and associated electronics is less than 15 nsec. The NE 102 scintillator has a decay time of 2.2 nsec and is thus suitable for use in the detection of temporal variations of the neutron flux. The neutron energy dependence of the light output of the NE 102 scintillator was assumed to be approximately linear, as given by Evans, et al.,[9] over the 2-3-MeV neutron energy range of interest.

The total yield of neutrons and the anisotropy of the neutron fluence (time-integrated flux) were determined by the use of a silver activation method in which neutron-induced gamma rays are counted (Publications 1 and 2). Nuclear emulsions were also used to determine the total neutron yield and the neutron energy distribution.

The results indicate that the energy spectrum of neutrons from d-d reactions in the plasma focus shows a sharp onset with average maximum energies of 2.8 and 3.2 MeV in the radial and the axial directions, respectively. The average half-width of the energy spectrum was 270 keV with a shot-to-shot variation between 150 and 400 keV. Simultaneous measurements in the axial and radial directions showed no appreciable difference in the half-widths and thus indicated randomly oriented ion velocities in the plasma.

The detailed description on these results and related discussions have been reported in Publication 3.

C. Neutron Fluence from a Plasma Focus - The analysis of the neutrons produced by fusion in high-temperature plasmas is a useful diagnostic tool for studying the nature of the plasma in various devices. In particular, measurements of the energy spectrum of the neutrons and its angular variation and measurements of the fluence of the neutrons and its angular variation have been made on the neutrons emitted by the plasma focus in Filippov- or Mather-type devices.

This study also deals with the measurements of the total yield and the angular variation of the fluence of the neutrons emitted from a plasma focus. The total yield of neutrons serves as a direct indicator of the over-all performance of a thermonuclear fusion device, and the angular variation of the fluence of neutrons is inherently related to the production mechanism of the neutrons in the plasma. These measurements, however, require rather complex detector systems, and the accuracy of the results is often unsatisfactory.

Several methods of measurements which superficially appear to be suitable for this application exhibit serious shortcomings upon closer scrutiny. The use of nuclear emulsions is limited to time-integrated measurements, and after long and tedious analyses gives results having large uncertainties. The use of a fast scintillator detector system would seem to be suitable for observing the neutron fluence as well as the temporal variation of the neutron flux. However, the extremely high flux and short duration of the burst of neutrons from a plasma focus surpass the time resolution capabilities of a pulse-counting system to be used for fluence measurements. Nevertheless, fast scintillator detector systems have been used to obtain measurements of the angular variation of the flux of neutrons from a plasma focus, which revealed a large anisotropy in the emission of neutrons from the plasma focus. The measurement of the activation induced by the neutrons in a silver target by beta counting is a widely used method for determining the absolute fluence and the angular variation of the fluence of neutrons emitted by a plasma focus. However, beta rays are emitted by four different modes of decay in the activated silver; thus, the accuracy of this method is limited by the nondiscriminating nature of the Geiger counter, and also by its characteristically long dead time.

Since the angular variation of the fluence of neutrons emitted by a plasma focus is expected to be small (a factor less than 2), an improvement in the accuracy of fluence measurements is desirable if these measurements are to be used to identify the mechanism of the production of neutrons in a plasma focus. In our work we have attempted to make more accurate measurements of the fluence of the neutrons and of the angular variation of the fluence by measuring the neutron-induced activity of the silver target by gamma spectrometry in lieu of beta counting. Our results are compared with the predictions of several models which have been proposed as the mechanism of neutron production in a plasma focus. The models considered are the moving thermal-plasma model[3], the beam-target model[1], and the converging-ion model (See Publication 3). The evaluation of the gamma counting system, the details of the experiment, its results and discussion have been reported in Publication 1, 2, and 4. In conclusion we have shown that the neutron fluence can be measured with increased accuracy by using gamma-ray counting in a silver-activation method. A detector system with an estimated uncertainty of less than 16% has been used to measure the neutron fluence of the plasma focus. The angular variation of the neutron fluence and the dependence of the neutron fluence anisotropy on the total yield have been determined.

The neutron fluence was found to be rather concentrated in a cone on the axis of the gun with a half-angle of 30 deg, and to fall off rapidly outside of this cone. Four speculative models for neutron production in a plasma focus are considered and the expectations from these models are compared with our data. No model is found to be satisfactory for interpreting our results, although a diffuse source distributed along the axis could be assumed for an explanation.

To resolve present difficulties concerning the mechanism of neutron production in a plasma focus, it is necessary to further improve the accuracy of the neutron measurements and to extend observations over a wide range of conditions affecting the formation of the plasma focus. It should be realized that the use of the axial-to-radial anisotropy alone is not sufficient for distinguishing a suitable model. Publication 27 presents anisotropy of neutron fluence from the plasma focus in detail.

D. Converging-Ion Model of a Plasma Focus

As pointed out in Publications 1-3 the moving thermal plasma model or the axial beam-target model can not explain the observed neutron energy spreads on anisotropy of neutron fluence.

We have proposed a new model which we call the converging ion model. Figure 4 shows the advance in time of the current sheet collapse above the center electrode of the gun. We postulate that the neutrons are produced at each instant of time by a three-dimensional convergence of ions into a small volume centered at the region of collapse as shown by the asterisks in Figure 5. Thus, in the laboratory reference system, the neutron producing region is observed to move up the axis of the gun with velocity V_{plasma}, since the region of collapse occurs farther and farther from the end of the center electrode on the axis of the gun as time increases. However, at a given instant the center of mass of the converging ions can have a velocity V_{cm}*, which may be different from the observed velocity V_{plasma}, according to the angular distributions of velocity and density of the ions in the laboratory frame of reference. Thus, V_{cm}* is not a directly observable quantity, but the observed neutron energy and fluence anisotropies are dependent upon it. This facet of the model provides an explanation for the apparent paradox[3] between the velocity of the neutron producing region along the axis of the gun observed in the laboratory, and the much higher velocities required to account for the measured neutron fluence and energy anisotropies. We assume that in the center-of-mass reference system with V_{cm}* along the axis of the gun, the neutron producing region consists of three-dimensional convergence of mono-energetic ions of energy E_d^{cm}. While there is symmetry about the axis of the gun in the laboratory reference system, ions converging from different directions in the axial half-plane (part of axial plane to one side of axis) have a distribution of energies E_d^{lab}, as shown in Figures 6(a) and (b).

The center-of-mass deuteron energies for the converging ion model required by our experimental data are presented in the fourth column of Table II. We assume an ion density of 5×10^{18} cm^{-3} and a volume of 6×10^{-4} cm^3 for the neutron producing region for the converging ion model. We use the reaction rates and the neutron energy spectrum half-widths calculated by Lehner and Pohl[10] for a three-dimensional monoenergetic ion distribution to obtain the center-of-mass ion energies required to explain the measured total neutron yields and neutron energy spectrum half-widths. Center-of-mass deuteron energies of 80 and 34 keV are required to give the measured total neutron yields of 1.0×10^{10} and

2.4×10^9, respectively. The measured average, maximum and minimum neutron energy spectra half-widths require center-of-mass deuteron energies of 53, 118, and 16 keV, respectively. The measured maximum axial-to-radial neutron energy anisotropy requires a center-of-mass velocity of 2.7×10^8 cm/sec. The measured 1.48 and 1.28 axial-to-radial neutron fluence ratios require center-of-mass velocities of 4.4×10^8 and 2.7×10^8 cm/sec, respectively.

The center-of-mass deuteron energies E_d^{cm} which account for the measured total neutron yields are seen to be in good agreement with the values required to explain the measured neutron energy spectrum half-widths, if we recall that the neutron energy measurements are averages over shots covering a wide range of total neutron yields.

Since for simplicity we have assumed an essentially uniform ion density in the neutron-producing region, we can calculate the spatial ion energy distribution in the laboratory reference frame using the center-of-mass velocity corresponding to the measured maximum axial-to-radial neutron energy anisotropy ($V^*_{cm} = 2.7 \times 10^8$ cm/sec), and the 80-keV deuteron center-of-mass energy obtained from the measured maximum total neutron yield. The resulting energy distribution in the laboratory frame is shown in Fig. 5(b). The deuteron energies range from a maximum of 313 keV in the axial direction pointing away from the center electrode, to 0 keV in the axial direction toward the center electrode. It should be noted that the acceleration of ions to energies greater than 300 keV is compatible with the observation by hard X-ray spectrometry of electron energies up to 500 keV in the plasma focus (See Publication 5 and 6).

The acceleration mechanism needed to produce the ion energy distribution predicted by the converging ion model has not as yet been determined. A promising mechanism is magnetic field annihilation at a neutral point which is considered by many to account for solar flare phenomena. The vortex burning proposed by Bostick et al.[11] may also be a microprocess which will produce an ion velocity distribution similar to our model. Other possibilities are the Fermi acceleration mechanism and the E × B acceleration mechanism proposed by Bernstein. Further study is needed to determine whether any of these mechanisms will give the velocity distribution required by our model.

The results of time-of-flight measurements neutron energy and measurements on neutron fluence anisotropy can be explained with the converging ion model. The converging ion model was found to be in closer agreement with our experimental data than the other proposed models, such as moving thermal plasma model and axial beam target model.

E. Hard X-Ray Spectra Determined by Nuclear Emulsions

A plasma focus produced by fast collapse of current sheets at the end of a coaxial electrode is a copious source of neutrons (from d-d or d-t reaction) and X-rays. Both the boiler model and the beam-target model can give rise to anisotropy in the production of neutrons and X-rays. The boiler model is based on the assumption that ions and electrons are thermalized in the plasma focus at a kT of a few keV and anisotropy of the neutron yield and spectra are results of plasma CM motion. The beam-target model considers a high current of charged particles accelerated in an electric or magnetic field giving a different production mechanism. Accurate spectral distributions of neutrons and X-rays would distinguish between these models. However, the determination of the spectral distribution of X-rays is difficult because the absorption coefficients for most elements are near a minimum for the energy range in consideration. In this note we report the spectrum of hard X-rays from the plasma focus determined using electron sensitive nuclear emulsions and compare it with the predictions of the proposed models.

The plasma focus apparatus at Langley Research Center is a Mather type powered with a 20-kV, 25-kJ capacitor bank. Hard X-rays with a maximum energy in excess of 500 keV are emitted simultaneously with neutrons (at resolution of 20 nsec) at the maximum compression of the plasma. No correlation was found between the intensities of neutrons and X-rays, excluding the possibility of significant neutron induced gamma-ray emission. The possibility of hard X-ray emission from the electrode surface has been excluded since production showing the same timing characteristics is observed with a hollow centre electrode as well as with a solid electrode. Figure 7 shows the hard X-rays monitored at 80 m from the plasma focus with a 3-in. thick scintillation detector which had a 3 mm lead shield cap. Because of time-of-flight, this detector separates the X-ray pulse from the neutron signal as indicated in Figure 7. Figure 8 is a pinhole photograph of the X-ray source in the apparatus. This shows the plasma focus is located approximately 2 cm above the surface of the electrode and has a volume of 1 cm long and 2 mm diameter cylinder.

Experiments were carried out to determine the spectral distribution of electron tracks produced in the emulsion by either photoelectric or Compton effect of X-rays from the plasma focus. The 600-μ-thick Ilford emulsions, stacked behind a 1.5 mm-thick lead absorber, were placed at a distance of 90 cm from the source on the axis of the electrode. The electron ranges were measured with Leitz scanning microscopes equipped with an 18 μ reticle grid.

The histogram in Figure 9 is a result of electron range measurements with 3807 tracks (longer than 18 μ) observed over background. The ranges were converted to electron energies using the relation given by Barkas[12]. A few tracks extended more than 600 μ indicating electron energies of greater than 500 keV. The dotted curves represent the expected electron track distributions, arbitrarily normalized, for three different models of the source. The curves were obtained by taking account of the attenuation through the lead absorber and the efficiency of nuclear emulsion. The expected number of electron tracks in emulsion per unit energy range N(E) is calculated from

$$N(E) = (4\pi)^{-1} A(E)T(E)N_{\gamma}(E)d\Omega$$

where $A(E)$, $T(E)$ and $N_{\gamma}(E)$ are the efficiency of nuclear emulsion, the attenuation through the absorber used and number of incident photons per unit energy interval. The efficiency of nuclear emulsion A(E) is determined using the chemical composition given by Barkas,[12] and the absorption coefficients by Brown.[13]

Three spectra of incident photons are considered for $N_\gamma(E)$. These are that of thermal plasma, thick-target bremsstrahlung expected from the beam target model, and a fitted power law distribution. It is clear that a Maxwellian distribution alone cannot account for the high energy spectrum. The curve for a thermal plasma assumed a $kT = 10$ keV; this is the maximum temperature one could reasonably assign for the plasma focus. The curve for thick target bremsstrahlung assumes an electron beam with kinetic energy of 500 keV. This model, by itself, cannot fit the observed spectrum. The power law curve is derived from the electron distribution, $f(E) \propto E^{-\gamma}$ with the best fit value of $\gamma = 4 \pm 1$ for $E > 150$ keV.

The result is in agreement with the power law distribution reported for the energy range up to 40 keV by Meskan et al. (1967). It is also interesting to note that such distribution of hard X-rays up to 80 keV was also observed in a solar flare as reported by Friedman[14]. These authors indicate nonthermal electron distributions in the plasmas.

We can conclude that the hard X-ray spectrum observed with nuclear emulsions are produced by nonthermal, power-law-distributed electrons in the plasma and the ion distribution does not agree with proposed models by others for a plasma focus such as the moving thermal plasma or the axial beam-target model. Publication 4, 5 and 6 deals with this subject in detail.

F. Hard X-Ray Sources in a Plasma Focus

Emission of hard X-rays with photon energy $E_\gamma > 100$ keV from a plasma focus has been observed and its spectrum has been determined. However the mechanism of hard X-ray production is obscure and interpretations of the phenomena are often contradictory. Maissonier, et al. speculated that the high energy photons from the plasma focus are neutron-capture gamma rays from the surrounding walls of the apparatus. This interpretation, however, can not explain the fact that no correlation exists between the neutron flux and the hard X-ray intensities. Furthermore we observed such hard X-rays are emitted when helium was used as working gas for which no neutron production could be expected.

This work was carried out to obtain the spatial resolution of hard X-ray source - the plasma focus which would clarify the mechanism of hard X-ray production in the plasma focus.

Since the sensitivity of photographic emulsions are too low to detect hard X-rays ($E_\gamma > 100$ keV), measurements were made with an array of thermoluminescence detectors (TLD 700) placed on the image plane of a pinhole camera as shown in Figure 10. The results shown in Figure 11 indicate that the hard X-rays are emitted mostly from near and on the center electrode surface. The area of the maximum emission is centered approximately 5 mm above the electrode surface. The hard X-ray source extends less than 1 cm along the axis, different from the neutron emitting volume which extends > 4 cm above the electrode. These results indicate that hard X-rays from a plasma focus are produced by accelerated electrons rather than gamma-rays associated with the nuclear reaction upon neutron irradiation on the walls. Publication 7 and 8 deal with this study in detail.

G. Electron Dynamics in a Plasma Focus

The intensity of X-rays from a plasma focus was measured as a function of position of emission, time, energy and angle, with resolution in several of these variables simultaneously. The low energy X-rays emanated from the dense focus region, but the high-energy components were mostly from the anode. Emission from the focus occurred some 20 ns prior to that from the anode, but the latter continued for 500 ns. Spatial estimates of electron energy were made; the electrons appeared to gain energy as they traveled from the plasma focus toward the anode, and possessed an "average" energy of about 10 keV near the anode surface. The time integrated intensity was also measured versus the angle θ from the axis of symmetry for $0 < \theta < \pi/2$ and for $\theta = \pi$, or behind the anode, in three energy ranges. Considerable anisotropy was revealed; the polar diagram of medium energy ($\simeq$ 20 keV) X-rays resembled a cardioid, but that for higher energy ($\simeq$ 100 keV) showed a lobe into the anode, with a forward-to-back ratio of about 50, indicating the plasma was near collisionless with run-away relativistic electrons in severaly anisotropic velocity distributions. By considering Bremsstrahlung emission from relativistic electrons, an explanation is suggested for the radiation patterns, and conversely the patterns are used to invoke the electron trajectories. The electron trajectories are consistent with the results of the spatial energy analysis. The electric fields required to produce such electron trajectories are also consistent with the converging ion model of neutron production, proposed previously. This work was carried out in cooperation with Dr. W. Harries of Old Dominion University. Publication 9 will discuss this subject.

H. Li-Target in a Plasma Focus - This experiment was carried out with the purposes of determining an upper limit of the fast ion energy by utilizing the energy threshold (200 keV) for the nuclear reaction $Li^7(d,n)Be^8$. The lithium rod of 50 mm dia. is placed in the top of the center electrode. Neutrons are monitored at both 3 m and 80 m from the plasma focus. Figure 12 shows the time-of-flight neutron spectrum at 80 m. The 13.3 MeV neutrons by Li(d,n)Be is clearly observed in addition to the D(d,n) He neutrons. This indicates > 200 keV deutrons are emitted from the plasma focus. The yield Y of the 13.3 MeV neutrons 10^8 is comparable to that of the d-d neutrons. By using the reaction rate $\langle \sigma V \rangle$ for 200 keV deutrons, the number of deutrons n_d falling on the lithium target is calculated as follows:

$$Y = n_{Li} n_d \sigma V(\mathrm{vol}) \cdot t_p$$

where $n_{Li} = 10^{22} cm^{-3}$, $\langle \sigma V \rangle = 1.8 \times 10^{-19}\ cm^3 sec^{-1}$ vol = volume = $10^{-3} cm^3$ and t_p = reaction time = $10^{-7}s$. This result indicates the number density of fast deutrons n_d, is 10^{15} cm^{-3}. This is many orders of magnitude higher than the number of fast deutrons expected from a plasma of a few keV temperature. No publication has been made on this experiment.

I. Production of a Fissioning Uranium Plasma

The emission spectra of a uranium plasma have drawn the interest of many authors who are engaged with the development of gas-core reactors and nuclear-pumped lasers. However the uranium plasmas that have been studied were nonfissioning and created in electric arcs, in shock tubes, or by lasers. The production of fissioning plasma is necessary to account for the effect of nonthermal fission products on the radiative properties of the uranium plasma. It was proposed to use a high-temperature oven in the high-flux neutron field of a nuclear reactor. However, the plasma in the oven attains a temperature and a density far below those required for a gas-core reactor. In another attempt at producing a fissioning uranium plasma, a discharge chamber coated with uranium oxide has been placed in a high-flux neutron field by Walters and Schneider.[15] A plasma in a state of nonequilibrium was obtained, and the effect of fissions on the radiation from the plasma was detected. These methods cannot be expected to create plasma conditions typical for the gas-core reactor and also require a large-scale nuclear reactor to maintain a sufficient neutron flux.

An inexpensive method of producing a fissioning uranium plasma that approximates gas-core reactor conditions is developed. A plasma-focus apparatus that provides an intense neutron emission and a strong heating mechanism simultaneously produces a fissioning uranium plasma. The fission yield was determined by high-resolution gamma spectrometry.

The plasma-focus apparatus (NASA-LANGLEY PFI) consists of a pair of coaxial electrodes and is energized by a 25 kJ capacitor bank. A 15-g rod of 93% enriched ^{235}U is placed in the end of the center electrode where an intense electron beam impinges during the plasma-focus formation. The resulting uranium plasma is heated to about 5 eV. Fission reactions are induced in the uranium plasma by neutrons from the d-d reaction which were moderated by the polyethylene walls. The fission yield is determined by evaluating the gamma peaks of ^{134}I, ^{138}Cs, and other fission products, and it is found that more than 10^6 fissions are induced in the uranium for each focus formation, with at least 1% of these occurring in the uranium plasma. This technique is most convenient and inexpensive for the study of a fissioning uranium plasma and can be extended to the production of other metallic plasmas in a high neutron flux. Publications 10, 11 and 12 report the production of a fissioning plasma in detail.

J. Radiation from a Uranium Plasma

The uranium plasmas produced in the plasma focus apparatus emit a wide range of electromagnetic radiation under similar conditions to a plasma core reactor. Since the radiation emitted by the fissioning uranium plasma core will play an important part in the operation of such a reactor, a knowledge of the radiation spectrum of such a plasma is necessary in order to establish reliable design criteria for the reactor.

The radiation emitted by uranium plasmas, containing both depleted U^{238} and enriched U^{235}, in the spectral range from 350 nm to 1000 nm, has been investigated with the objectives of: (1) determining the absolute intensity of the radiation emitted as a function of wavelength; (2) determining if any nonthermal radiation is produced by the plasma; and (3) determining if there are any detectable effects on the radiation spectrum due to induced fissions in the U^{235}. These measurements are the first laboratory data on the radiation emitted by uranium plasmas which are near the anticipated gas-core reactor conditions. Therefore, these measurements are expected to contribute to the establishment of design criteria for the development of plasma-core reactors.

The uranium plasma was produced by inserting a disk of pure uranium metal into the tip of the center electrode (anode). The device is normally operated at a filling pressure of 6.7×10^2 Pa (5 Torr) of deuterium. When the capacitor bank is discharged, a current sheet is formed and is accelerated upward between the electrodes by the $\vec{J} \times \vec{B}$ force. Maximum current is obtained as the current sheet reaches the end of the electrodes. The rapid radial collapse of the current sheet produces a dense, high-temperature plasma which emits intense bursts of charged particles and neutrons (from D-D reactions). The charged particles bombard the uranium sample creating the uranium plasma. The neutrons which are produced induce fissions in the plasma when U^{235} is used. A carbon arc was used as the radiation standard and the calibration of the spectrometer-photomultiplier system was made "in-situ." At each wavelength position a narrow band filter was inserted in front of the entrance slit to insure that no second-order radiation reached the monochromator. An exit slit width of 1 mm was used in these measurements corresponding to a band pass of 1.7 nm. The detector consisted of a high-gain photomultiplier tube and its output was recorded on an oscilloscope. All measurements were made one half cm above the center electrode and at the peak intensity of the emitted radiation.

The experimental results obtained for the U^{238} and U^{235} plasma show no observable difference in the two spectra.

A comparison of these experimental results with blackbody curves as well as the results obtained from a laser produced U^{238} plasma does not match any of the blackbody curves in this region. This is not surprising due to the existence of temperature and density gradients in the plasma. The blackbody curves should, however, provide some basis for comparison in this region.

No nonthermal radiation from the plasma was observed in this region. Also, no effects on the spectrum which could be attributed to induced fissions in the U^{235} were observed. This last result was anticipated as the energy due to the total number of induced fissions is small compared to the total energy of the plasma.

For this investigation, N. W. Jalufka, M. D. Williams and D. R. McFarland of NASA Personnel had active participation. Details of the results have been reported in Publications 13 and 14 (NASA TM X-71942).

K. Ultraviolet and Soft X-ray Emission from a Uranium Plasma

Emission of UV and soft X-rays from the uranium plasma produced in the plasma focus apparatus is investigated to help determine the design parameters of the gas core reactor that are presently being developed.

Spectral emission from the plasma was recorded on film and with a photomultiplier tube detector. The first such recordings were made with a one-meter Seya-Namioka spectrograph equipped with a platinum coated grating ruled at 600 lines/mm at a 1° blaze angle. With a specially developed differential pumping system which could maintain 10^{-4} Torr in the spectrograph with several Torr pressure in the plasma focus, the spectrograph was able to record for the first time the spectrum of a fissioning uranium plasma in the spectral region of 100-900 Å.

These spectral data were compared with similar data from a non-fissioning U^{238} plasma in order to determine the spectral effect of the fissions. Figures 13 shows that there was some enhanced emissions from the fissioning uranium plasma below 90 Å. However, the spectrograph was known to respond poorly in that spectral region, so the results were not conclusive.

A grazing incidence spectrograph was substituted for the Seya-Namioka spectrograph. It extended measurement capability to lower wavelength with greater resolution and allowed further investigation of the spectral region below 90 Å. The spectra were recorded on Kodak 101-01 film for high resolution of wavelengths and relative line intensities. An Amperex 150 AVP photomultiplier tube coated with sodium salicylate was used in the spectrograph to display time resolved spectra on a Tektronix 555 oscilloscope. Neutron pulses detected by a photomultiplier/scintillator combination were displayed on the same screen and the traces were recorded on film.

Figures 14 is density traces of the film spectrum for typical U^{238} and U^{235} plasmas. The general features of the traces remained the same on all spectrograms. However, there was a large difference in intensity especially in the large 93 Å peak. These intensity variations could not be correlated with neutron production or any other experimental parameter and are now believed to be a manifestation of the non-reproducibility of the plasma focus.

Although 10^4 fissions occur in the U^{235} plasma the energy deposited by fission fragments is so small that no evidence of the effects of fissions on the spectral range from 30 Å to 900 Å could be detected.

Soft X-rays from the uranium plasma are recorded with a bent crystal X-ray spectrometer. Figure 15 shows a typical spectrum obtained with Kodak NS X-ray film. The spectrometer covers a range of 3 to 9 Å. With the uranium insert the intensity of the soft X-rays in the range markedly increased from that of the copper insert. This is expected since the white X-ray emission is dependent on Z^2, where Z is the atomic number. However the uranium spectra shows characteristic lines at 4.7, 4.9, 5.6, 8.7 and 8.8 Å. Especially strong emission of lines at $\lambda < 4$ Å may be due to the non-thermal electron beams ($E_\gamma > 5$ keV) from the plasma focus.

Since one expects a large density of high energy electrons associated with the fission fragments in a gas core reactor the effects of intense X-rays on the first wall of the reactor should be given serious consideration. Our results indicates that not only the bremsstrahlung emission but also line emission will give significant contribution to the total X-ray energy.

L. Applications of a Plasma Focus

The intense neutron emission of 10^{17} s^{-1} by d-d fusion in a plasma focus may be exploited for applications other than fusion-plasma research. The production of a fissioning uranium plasma by inserting a U^{235} in the end of the center electrode as described in the foregoing chapters is an example of these. The applications of the plasma focus were also extended to production and life-time measurements of short-lived isotopes and fast-neutron radiography. Some preliminary studies on these applications have been made.

D. G. Wood of Kaman Nuclear has used a source with a total flux strength of 4×10^{10} n/sec for fast neutron radiography and obtained a useful result. The sample was located at 5 meters away from the source and exposed for 15 minutes. Therefore, the neutron fluence f can be estimated as follows:

$$f = Ft/4\pi r^2 \qquad (1)$$

where F is total flux, t, exposure time and r, the distance from the source to the sample. Using the given values of $F = 4 \times 10^{10}$ n/sec, $t = 15$ minutes or 900 sec, and $r = 500$ cm, we get $f = 1.2 \times 10^{6}$ n/cm^2. We may consider this value as the fluence required for a fast neutron radiography.

A plasma focus produces 5×10^{9} n/shot of average total yield and a repetition rate of 1 shot per 2 minutes can be made. The sample could be located as close as 10 cm from the focus.

We can calculate the number of shots N to obtain the required neutron fluence for fast neutrography with the relation

$$f = YN/4\pi r^2$$

where Y is the total neutron yield, 5×10^{9} n/shot. Hence

$$N = \frac{4\pi r^2 f}{Y}$$

At $r = 25$ cm

$$N = 4\pi(25)^2\ 1.2 \times 10^{6}/5 \times 10^{9} = 1.884$$

$$= 2 \text{ shots}$$

Since 2 shots of plasma focus formation could be made in 2 minutes this will have temporal advantage over the use of the source mentioned above.

By using a moderator-collimator, a thermal neutron radiography can be obtained as for other neutron sources.

Some advantages of using a plasma focus for the neutrography are as follows:

1. Inexpensive: The cost of neutrons produced in different devices have been compared and it is shown that a plasma focus device is the most inexpensive source of neutrons. The cost of initial capital investment is 10^6 neutrons per dollar and substantially cheaper than any other neutron source.

2. Little gamma background: Since the neutron is produced by d-d reaction no gamma ray is associated. X-rays can be shielded with a proper absorber.

3. A point source: The plasma focus has submillimeter size and without a collimator a good resolution of the picture can be obtained.

4. Radiation safety: Since a plasma focus lasts only a tenth of a microsecond, no radiation hazard is to be expected during down time.

The following is a summary of possible applications of a plasma focus as neutron, X-ray and deutron sources.

APPLICATION OF A PLASMA FOCUS

AS PULSED NEUTRON SOURCE:

Production of a fissioning uranium plasma - a sample of gaseous-core reactor plasma

Fast neutron radiography

Production and study of ultra-short-lived isotopes

Nuclear laser pumping

AS INTENSE AND PULSED X-RAY SOURCE:

Dynamic study of solid using 100 ns hard X-rays (e.g., shock in metal; phase transition in alloy, etc.)

AS ACCELERATED DEUTERON SOURCE:

Nuclear reactions by deuterons (e.g., $^{7}Li(d,n)^{8}Be$ with 13.6 MeV neutron production)

These applications are discussed in Publications 15 and 16.

M. Hypocycloidal-Pinch Apparatus

The plasma focus apparatus is most successful in approaching Lawson's criterion for thermonuclear fusion reactor (see Fig. 16). However, it is difficult to extend to a large-scale reactor development due to its geometrical limitations. Attempts to couple two plasma focuses have been unsuccessful for both Mather and Filipov types. To overcome these shortcomings a new type of pinch device made of electrodes in a disk shape called a hypocycloidal-Pinch (HCP) apparatus was invented by this investigation in 1970.

Figure 17 shows a plan view and a cross section through the apparatus. Figure 18 is a cut-out view of the apparatus to show the arrangement in three dimensions. There are two disk cathodes and a common disk anode. Two current sheets collapse radially toward the center of the apparatus. The initial breakdown takes place over the surface of the pyrex glass which insulates the two electrodes. As for the regular plasma focus apparatus, the current sheets are rapidly detached from the surface by the inverse pinch force. This minimizes the evaporation of insulator material into the current sheets.

Furthermore, this geometry contributes to the symmetrical shaping of the current sheets.

The hole on the axis of the center electrode allows the current sheets to interact and form a pinched discharge region resembling a hypocycloid in shape and thus the plasma undergoes a three-dimensional compression in the center hole.

It is anticipated that the hypocycloidal pinch apparatus will provide improvements over the coaxial plasma focus in (1) a longer plasma confinement time (2) larger plasma volume (3) easy access to additional heating by laser or electron beams and, (4) the possibility of scaling up to a multiple array for high power operation.

Figure 19 shows the prototype unit used for this study. It is energized by 20 kV, 30 kJ capacitor bank and deuterium is used as filling gas. It has a rundown radius of 10 cm with a 5-cm diameter center hole. The spacing between the anode and cathode disks is 2.5 cm.

The operating procedure of the HCP apparatus is similar to that of the coaxial plasma focus. The following sequence is used for each run:

(1) Filling the apparatus with working gas at a desired pressure,

(2) Changing the capacitor bank to the required voltage, and

(3) Firing of the trigatron switches to discharge the stored energy into the HCP apparatus.

The prototype system has the following electrical parameters: capacitance, 150 μF; external inductance, 20 nH; inductance of the prototype, 4 nH; and the current rise time, 3 μs. Some preliminary studies were carried out to obtain design parameters for the prototype.

These studies were carried out to determine (1) effectiveness of perforation in the outer electrodes, (2) effect of the backstrapping of the current path on the speed of the current sheets, and (3) the size of the center hole.

It has been known that perforation of the outer electrode of a coaxial plasma focus is effective for promoting the rundown speed of the current sheet in the discharge chamber. To verify that such benefits of perforation can still be expected for the hypocycloidal pinch, an outer electrode with partial perforation was coupled with the center electrode. Figure 20 shows the time integrated photograph of the current sheet motion. Note that the current sheet does not reach the center hole from the solid area of the electrode in contrast to the luminous fronts shown in the directions of linear perforations (or lines of holes). This is vivid demonstration of the effectiveness of perforation. Therefore the prototype apparatus was constructed with 40% uniform perforation on the outer electrodes.

The backstrapping current path is commonly used on Tee-tube shock tubes to promote the speed of the current sheet in the expansion tube. However there is little quantitative information about its efficacy.

To determine the effect of "backstrapping" on the hypocycloidal pinch apparatus, two methods of cable connections, one providing the backstrapping, and the other without, were tested. Figure 21 illustrates these methods. Figure 22 shows the results of measurements on the velocity and acceleration of the current sheet. Note that at the pressure of 133 Pa, the velocity of the current sheet is 1.9 cm/μs without backstrapping while it is 4.1 cm/μs with backstrapping. The latter is 2.2 times greater than the former. The promoted velocity of the current sheet is observed over all pressure points in the range 133 to 399 Pa. The acceleration of the current sheet shows the same effect. These results were obtained with assistance of Larry A. Stauffer of VPI who was supported by NASA Summer Student Program. The dynamics of the current sheet have been studied for different diameters of the center hole. For hole diameters less than 3 cm, no focus formation was observed and non-uniform erosion of the surface of the hole was noticed. However, the collapse of the current sheets for a larger (5-cm diameter) hole is well organized and radial stability of the focused plasma is sustained for several μs.

The results of these tests have been helpful to determine the design parameter of the prototype constructed later.

The invention disclosure of the HCP apparatus to the NASA Technical Officer has been made on June 27, 1970 and the Patent Waiver [W1418] has been granted to Vanderbilt University.

N. Diagnostic Measurements of a HCP Produced Plasmas

The prototype (HCPI) of a hypocycloidal-pinch apparatus is used to make extensive diagnostic measurements on the dynamics of the current sheets, the size and the confinement time of the focused plasmas, plasma radiation, plasma temperature and plasma density. Figure 23 shows streak pictures taken through a slit placed across a diameter of the center hole. The strong emission of light from the focused plasma is attenuated through a 4D neutral density filter to prevent overexposure of the film. The objective lens of the camera is covered with a λ5600 ± 10 Å interference filter to allow observation of continuum emission only. The pictures reveal production of a luminous plasma on the axis which has radial stability for more than 5 microseconds. The diameter of the luminous plasma column is approximately 5 mm and it is well centered on the axis of the hole. Note that the diameter of the filter is small enough so as not to cover the edge of the hole. This allows observation of the hole edge in Figure 23. The boundary of the plasma is sharply defined and no MHD instabilities are detectable in the pictures. Figure 24 shows frame pictures of the same event. A still reference picture is also shown. The frame pictures were taken in sets of three at a time with different neutral density filters for each set. The filter density was increased as the compression progressed to prevent overexposure. The progress of symmetrical compression is well illustrated.

Figure 25 shows the axial motion of the focused plasmas. These pictures were obtained with the optical axis of the image converter camera oriented to form a 10° angle with the axis of the apparatus as illustrated in Figure 25(a). The still reference picture in Figure 25(b) shows the field of view of the camera. The streak picture in Figure 25(c) shows that there are three stages in the axial motion. First the current sheets collapse to form a 10-cm-long column on the axis with a dense focus at each end. Then axial compression follows and ~2 μs later its length is reduced to ~3 cm and a fading of visible radiation follows. Lastly, the plasma column splits into two focuses separated by a distance of ~5 cm which is the distance between the central planes of two electrode pairs. However, there are occasions when no axial compression is observed as shown on the streak picture in Figure 25(d). The two focuses seem to stay separated for their whole lifetimes.

Figure 26 shows the rundown speed of the current sheet measured on streak pictures taken with an image converter camera which is focused to a 1-mm-wide slit located along a radius of the discharge chamber. The time history of the advancing luminous front of the current sheet is then obtained from the image converter pictures and yields the rundown speed. The rundown speed V was measured as a function of the filling pressure p. For the deuterium pressure range from 67 to 2,000 Pa (0.5 to 15 Torr) it is in agreement with a snow-plow model which predicts $V \propto p^{-1/4}$. These measurements were made with the capacitor bank energy of 27 kJ at 19 kV.

Figure 27 is a time-integrated X-ray pin-hole picture taken on the axis of the apparatus. The X-rays pass through a 250-μm-thick beryllium foil that covers a 1-mm-diameter pinhole. The picture shows that soft X-ray emission is concentrated in a volume of diameter ~5 mm on the axis and that it is well separated from the wall surrounding the hole. The size of this volume is in agreement with the luminous plasma shown earlier in Figure 25.

Figure 28 compares temporal evolution of the voltage, the dI/dt at the center electrode, the X-ray emission detected by a fast scintillator-photomultiplier system, and the continuum emission in the visible. The dense-plasma formation in the hypocycloidal-pinch apparatus is characterized by a sharp spike on the voltage and the dI/dt signal and simultaneous onsets of strong continuum and X-ray emission, similar to a coaxial plasma-focus apparatus. However, the voltage signal from the center electrode, figure 28(a), does not show the high frequency oscillation following the spike that is often observed with the coaxial type. This may indicate lack of fast-growing instabilities in the hypocycloidal-pinch apparatus. Furthermore, the continuum and the X-ray emissions are sustained for a period of 5 μs after the current-sheet collapse. This time is more than an order of magnitude longer than that of a coaxial plasma focus. This is well illustrated in Figure 29 which compares the periods of X-ray emission from two apparatus.

The electron temperature T of the plasma is determined by the differential transmission of the X-rays through absorbing foils of different thicknesses. The intensities of the transmitted X-rays through 250, 500, 700, and 1,000 μm beryllium foils were monitored on the four sections of a Kodak NS X-ray film. With the assumption of a Maxwellian distribution, the intensity ratio of the transmitted X-rays can be used to determine the electron temperature of the plasma. For a typical run, after subtracting the gray level of the film, the intensity ratio of the transmitted X-rays through 250 μm and 500 μm foils is 0.55 which indicates the electron temperature of ≈1 keV.

The assumption of a Maxwellian velocity distribution for electrons is considered reasonable since the plasma lifetime of ~5 μs is very long compared with the electron thermalization time of the order of 10 ns. Also, the X-rays are detectable through a 1.5-mm-thick aluminum absorber, indicating that the high-energy tail extends beyond the 8 keV K-edge of aluminum. However, no X-rays were detectable behind lead foils, indicating emission of hard X-rays ($E_\gamma > 80$ keV) is small. Nevertheless, low-level neutron production has been observed with a scintillation neutron detector even at the comparatively low capacitor bank energy of 27 kJ.

The density of the plasma is estimated by the line broadening of D_α and D_β. The line broadening is measured on the time resolved spectra obtained with an image-converter camera-photomultiplier system. This system consists of a 500 gain TRW camera focused on the exit slit of a 1.5-m spectrometer which had a dispersion of 0.556 nm/mm. Since the line broadening in a high-density plasma is mainly due to the Stark broadening and since Doppler broadening is negligible, the half width of the lines can be used as a measure of plasma density. Figure 30 shows the plasma density variation in time obtained by this method. A densitometer is used to obtain the broadened line width. The broadening of the D_α line produced by the first pinch is so wide (>10 nm) that accurate pressure determination cannot be made. However, the broadening indicates that $n_e > 10^{18}$ cm^{-3}, the upper limit of the useful range of this method. This was expected from the compression ratio of ~100 estimated with the snow-plow model.

The particle confinement time is measured by means of high power CO_2 laser transmission. Figure 31 shows the experimental setup. A 50-J, TEA CO_2 laser beam with 150-ns pulse width is focused to a diameter of 5 mm by a germanium lens. The beam irradiates the full cross section of the focused plasma in the HCP apparatus. The laser firing time is varied so that the interaction at different times of the plasma life can be determined. The incident and the transmitted laser powers were measured with pyro-electric infrared detectors IR 1 and IR 2, respectively. IR 1 monitors a small fraction of the incident laser power which is reflected by a small mirror. IR 2 has a higher sensitivity than IR 1 and measures the transmitted or scattered laser power.

Figure 32 shows five sets of oscillograms which record the voltage at the center electrode of the HCP, the incident power of the CO_2 laser by IR 1, transmitted laser power by IR 2 at 180° and the X-ray emission, as indicated. Time t is the elapsed time from the onset of X-ray emission to the CO_2 laser firing as monitored by IR 1. Figure 32(a) shows the full transmission of laser radiation before (t = -0.2 μs) the plasma production on the axis. Less than 1 percent transmission is recorded for t = 0, 0.5, and 12 μs, (Figure 32(b), (c), and (d)). For these times the maximum sensitivity of the scope amplifier is used to verify the results. Figure 32(e) shows that at t = 72 μs there is 30 percent transmission through the cooling and expanding plasma. Note that both IR detectors have a fast rise time, <10 ns, but a long decay time characteristic of pyroelectric sensing elements. Only the leading edge of the pulse is meaningful.

The back and side scattering of the laser power by the plasma has also been investigated. For this purpose the IR 2 detector is located in 10° and 90° directions with respect to the optical axis as shown in Figure 31.

The sensitivity of the IR 2 (KT-1100, Laser Precision Corp.) was 0.125 μA/watt. When this detector is located at a distance of 1 m from the plasma, which is irradiated by a pulsed laser of 5×10^{8} watt (or 100 ns pulse of 50 J), the sensitivity of the detector is sufficient to give an observable signal for the total scattered power of as small as 5×10^{-3} times the incident power.

The laser firing time t is varied with respect to the onset of the X-ray emission, $t = 0$, as for the transmission experiment. Since the scattering is expected to increase with the plasma density, the laser firing time t is varied with a small interval of 100 ns between runs so that the scattering from the plasma at the maximum compression can be detected. However, for both 10° and 90° directions, no scattered intensity above the detector threshold was observed for the laser firings made in the period $-0.2 \leq t \leq 75$ μs. This indicates the total scattered intensity is less than 1 percent of the incident laser power.

The combined results of the transmission and scattering measurements lead to the conclusion that nearly complete absorption of the laser energy occurs in the plasma.

The absorption of CO_2 laser energy can be used to determine the density of the plasma. For an underdense plasma, the dominant absorption process is that of inverse bremsstrahlung due to electron-ion collisions. This process gives an absorption length ℓ

$$\ell_{ab} = \frac{5 \times 10^{27}\, T_e^{3/2}}{n_e^2\, Z\, \lambda^2} \left(1 - \frac{\lambda^2}{\lambda_e^2}\right)^{1/2}$$

Here λ is the wavelength in cm, λ_e is the wavelength of radiation at the plasma electron frequency ω_e; i.e., $\lambda_e = 2\pi c/\omega_e$ and $\omega_e^2 = 4\pi n_e/m_e$, T_e is the electron temperature in eV, n_e is the electron density in cm^{-3} and Z is the ionic charge.[17] By unfolding the relation $I = I_0 \exp(-x/\ell_{ab})$. n_e can be determined when T_e and Z are known. If $\lambda = \lambda_e$ or the plasma has a critical density, the absorption length is reduced to zero and the near complete absorption will occur. In this case, if radiation of sufficient intensity falls on the plasma it can create instabilities which lead to anomalous absorption of the radiation. For the plasma produced during the first compression in HCP, $T_e \approx 1$ keV, $Z = 1$ (since few impurity ion lines are observed above the continuum). Near complete absorption of the CO_2 laser ($\lambda = 10.6 \times 10^{-4}$ cm); i.e., $I/I_0 < 0.01$, through 5-cm long plasma column indicates that the plasma column provided more than 4.6 times the absorption length. This can be translated into $n_e > 7.8 \times 10^{18}$ cm^{-3}. For the later times, the absorption of radiation takes place in the hole ($T_e < 100$ eV) and impurity-rich ($Z > 1$) plasma with its density $n_e < 10^{18}$ cm^{-3}. Due to the limit in the sensitivity of the IR detector system, the determination of the temporal variation of n_e was not possible.

The impurity level of the plasma generated in the hypocycloidal pinch was investigated with time-resolved spectrometry. No detectable line emissions expected from wall erosion were observed above the continuum intensity during the first pinch period. The impurity line emissions became apparent only at later time as expected. Some of the impurity lines which have been identified include ion lines of oxygen and silicon.

The final compression and heating in Z-pinch devices, such as the coaxial plasma focus or the hypocycloidal pinch, are known to depend on the degree of symmetry that is maintained for the entire flight of the Z-pinch current sheets. In the hypocycloidal-pinch apparatus, the most serious excursion from symmetry may occur when one current sheet moving in the upper or lower chamber gets in front of the other, thereby arriving at the center hole before the other. However, we observe no appreciable delay between the arriving times of the upper and the lower current sheets at the center hole. The observations made in the streak mode, as in Figure 23, clearly show that the final collapse of the upper and the lower current sheets is simultaneous within the framing time of 50 ns. This is also confirmed by the shape of the X-ray pulse, as shown in Figure 28, for which one would expect double peaks corresponding to each collapse of the two current sheets if they occurred at two different times. Indeed, the observations indicate that the geometry of the hypocycloidal-pinch apparatus provides a self-stabilizing effect on current sheet dynamics, as discussed in Reference 18. The self-stabilizing effect can be easily understood by considering the advancing current fronts as two parallel-circuit elements with time-varying inductance as the load of a common power source. The ponderomotive force $\bar{J} \times \bar{B}$ exerted on the current sheet which lags behind, forming a circuit with a smaller impedance, will be stronger than the force on the current sheet that leads, resulting in an increase of acceleration to "catch up" to the leading front.

The other common phenomenon undesirable for a Z-pinch is nonsymmetrical spoking, or filamentation of the current sheet. For the hypocycloidal pinch no evidence was found of such spoking of the current sheets by means of either the fast camera pictures or the "foot prints" of the currents on the electrodes. The main reason for the uniform discharge at the outer periphery may come from the fact that the design of the HCP accommodates the inverse-pinch phase, similar to the coaxial plasma-focus apparatus. It is known that the initial breakdown in a form of an inverse pinch is important for symmetrical current-sheet formation in a plasma-focus apparatus. The inverse pinch is also helpful for reducing impurity level in the plasma since the current sheets will quickly leave the surface of the insulator. The uniform discharge at the periphery is also partially a result of careful construction to maintain a high degree of axial symmetry of the apparatus. It should be mentioned that the output cables from different switches are criss-crossed at the collector plates to ensure simultaneous breakdown at all points of the periphery.

The rundown speed of the current sheet of 5×10^4 m/s at 665 Pa (5 torr) is rather low compared with that of the coaxial plasma-focus apparatus, 3×10^5 m/s. However, this can be understood by taking account of the fact that the stored energy is divided into two chambers of the hypocycloidal pinch (HCP), while the coaxial plasma-focus apparatus (PF) has only one current sheet to be accelerated. Furthermore, in the HCP the current sheets are radially compressed from the beginning and tend to have a large mass pickup in contrast to the rather low mass pickup in the PF which runs down in an annular space with a constant cross section. Therefore, it is expected that a larger mass for the focused plasma in the HCP than in the PF and this is indeed confirmed by our measurements of the X-ray emitting volume (~5 mm diameter for the HCP and ~1 mm diameter for the PF) and the density of the plasma. The slower rundown speed in the HCP may be the result of the large mass entrainment. However, since the snow-plow model gives a scaling of the rundown speed with the capacitor-bank energy, a higher rundown speed should be obtainable by increasing the stored energy.

The results obtained with the HCP also shows a remarkable improvement in both energy and particle confinement times. The full width of the X-ray pulse extends to 5 μs with a sharp spike at the onset. This is an order of magnitude longer than the corresponding period of X-ray emission in the coaxial plasma-focus apparatus as shown in Figure 29. In fact, the X-ray emission in HCP continues until the end of the first half cycle of its discharge circuit. This may indicate that the plasma confinement time in HCP is limited only by the current decay. This also contrasts to the 150-ns X-ray spike without an extended tail observed in the spindle focus with a pair of disks by Ware and Mather.[19] The extended confinement of the plasma in the HCP seems to result from the interaction of two focuses in the magnetic-neutral plane formed by the cusp configuration of the current sheets in the center hole, which is a unique feature of the HCP. One should also note that the simultaneous arrival of the upper and lower current sheets on the axis of the center hole is necessary to form the symmetric cusp configuration of the current sheets. The excellent radial stability beyond the period of the initial spike observed in the HCP leads one to believe these requirements are fully met and the configuration is well maintained throughout the later period during which the plasma diffuses and expands as the currents oscillate and decay. This interpretation is further justified by the results of the CO_2 laser absorption experiment which indicates prolonged particle trapping near the axis for five periods of the circuit oscillations. Therefore, one could possibly achieve further extension of the containment time of the dense plasma produced at the first pinch by shaping the current wave form to a nonoscillatory mode with a crowbar circuit as is often adopted for the capacitor banks used for theta pinches.

The self-stabilizing mechanism of the hypocycloidal current sheets discussed earlier may be effective even after the collapse of the current sheets into the hole, thus resulting in the suppression of the fast-growing MHD modes. The self-stabilization mechanism after the collapse can also be understood by elementary consideration of the circuit induction with a virtual displacement of the current sheets. As shown in Figure 33, displacements from the equilibrium of the current sheets tend to reduce the inductance of the circuit to which the current sheet is attached. This in turn results in a stronger $\bar{J} \times \bar{B}$ force in the direction against the displacement. The force F on the current sheet displaced by δ is $F = -k\delta$ where k is a constant.[18] The negative sign indicates this force will act to restore the equilibrium. Note also that the restoring force is linear in this analysis. The restoring force resulting from displacement from an equilibrium position can be visualized in a different way. It is the compression of lines of force which leads to an increase in magnetic pressure on the current sheet.

The present results from the prototype thus show that a high-density, high-temperature plasma of a rather large volume (~ a few cubic centimeters) can be confined for a long time (>5 μs) with the hypocycloidal-pinch apparatus. Energy confinement of tens of kilojoules and copious X-ray and neutron production in the HCP are expected when an adequate power source is used in the future.

The geometry of the HCP is such that there is easy access for laser or electron beam heating. Since the electron density of the plasma in the hypocycloidal pinch approaches the critical density for the CO_2 laser frequency, anomalous plasma heating to achieve thermonuclear fusion temperatures may be possible. This mechanism is predicted to be the most efficient for plasma heating.[17] Sufficiently powerful CO_2 lasers for this mechanism to be operational also have been developed. However, no other suitable plasma source has previously been available for testing the anomalous heating mechanism.[17] The coaxial plasma focus has been proposed as a plasma with sufficiently high density for testing and mechanism. However, few successful experimental results have been reported to date. Its small volume and brief lifetime do not render clear observation of the effects of the interaction. The nearly complete absorption of CO_2 laser energy by the plasma in the HCP apparatus gives strong encouragement for this approach although no apparent evidence for strong development of parametric instabilities, expected from the anomalous heating, has yet been observed, perhaps because the energy (50 J) of the laser that was used contributed only a small fraction of the plasma energy of 900 J. It may be necessary to increase the laser output to the range of kilojoules to reach the "strong pump-field regime" for clear observation of the effect[20].

Since the geometry of the hypocycloidal-pinch apparatus consists of a set of disks, a multiple array to form a linear or toroidal system could be constructed, as shown in Figure 34. Such a system is not only capable of accommodating a large energy input, but will also improve the plasma containment time since the axial outflow will be reduced by the closed ends.

In conclusion, successful production of a long-lived high-density and high-temperature plasma in a large volume in the prototype of the hypocycloidal-pinch apparatus has been demonstrated. The plasma is observed to have nearly complete CO_2-laser-energy absorption for a time longer than a quarter cycle of the discharge. The CO_2-laser absorption indicates a plasma density greater than 10^{18} cm^{-3}. The plasma temperature is about 1 keV and the plasma confinement time is 5 μs. It is optimistically suggested that this geometry could be adopted to develop a large-scale fusion-power reactor because of its advantages in plasma volume, containment time, easy access to additional heating by a laser or electron beam, and the possibility for scaling-up to a multiple array. Publications 20, 21, 22 and 29 deal with diagnostic measurements on a hypocycloidal pinch in detail.

O. Current Sheet Dynamics in a HCP Apparatus

This work has been carried out at the Vanderbilt University by John P. Barach. A small hypocycloidal pinch was constructed for study of the current sheet dynamics. Small magnetic probes were used to map the magnetic field lines as the current sheets rundown toward the center hole. The device has a peak current of 1.4×10^6 A and operates in helium at a pressure of 2.8 Torr. The inward-going current sheet is observed which has flow speeds of about 2×10^6 cm/s. The plasma assembled near the center has a temperature of 8 to 10 eV. A magnetic well is indeed formed at the center of the device as expected.

Figure 35 displays contours of the magnitude of B_ϕ at the moments 1.4 and 2.8 μs after the arc strike. Inspection of these plots leads to various conclusions as follows. (1) The current sheet has a complex shape and behavior making it hard to, for example, determine a single number for the run-down or snow-plow speeds. The piston we observe is evidently "leaky". (2) The current flows from over much of the electrode surface and is not confined to a narrow region which might move radially inward down the electrodes. Only 42% of the total current flows within r = 3 cm from the axis. (3) A roughly "spindle-shaped" pinch is indeed formed at small r and small z. Since the magnetic force density is directed roughly perpendicular to the contour lines a magnetic "well" may be visualized in the figures. At t = 2.8 μs a boundary may be seen ($z = 1$, $r = 2$) to ($z = 2$, $r = \frac{1}{2}$). It is estimated the plasma pressure of 10^6 N/m^2 or kT = 8 eV. (4) The current sheet thickness is observed to be about 0.4 cm, and has a Spitzer conductivity of ca. 960 mho/cm.

However nothing about the small volume focus event itself could be determined with magnetic probe measurements. (5) The plasma temperature observed is 8-10 eV, 3 times lower than that of a coaxial plasma focus for the rundown phase. This may be due to the low rundown speed in the hypocycloidal pinch which is under powered for the mass of the gas in the chamber.

This work will be published in Physics of Fluids shortly (Publication 17).

P. Current Drop in a Plasma Focus

Many authors have attempted an explanation of a plasma focus formation by numerical simulation of the plasma dynamics during the compression phase. The current drop is considered merely as the consequence of the plasma disturbance. However, we believe the current-drop induced field is the most important factor for hard X-ray and neutron production from the plasma focus. Therefore we gave this subject further consideration.

The possible causes for the current drop in the plasma focus are as follows:

Induced emf, IdL/dt. The imploding current sheet can be considered as a variable inductor in the circuit and the induced emf (IdL/dt) can be calculated easily. For electrical parameters for a typical plasma focus apparatus with 5 and 10 cm dia. electrodes, $I_{max} = 10^6$ A and

$$V_r = 2 \times 10^{+7} \text{ cm/s}$$

then

$$I(dL/dt)_{max} \sim 100 \text{ keV}$$

One should note that this field is in the opposite direction to the initially imposed field. This field may alter the shape of the current pulse selfconsistently but not sufficient to explain the hard X-ray ($E_\gamma > 100$ keV) and anisotropic neutron emission observed.

Often used equivalent circuit includes the external circuit and current sheet only neglecting the shock heated plasma (see Figure 37).

The voltage across the current sheet V is

$$V = \frac{d}{dt}(L_{CS}I) + IR_{CS}$$

$$= L_{CS}\dot{I} + \dot{L}_{CS}I + IR_{CS}$$

For the compression is timed at $\dot{I} = 0$ and IR_{CS} very small $V \approx \dot{L}_{CS}I$.

However, this circuit may be over simplification for the circuit involving the complex plasma, i.e., MHD interaction is completely neglected. The following phenomena have been noted by many authors.

M = 0 Necking. At the end of the plasma pinch in the axial column an M = 0 instability grows as for any linear z-pinch. Recently this instability has indeed been observed in plasma focuses with interferograms and soft X-ray channel plates in ns time resolution. However, the sustained neutron emission for over 100 ns and multiple focus formations are not fully explainable with the MHD instability of ~10 ns time scale.

Impurity cooling. This mechanism ascribes the current drop to the injection into the current sheet of high-z impurities from the electrode surface, thus abruptly cooling the sheet by enhanced radiation (Gullickson) to the point where the electron thermal velocity is less than the directed velocity, triggering a microinstability. Bazdenkov, et al. advocate that the dense neutral vapor from the anode lowers the plasma conductivity to result magnetic field diffusion and consequently the particle acceleration. This mechanism may not explain the ~20 ns onset time of the current drop or hard X-ray emission time.

Annihilation of Vortices. Bostick et al. find that a magnetic structure of localized vortices is the main current carrier in the plasma focus apparatus. The annihilation of each pair of vortices in the structures can result in explosive decays of the current and particle acceleration. However, this mechanism needs further clarification for universal acceptance.

Current sheet runaway. This is recently reported by Gureev et al. in Soviet J. of Plasma Physics. At near the axis the current sheet suddenly dissociates and produces a large electric field to accelerate particles. No basic mechanism for the phenomenon has been proposed.

Until recently, little attention was given to motional emf $\bar{V} \times \bar{B}$ in its full extent, although the simulation with MHD code is based on the equation including this emf. According to T. G. Cowling, a simple development of the MHD equation results in an expression for a point fixed in the fluid as follows:

$$\frac{\partial B}{\partial t} = \nabla \times (\bar{V} \times \bar{B}) + \nabla^2 \bar{B}$$

Associated parameters are:

$$\tau = 4\pi\mu\sigma L^2 \qquad \text{e.m.u.}$$

$$\eta = (4\pi\mu\sigma)^{-1} \qquad \text{e.m.u.}$$

The effective electric field $\bar{E}^*$ on a point in the fluid is

$$\bar{E}^* = \bar{E} + \bar{V}\times\bar{B}$$

where $\bar{V}\times\bar{B}$ is the motional emf E_m.

Figure 36 illustrates the MHD relation with this motional emf E_m generated in the shock heated plasma ahead of the current sheet. The azimuthal magnetic induction B_ϕ is inversely proportional to the radius as shown in the upper figure. In the lower figure $J_z\ \delta(\phi)$ is a current carrying filament directed toward $+z$ while the E_m is induced anti-parallel to this. V_r is the radial velocity of the current sheet.

The magnetic Reynolds number R_m is

$$R_m = \frac{LV}{\eta} = 4\pi\mu\sigma VL$$

where L is the scale length of the fluid. For the shock heated plasma in the surface of the magnetic flux, may typically have

$\sigma = 10^{-7}$ emu or 100 mho cm^{-1}

$L = 0.3$ cm distance between B_{max} and $1/4\ B_{max}$

$V = 10^7$ cm/s

to give $R_m \approx 4 > 1$

The diffusion time of the magnetic field $\tau = 4\pi\mu\sigma L^2$ is

$\tau = 113$ ns

We see a strong MHD interaction of the plasma flow and the magnetic induction B. Also, we note that the $\bar{V} \times \bar{B}$ field can result in an internal current loop near $r = 0$ since there is a strong $\nabla B \sim r^{-2}$.

Therefore, we propose the equivalent circuit for the plasma focus apparatus to include E_m as shown in Figure 37. Here the subscripts e, cs, p denote the external circuit, the filamentally current sheet, and the shock heated plasma. The branch circuit with a variable resistance R_p of the shock heated plasma, and a generator G to represent the motional emf $V_r \times B$ is included, to include the MHD interaction described above. The value of $E_m = V_r \times B$ can be derived from V_r measured on a streak picture as shown and B via the relation with the monitored current I, i.e.,

$$B = \frac{\mu_o I}{2r}$$

Figure 38 illustrates that the E_m is steepened near the axis ($\gamma = 0$) by the slopes of both V_r and B. It is 300 kV/cm at $r = 1$ mm. Therefore, the E_m is only effective a few mm from the axis. This matches the effective time of ~10 ns before the maximum compression. Newman, et al. have recently used this field to explain the hard X-ray emission from the plasma focus.[21] The computer simulation results presented by Hohl also indicated there is electron acceleration during the compression phase as well as during the current reduction phase. However, our hard X-ray observation shows that no electron acceleration away from the electrodes attributable to this field.

Disagreement between results of the observation and the simulation may be due to the fact that the simulation neglects local current loops in the plasma column. It has been observed that a strong gradient B embedded in a moving plasma volume can be trapped by the local current loop and even be transported by the plasma. To fully account for these, a selfconsistent simulation, including the strong gradient B field and resulting local current loops may be necessary.

Three effects of the strong motional emf near the axis are as follows. The first effect is disruption or destruction of the currrent filaments similar to solar flare events. The particle acceleration is the consequence of the current drop or field annihilation. The second effect is that since the motional emf is induced only near the end of the compression phase when the magnetic field ~100 Tesla with a strong gradient behind it, it does not accelerate electrons away from the electrode. For $B = 100$ T the cyclotron frequency is $\sim 10^3$ times of the collision frequency. We should note that the high motional emf is incuded only for <10 ns before the current sheet is stopped or $V_r = 0$. Thirdly, we consider particle drift by $E_m \times B$. This drift oppose $E \times B$ drift, so we expect a deceleration of the current sheet implosion. In fact, this mechanism may determine the size of the focused plasma column and the sustainment time of the plasma focus.

In conclusion, we hope that this speculation could stimulate self-consistent simulations of a plasma focus which may lead us to a better understanding of events occurring the transition period from the compression phase to the current reduction phase.

Publication 18 reports on the effects of the motional emf in the plasma focus apparatus.

Q. 50-kJ Plasma Focus Apparatus PFII

The 50-kJ plasma focus apparatus PFII was installed in 1971 for increased neutron production. The PFII apparatus is utilized for establishing a scaling law of the plasma focus and investigation of high voltage effects on its characteristics. These studies have been made in comparison with the results of PFI. Neutron energies from two plasma-focus apparatus PFI and PFII were measured with the time-of-flight method to determine the effects of the applied voltage. Both devices were operated under similar conditions except for the applied voltage. The neutrons from PFII with a 40-kV capacitor bank show that, while the radial energy remains unchanged, the axial-to-radial energy difference is twice as large as the difference observed with PFI using a 20-kV bank. With 40 kV, the highest-energy neutrons are often separated from the neutrons of lower energy. These results indicate that two different modes of neutron production are operative in the plasma focus. We have also observed 14-MeV neutrons that are attributable to the secondary D-T reactions of fusion products.

Publication 19 reports the results of this investigation.

R. 150-kJ Hypocycloidal Pinch Apparatus

The diagnostic measurements on the prototype hypocycloidal pinch, as reported in a previous chapter, confirmed that the expectations on plasma stability, size, density, and temperature, have been indeed fulfilled.

According to the snow-plow model the rundown speed of the current sheet can be increased by increasing the capacitor bank energy. To obtain a rundown speed of 3×10^5 m/s with 5 Torr D_2 which is comparable to that of the coaxial-type plasma focus, a six-fold increase of the bank energy is needed. With the existing capacitors and additional capacitors on order, a 150-kJ capacitor bank has been installed. The 150-kJ bank system has modules consisting of three 50 kV capacitors, 24 trigatron switches, and a 20-cm diameter HCP apparatus. A rise time of 4 μs was obtained with eight output cables from the switch. (The prototype HCP I uses four output cables per switch and has a rise time of 3 μs.) The system will be tested for simultaneous firing of switches. A 90 kV trigger unit has been constructed for this purpose. This program will be continued under a new grant.

III. SUMMARY

The investigation of high-energy radiation from a plasma focus has been conducted to understand the mechanism of hard x-ray and neutron production in the plasma. Neutrons are studied by means of a time-of-flight method with a flight path up to 80 m, silver activation counters and fast scintillation detectors, while x rays are investigated with absorbing foil pin-hole camera system, scintillation detectors, and crystal spectrometers. Nuclear emulsions were also used for both neutron and hard x-ray analyses.

The anisotrophies in energy and fluence of neutrons produced by D(d,n)He reactions in the focused plasma indicate that the proposed converging ion model agrees better than any other models previously speculated. The results of hard x-ray observation also support the converging ion model.

Demonstration of various applications of a plasma focus including production of a fissioning uranium plasma, nuclear reactions with a Li target, neutrography and production of short-lived isotopes are discussed.

The high-voltage effects on neutron energy have been studied with a 50-kV apparatus.

A new geometry, called a hypocycloidal pinch, has been invented and preliminary studies were made. The results indicate that significant improvements in the performance of the plasma focus can be expected.

INVENTORY OF RESIDUAL EQUIPMENT AND PROPERTY

No residual equipment or property has been acquired with grant funds having acquisition cost of over $1,000 for the entire grant period. The status of one capacitor bank furnished by NASA Langley Research Center under this grant is as follows.

Location: Vanderbilt University
Stevenson Science Center

Number of Capacitors: Total 22
usable - 21 (near the end of their life)
Damaged - 1

Number of switches: 12 (Trigatron type)
all usable
Estimated value - $200

The capacitor bank will be transferred to the new NASA Grant NSG 1235.

Final Report, NASA Grant NGR 43-002-031, February 1969-August 1975.

Vanderbilt University, Ja H. Lee, Principal Investigator

FINAL DISCLOSURE OF INVENTIONS REPORT

The following invention report has been made under this grant.

Invention: Hypocycloidal-Focus Device

Letter of disclosure: June 27, 1970

Formal disclosure and
application for waiver of title: February 8, 1972

Waiver granted : W-1418 March 29, 1973

A patent application on this invention has been made by the principal investigator through Vanderbilt University.

IV. PUBLICATIONS

1. "Angular Variation of Neutron Yield from a Plasma Focus by Neutron-Induced Gamma Spectrometry," L. P. Shomo, K. H. Kim, and J. H. Lee, Bull. Am. Phys. Soc. 15, 814 (1970).
2. "Dependence of Neutron Fluence Anisotropy on the Neutron Yield of a Plasma Focus," L. P. Shomo, J. H. Lee, and K. H. Kim, Bull. Am. Phys. Soc. 15, 1463 (1970).
3. "Neutron Production Mechanism in a Plasma Focus," J.H.Lee, L.P.Shomo, M.D.Williams, and H.Hermansdorfer, Phys. Fluids 14, 2217-2223 (1971).
4. "An Investigation of Hard X-Rays from a Plasma Focus," J.H.Lee, C.E.Roos, and D.S.Loebbaka, Sixth NASA Intercenter and Contractors Conference at Langley Research Center, December 8-10, 1969.
5. "An Investigation of Hard X-rays from a Plasma Focus," J.H.Lee, D.S.Loebbaka, and C.E.Roos, Bull. Am. Phys. 15, 642 (1970).
6. "Hard X-ray Spectrum of a Plasma Focus," J.H.Lee, C.E.Roos, and D.S.Loebbaka, Plasma Physics 13, 347-349 (1971).
7. "Fine Structure of Hard X-Ray Emission from a Plasma-Focus Apparatus," J.H.Lee, W.L.Harries, and D.R.McFarland, Bull. Am. Phys. Soc. 19, 511 (1974).
8. "Space and Time-Resolved Observations of X-Ray Production in Plasma Focus Apparatus," J.H.Lee, W.L.Harries, and D.R.McFarland, IEEE Internat. Conf. on Plasma Science, May 15-17, 1974, Knoxville, TN.
9. "Trajectories of High-Energy Electrons in a Plasma Focus," W.L.Harries, J.H.Lee, and D.R.McFarland, Bull. Am. Phys. Soc. 20, 1370 (1975).
10. "Plasma-Focus-Produced Neutrons for Study of Induced Fission in Uranium," J.H.Lee, D.R.McFarland, and K.H.Kim. Submitted to Am. Phys. Soc. Mtg., Bloomington, Indiana, Nov. 1-3, 1973. Bull. Am. Phys. Soc. 18, 1411 (1973).
11. "Production of a Fissioning Uranium Plasma," J.H.Lee, F.Hohl, K.H.Kim, and D.R.McFarland, submitted to American Nuclear Society Meeting, San Francisco, California, Nov. 11-16, 1973.
12. "Production of a Fissioning Uranium Plasma Near Gas-Core Reactor Conditions," J.H.Lee, D.R.McFarland, F.Hohl, and K.H.Kim, Nuclear Technology 22, 306 (1974).
13. "Absolute Intensity of Radiation Emitted by Uranium Plasmas," N.W.Jalufka, M.D.Williams, J.H.Lee, and D.R.McFarland, Internat. Conf. on Plasma Science, IEEE, Univ. of Tenn., Knoxville, TN 1974.
14. "Absolute Intensity of Radiation Emitted by Uranium Plasmas," N.W.Jalufka, M.D.Williams, J.H.Lee, and D.R.McFarland, NASA TM X-71942, April 1975.

15. "Applications of a Plasma Focus," J.H.Lee, D.R.McFarland, and K.H.Kim, submitted to Am. Phys. Soc. Plasma Division Meeting, Philadelphia, PA, Oct. 21-Nov. 3, 1973. Bull. Am. Phys. Soc. 18, 1364 (1973).

16. "Time of Flight Study of Neutrons and Gamma Rays from a Plasma Focus." Presented at the Annual Mtg. of Div. of Plasma Physics, APS, at Miami Beach, FA, Nov. 13-16, 1968.

17. "Current Sheet Measurements in a Hypocycloidal Focus Device," John P. Barach and Carl R. Henderson, to be published in Phys. of Fluids (1976).

18. "Current Drop in a Plasma Focus," J.H.Lee and J.P.Barach, Bull. Am. Phys. Soc. 20, 1235 (1975).

19. "Effects of High Voltage on Neutron Energies from a Plasma Focus," J.H.Lee and D.R.McFarland, Bull. Am. Phys. Soc. 17, 1023 (1972).

20. "Diagnostic Measurements on a Hypocycloidal Pinch," J.H.Lee and D.R.McFarland, APS Div. of Plasma Physics Mtg., Oct. 28-31, 1974, Albuquerque, NM. Bull. Am. Phys. Soc. 19, 946 (1974).

21. "Absorption of CO_2-Laser Radiation in a Hypocycloidal-Pinch Plasma," J.H.Lee and D.R.McFarland, Paper C19, 3rd Topical Conference on Pulsed High Beta Plasmas, UKAEA Culham Lab., Sept. 9-12, 1975.

22. "Dense Plasma-Focus Production in a Hypocycloidal Pinch," J.H.Lee, D.R.McFarland, and F.Hohl. NASA TN D-8116, NTIS, Springfield, VA 22161 (1975).

23. "Investigation of X-ray Emission from a Plasma Focus," N.W.Jalufka, and J.H.Lee, Bull. Am. Phys. Soc. 15, 815 (1970).

24. "Investigation of Current Sheet Collapse in a Plasma Focus Apparatus," N.W.Jalufka and J.H.Lee, Bull. Am. Phys. Soc. 15, 1462 (1970).

25. "Bremsstrahlung Emission During Current-Sheet Collapse in a DPF," J.H.Lee and N.W. Jalufka, Bull. Am. Phys. Soc. 16, 1284 (1971).

26. "Current Sheet Collapse in a Plasma Focus," N.W.Jalufka and J.H.Lee, Phys. Fluids 15, 1954 (1972).

27. "Anisotrophy of the Neutron Fluence from a Plasma Focus," J.H.Lee, L.P.Shomo, and K.H.Kim, Phys. Fluids 15, 2433 (1972).

28. "Near Ultra-Violet and Visible Emission of a Plasma Focus," N.W.Jalufka, J.H.Lee, and D.R.McFarland, Bull. Am. Phys. Soc. 17, 1023 (1972).

29. "Hypocycloidal Focus," J.H.Lee and D.R.McFarland, Bull. Am. Phys. Soc. 18, 1369 (1973).

30. "Electron Dynamics in a Plasma Focus Based on X-Ray Measurements," W.L.Harries, J.H.Lee, and D.R. McFarland, APS Division of Plasma Physics, Oct. 28-31, 1974, Albuquerque, NM.

31. "Electron Dynamics in a Plasma Focus," D.R.McFarland, W.L.Harries, and J.H.Lee, to be published in NASA Technical Memorandum, 1976.

32. "Production of Dense Plasmas in a Hypocycloidal-Pinch Apparatus," J.H.Lee, D.R.McFarland, and F.Hohl. Submitted for publication in Physics of Fluids, 1976.

V. REFERENCES

1. N.V.Fillipov, T.I.Fillipova, V.P.inogradov, Dense, High-Temperature Plasma in a Noncylindrical z-Pinch Compression. Nuclear Fusion, Pt. 2, Supp. p. 577 (1962).

2. J.W.Mather, Investigation of the High Energy Acceleration Mode in the Coaxial Gun. Phys. Fluids Supplement, S 28, 1964.

3. P.J.Bottoms, J.P.Carpenter, J.W.Mather, K.D.Ware, and A.H.Williams, in Plasma Physics and Controlled Nuclear Fusion Research (International Atomic Energy, Vienna, 1969), Vol. II, p. 67.

4. N.V.Filippov and T.I.Filippova, in Plasma Physics and Controlled Nuclear Fusion Research (International Atomic Energy Agency, Vienna, 1966), Vol. II, p. 405.

5. C. Patou, A. Simonnet, and J.P.Watteau, Phys. Letters 29 A, 1 (1969).

6. M.J.Bernstein, Phys. Rev. Letters 24, 724 (1970).

7. M.J.Bernstein and F.Hai, Phys. Letters 31 A, 317 (1970).

8. J.H.Lee, H.Conrads, M.D.Williams, L.P.Shomo, H.Hermansdorfer, and K.H.Kim, Bull. Am. Phys. Soc. 13, 1543 (1968).

9. H.C.Evans and E.H.Bellamy, Proc. Phys. Soc. (London) 74, 483 (1959).

10. G.Lehner and F.Pohl, Physik 207, 83 (1967).

11. W.H.Bostick, L. Grunberger, and W.Prior, in Proceedings of the Third European Conference on Controlled Fusion and Plasma Physics (Wolters-Noordhoff, Broningen, The Netherlands, 1969), p. 120.

12. W.H.Barkas, Nuclear Research Emulsions. Academic Press, New York, 1963.

13. W.D.Brown, X-Ray Attenuation and Absorption Coefficients. X67-13708, Boeing Co., Seattle, Wash., 1966.

14. H.Friedman, Physics of Solar Flares. NASA SP-50, p. 147, 1963.

15. R.A.Walters and R.T.Schneider, Trans. Am. Nucl. Soc., 15, 634 (1972).

16. D.E.Wood, Technical Note 115, Kaman Nuclear.

17. J.M.Dawson, A.Hertzberg, R.E.Kidder, G.C.Flasses, H.G.Ahlstrom, and L.C.Steinhauer, CN-28/D-13 in Fourth Conf. on Plasma Phys. and Controlled Nuclear Fusion Research, IAEA, Madison, WI, 17-23 June 1971.

18. F.J.Mayer, Bull. Am. Phys. Soc. 15, 1462 (1970), and private communication.

19. K.D.Ware, and J.W.Mather, LA-5178-MD, Los Alamos Scientific Laboratory, Los Alamos, NM, 1973.

20. W.L.Kuruer, and J.W.Dawson, Phys. of Fluids 15, 446 (1972).

21. C.E.Newman and Vahé Petrosian, Phys. Fluids 18, 547 (1975).

VI. LIST OF FIGURES

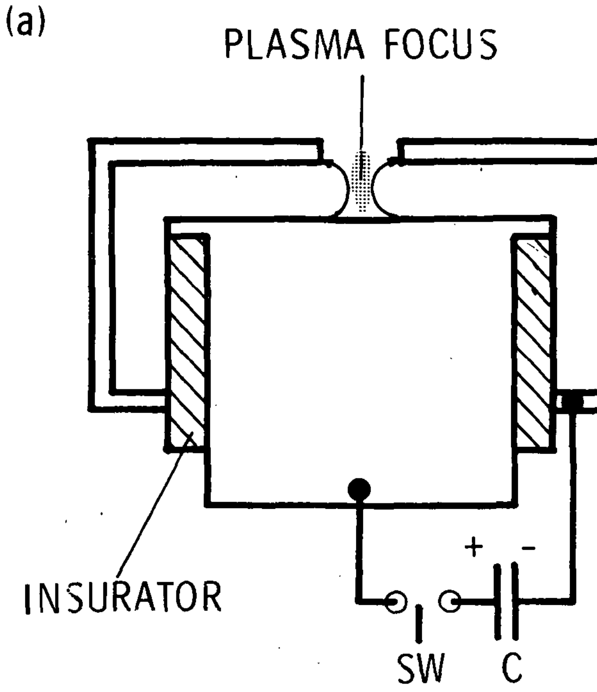

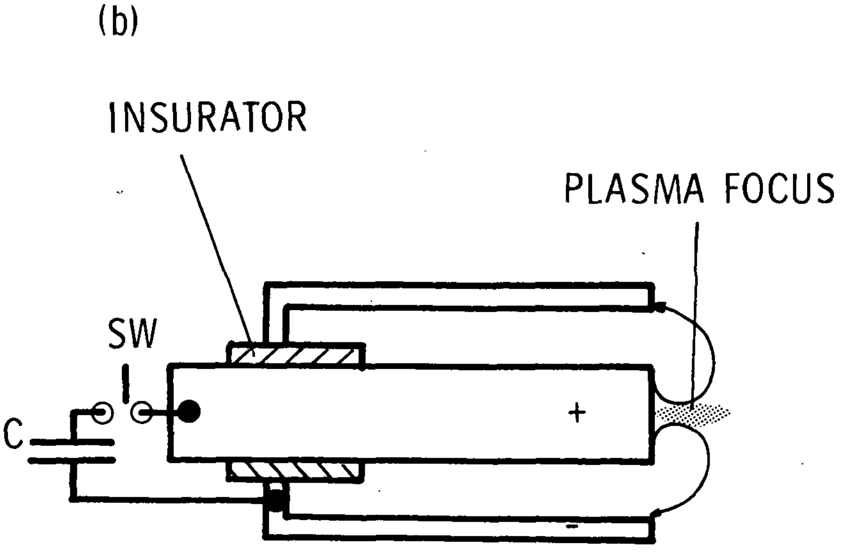

Figure 1.- Two geometries of plasma focus apparatus. (a) Fillipov type and (b) Mather type.

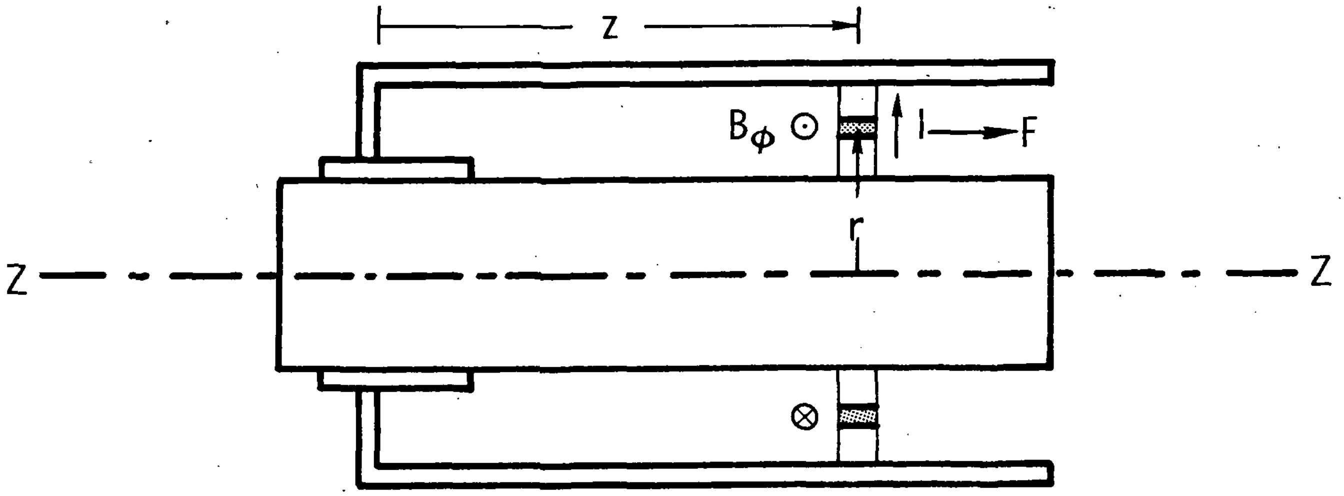

Figure 2.- Snow-plow model of current sheet motion. I total current, B_ϕ azimuthal magnetic induction due to the current, and r,z cylindrical coordinates.

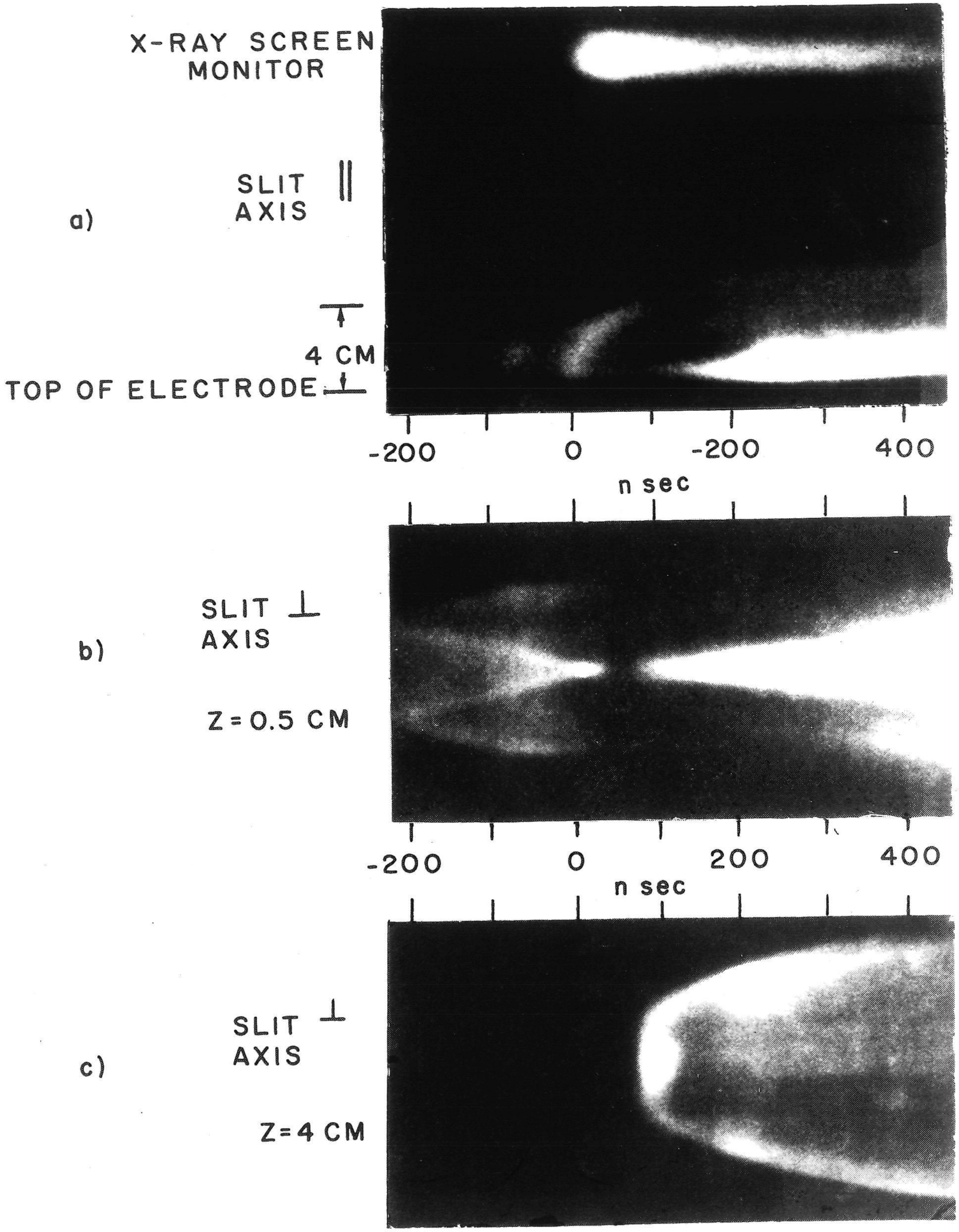

Figure 3.- Compression of the current sheet observed in streak mode of an image converter camera. (a) The observing slit is parallel to the axis of the apparatus, (b) the slit is perpendicular to the axis and a height of 0.5 cm above the top of the electrodes, and (c) as for (b) but at 4 cm above. X-ray emission is monitored with an intensifying screen and light pipe which illuminates the photocathode of the image converter camera.

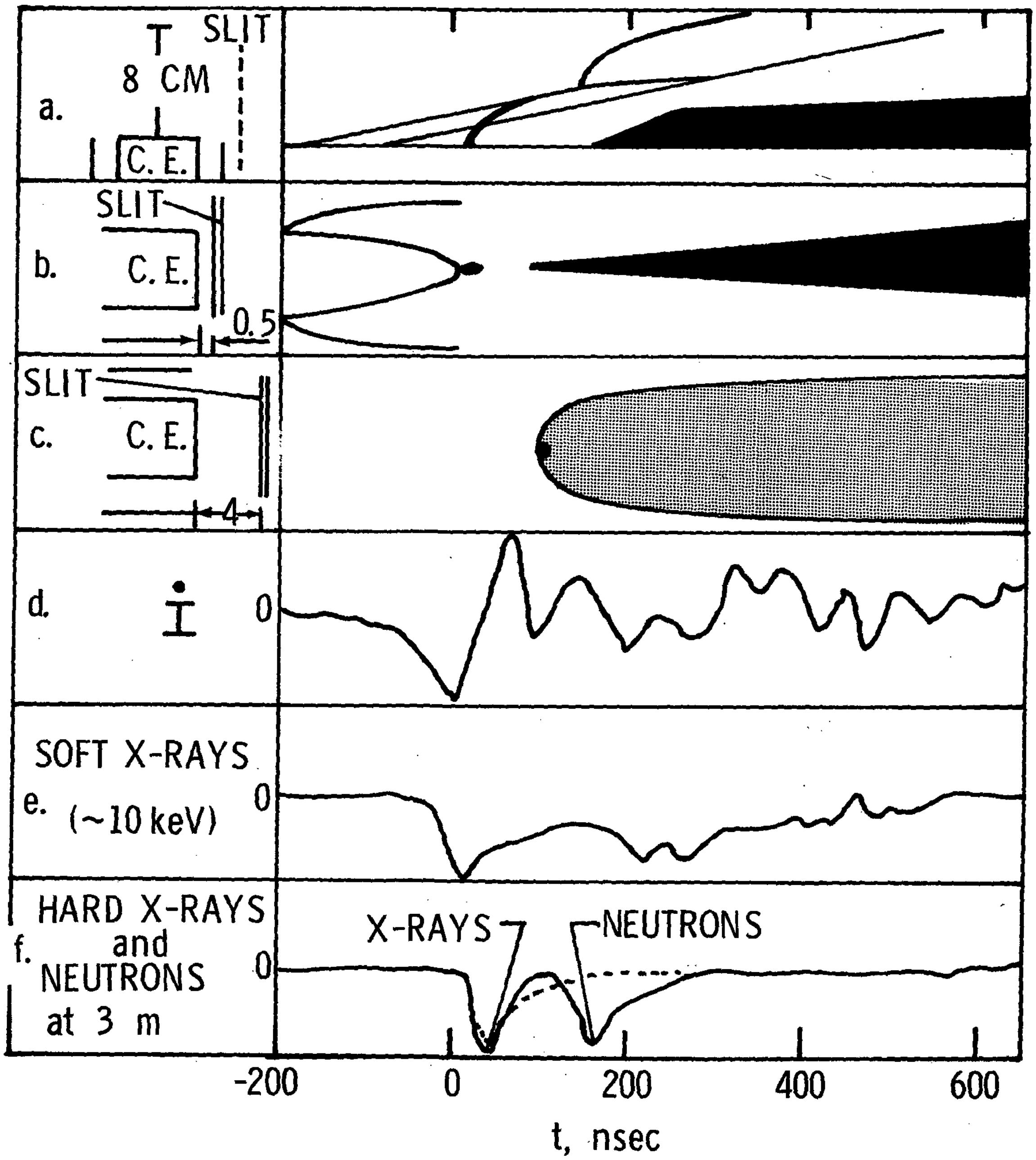

Figure 4.- Temporal evolution of various parameters. (a), (b), and (c) sketch of Fig. 3, (d) the variation of İ, (e) soft x-ray emission monitored by thin scintillation-photomultiplier system, and (f) hard x rays and neutrons monitored by 3" thick scintillator at 3 m from the plasma focus. The dotted line is time-of-flight correction to show the onset time of neutron signal.

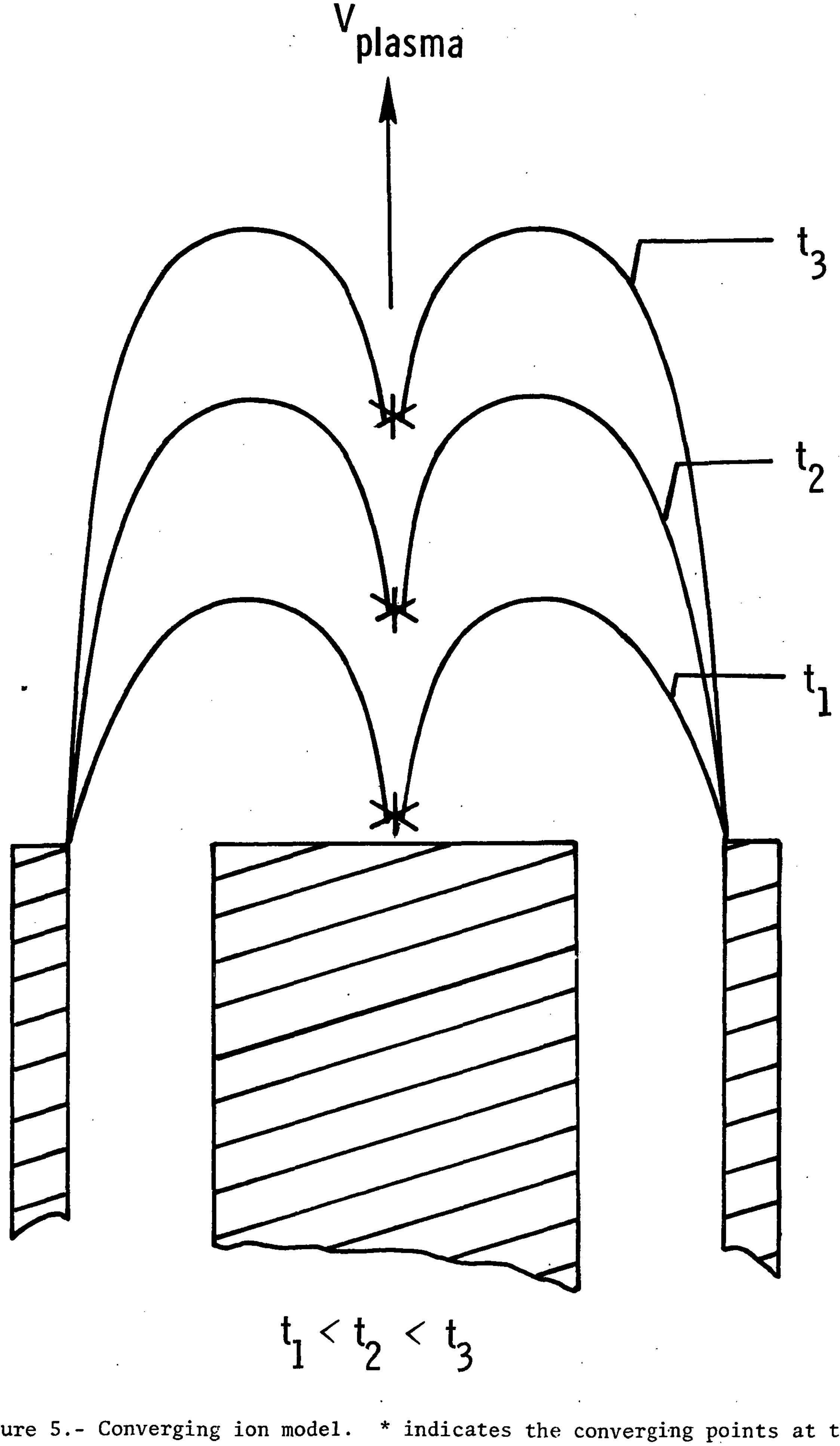

Figure 5.- Converging ion model. * indicates the converging points at three different times.

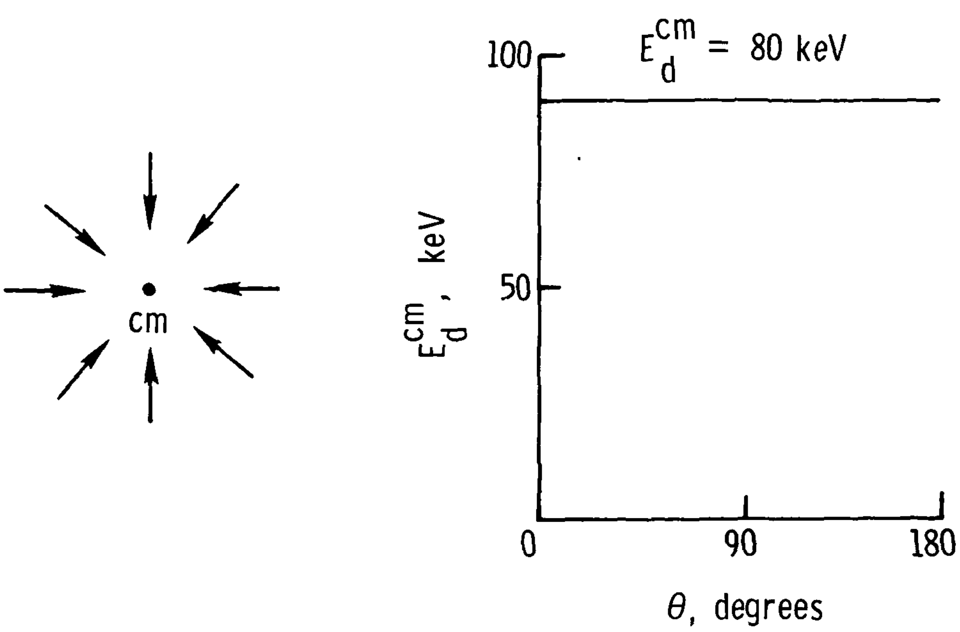

(a) Center of mass system

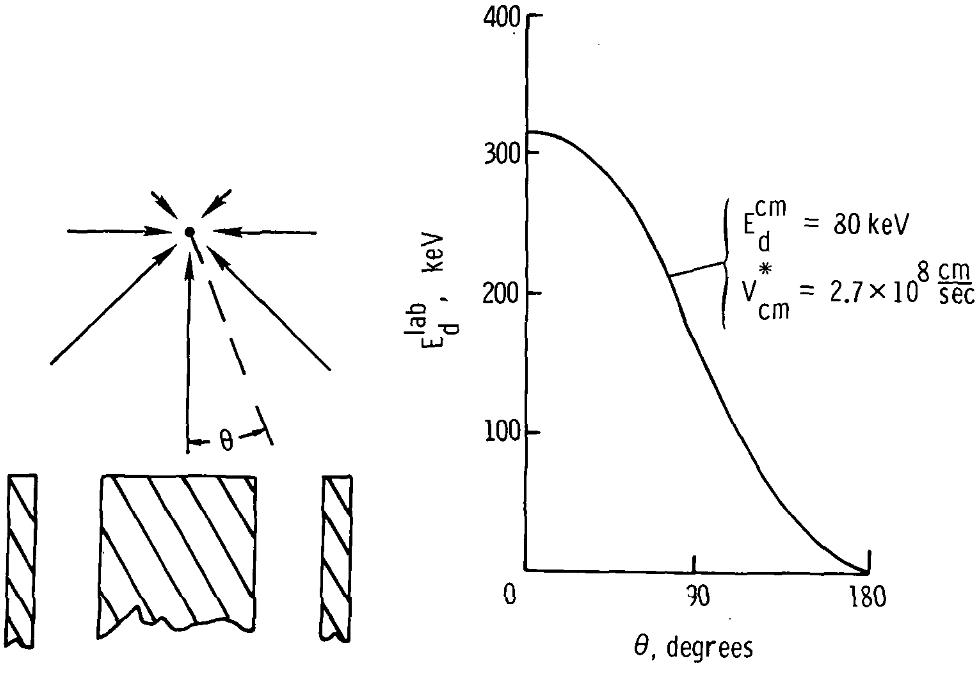

(b) Laboratory reference system

Figure 6.- Velocity and energy distribution of converging ions (a) in the center of mass system and (b) in the laboratory system.

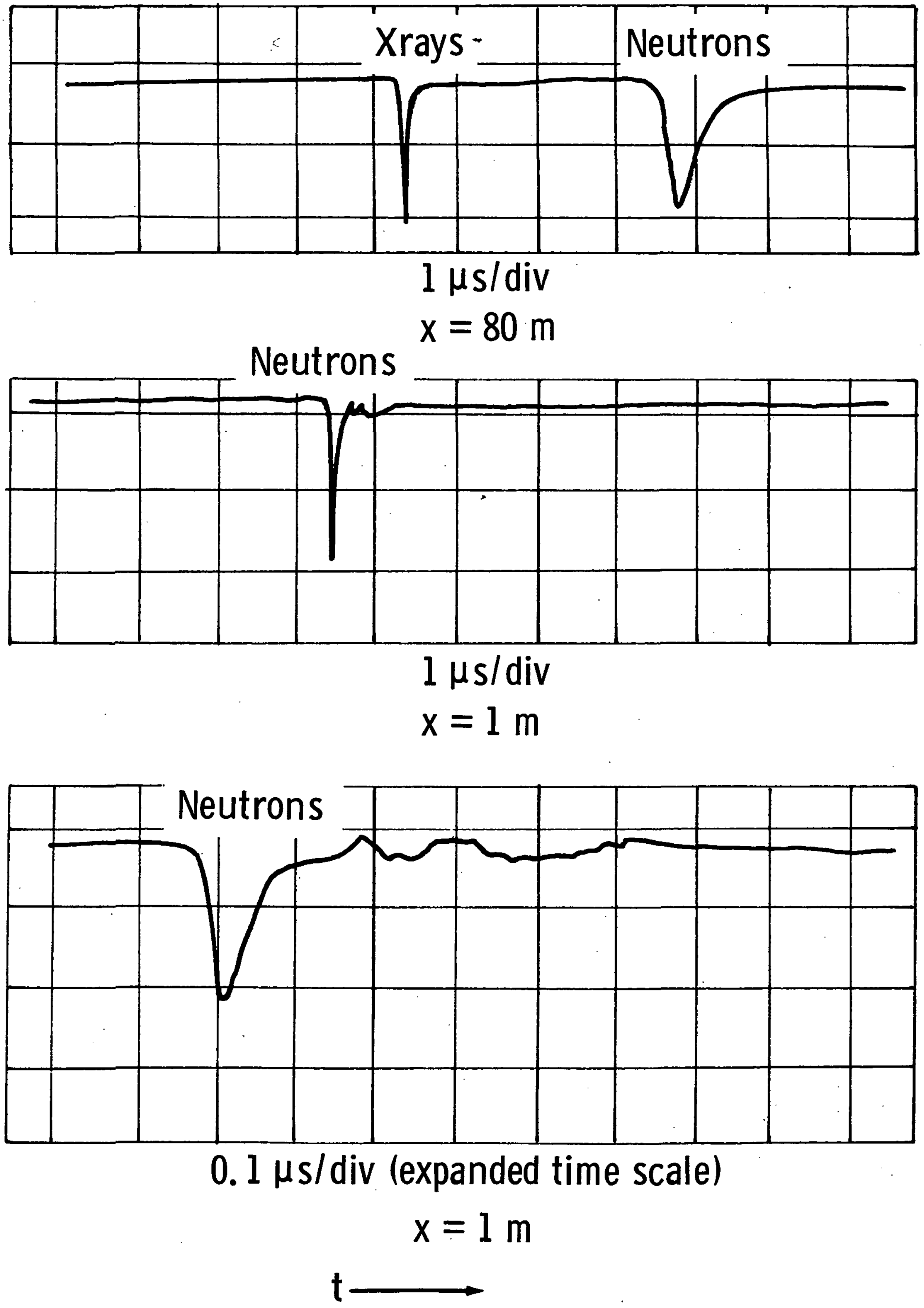

Figure 7.- Hard x-ray and neutron signals from 3" thick scintillation detector at 80 m and 1 m from the plasma focus. The detector had a 3-mm thick lead absorber.

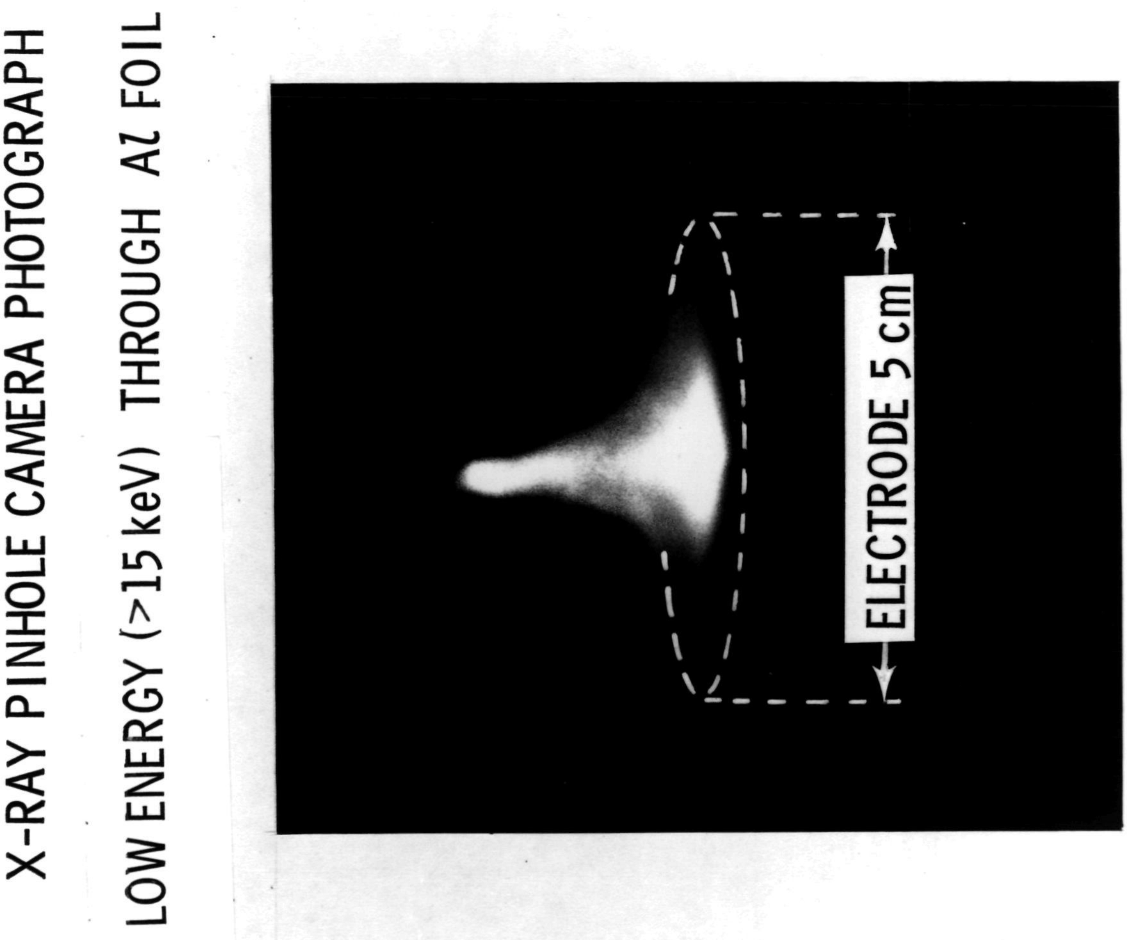

Figure 8.- X-ray pinhole camera photograph. Aluminum absorber is used to observe the x-ray source with photon energy > 15 keV.

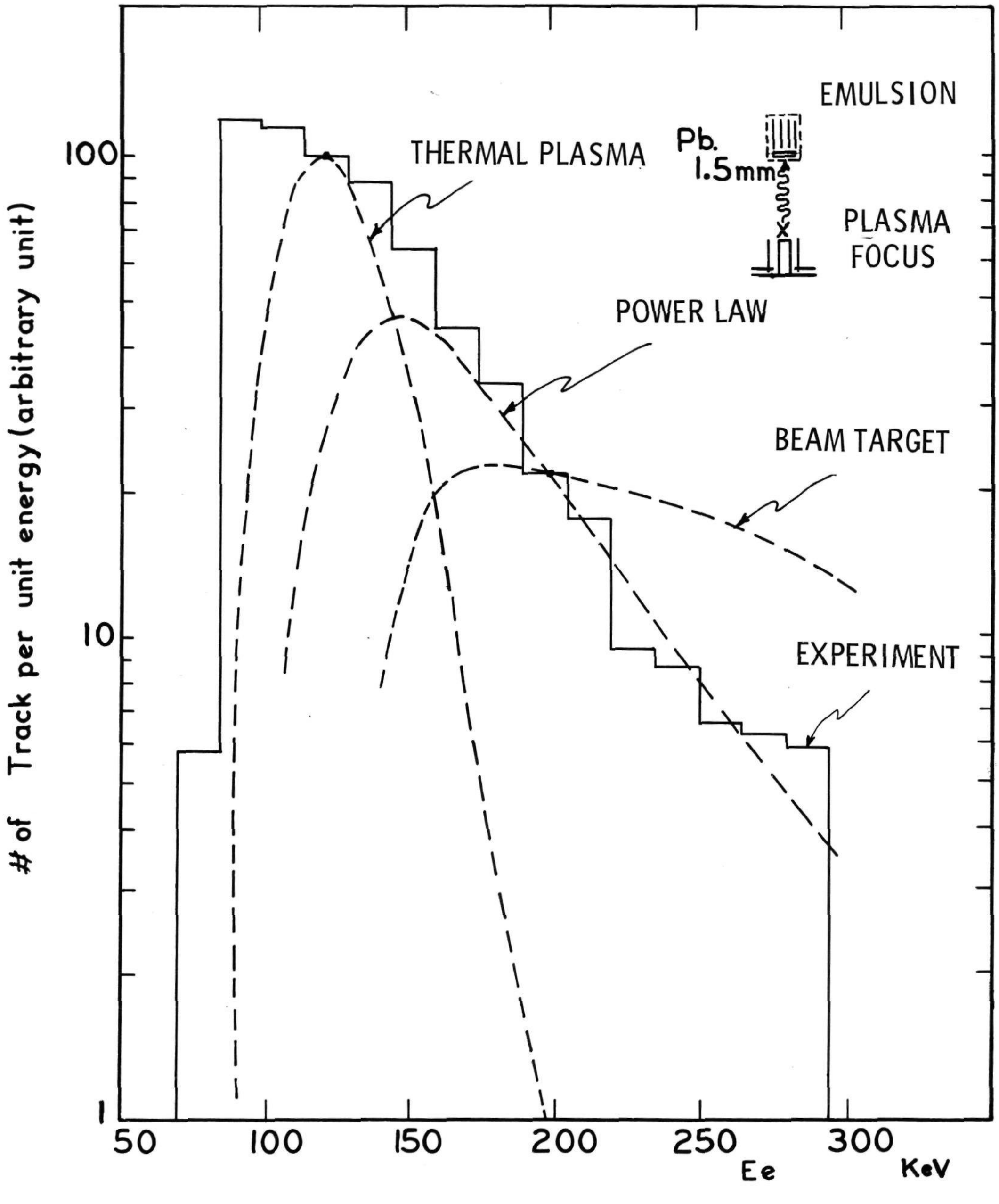

Figure 9.- Electron track distribution in emulsion exposed to hard x-rays from the plasma focus. The electron ranges are converted to energy using the relation given by Barkas.

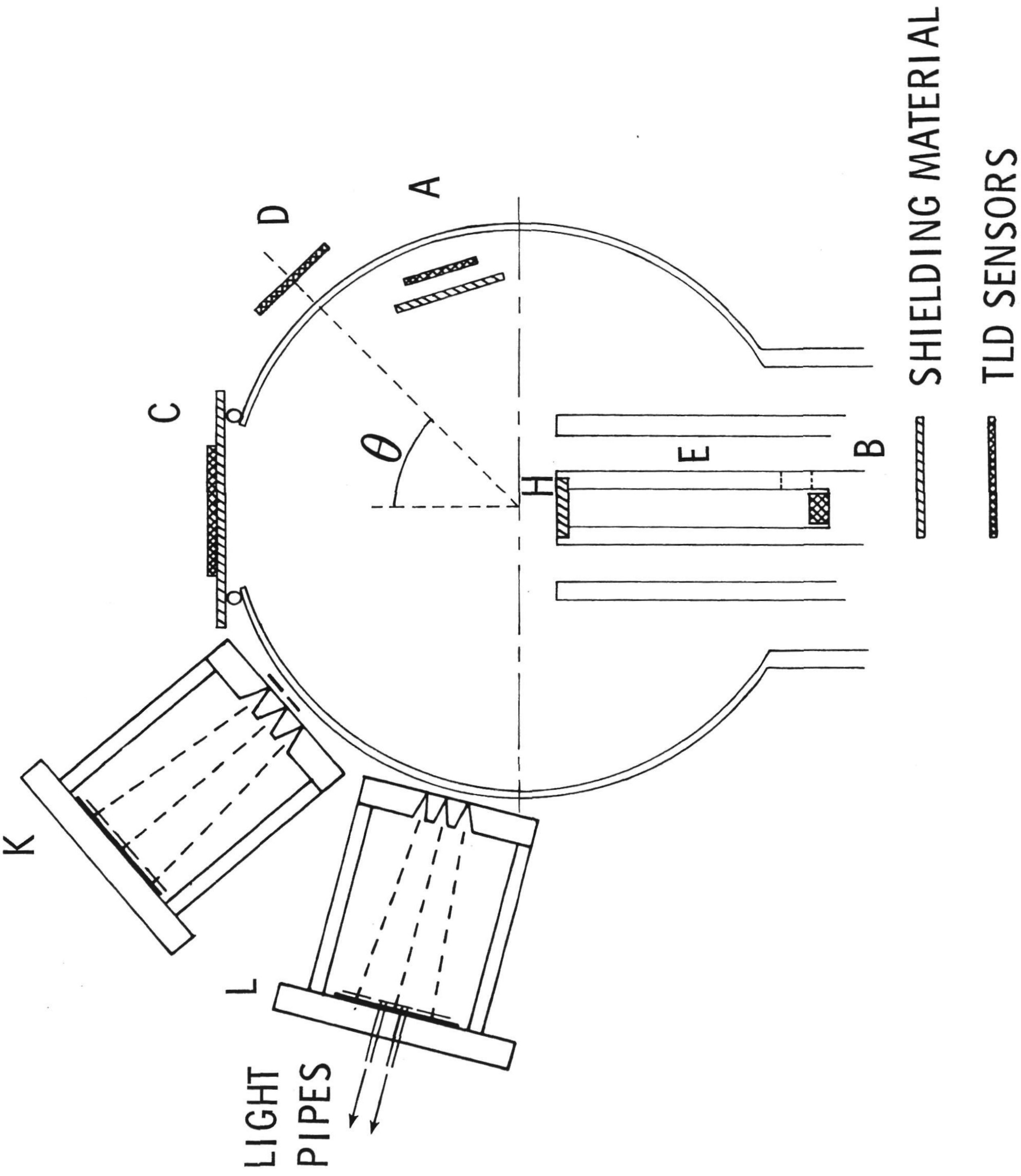

Figure 10.- Pinhole camera -- TLD array system to measure spatial distribution of hard x-ray sources in the plasma focus. The second pinhole camera is equipped with light pipes to observe temporal variation of x-ray intensity at two different points of the image plane. Note that the pinhole camera has triple pinholes.

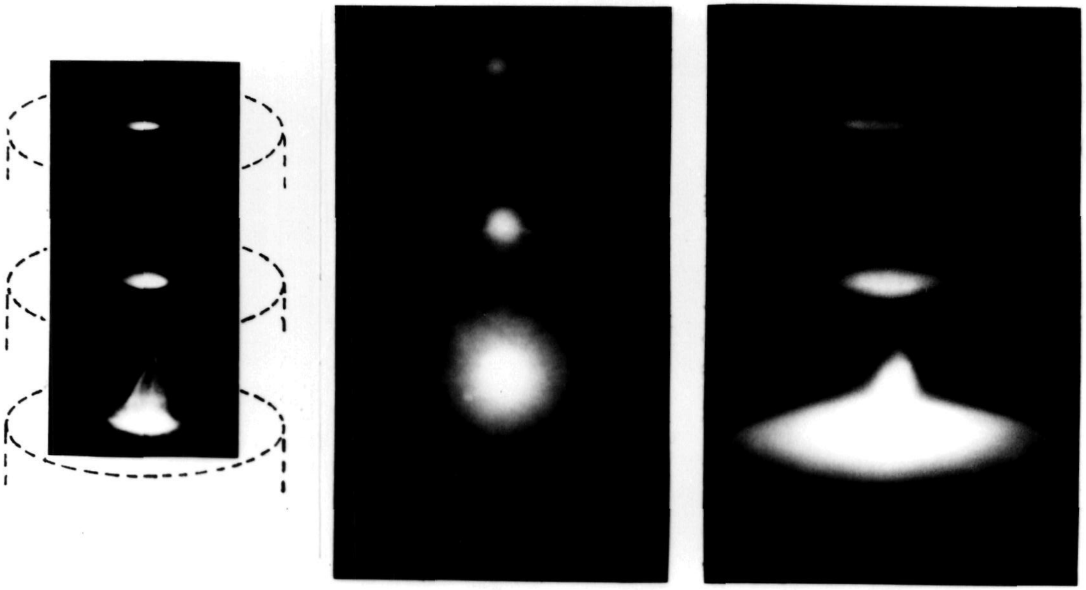

(a) (b) (c)

			41					
			45					
		18	118					
			9					

			5					
			366	167				
	103	306	1130	1210	249	34		
359	815	1800	4050	4110	2000	903	351	96
114	231	460	1070	1220	574	346	200	111
			2	8	4	2		

(d)

Figure 11.- Pinhole photographs (a), (b), (c), and TLD readings (d) of the x-ray source in the plasma focus.

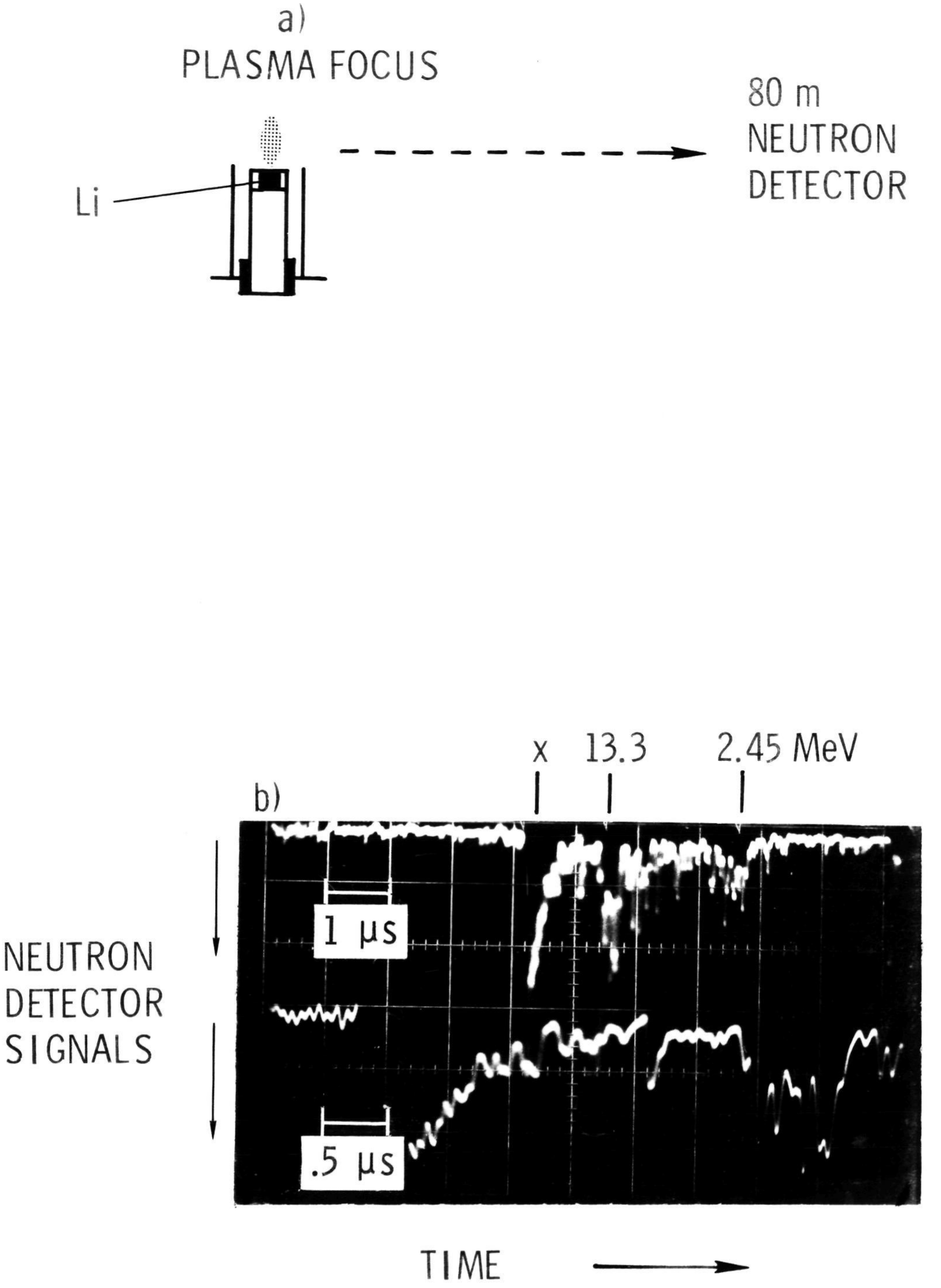

Figure 12.- Time-of-flight neutron spectra at 80 m when a Li target is placed on top of the center electrode. In addition to the 2.45 MeV neutrons by D(d,n)He, the 13.3 MeV neutrons by Le(d,n)Be are observed. The lower trace is on expanded time scale to show the details of the neutron signal.

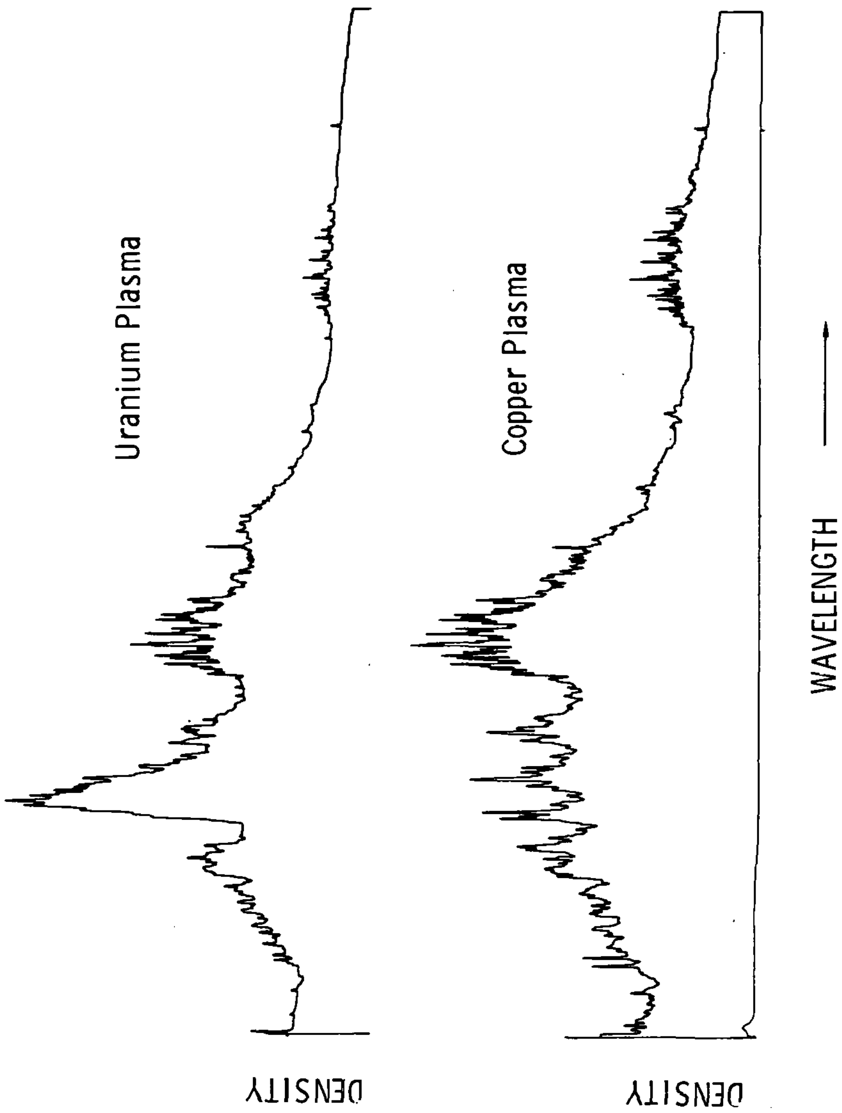

Figure 13.- UV spectra of a uranium plasma and a copper plasma for $30 < \lambda < 300 Å$. The pronounced peak near 90 Å is characteristic of the uranium plasma.

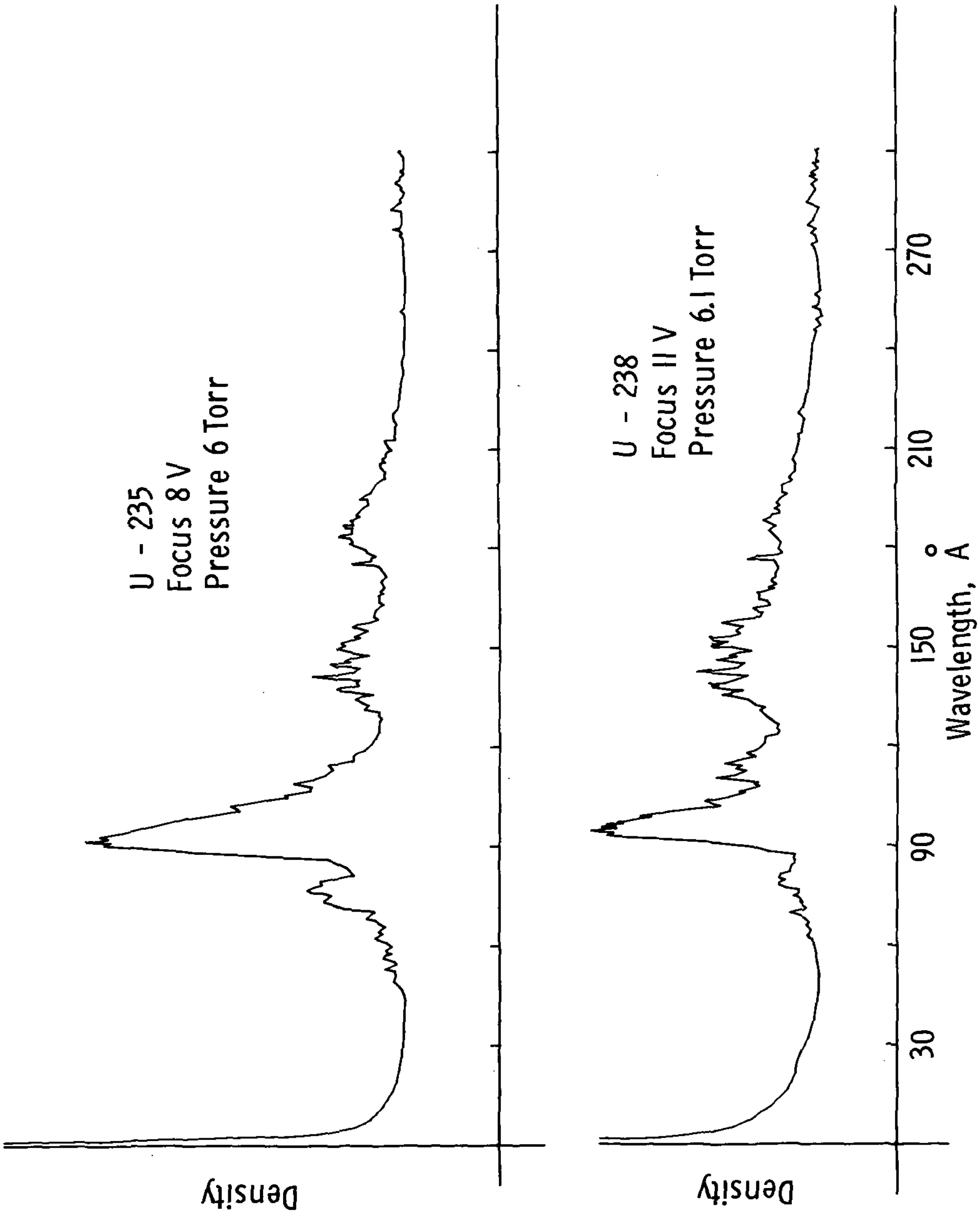

Figure 14.- UV spectra of U-235 and U-238 plasmas. Except minor differences in detail, no difference can be found in the spectra.

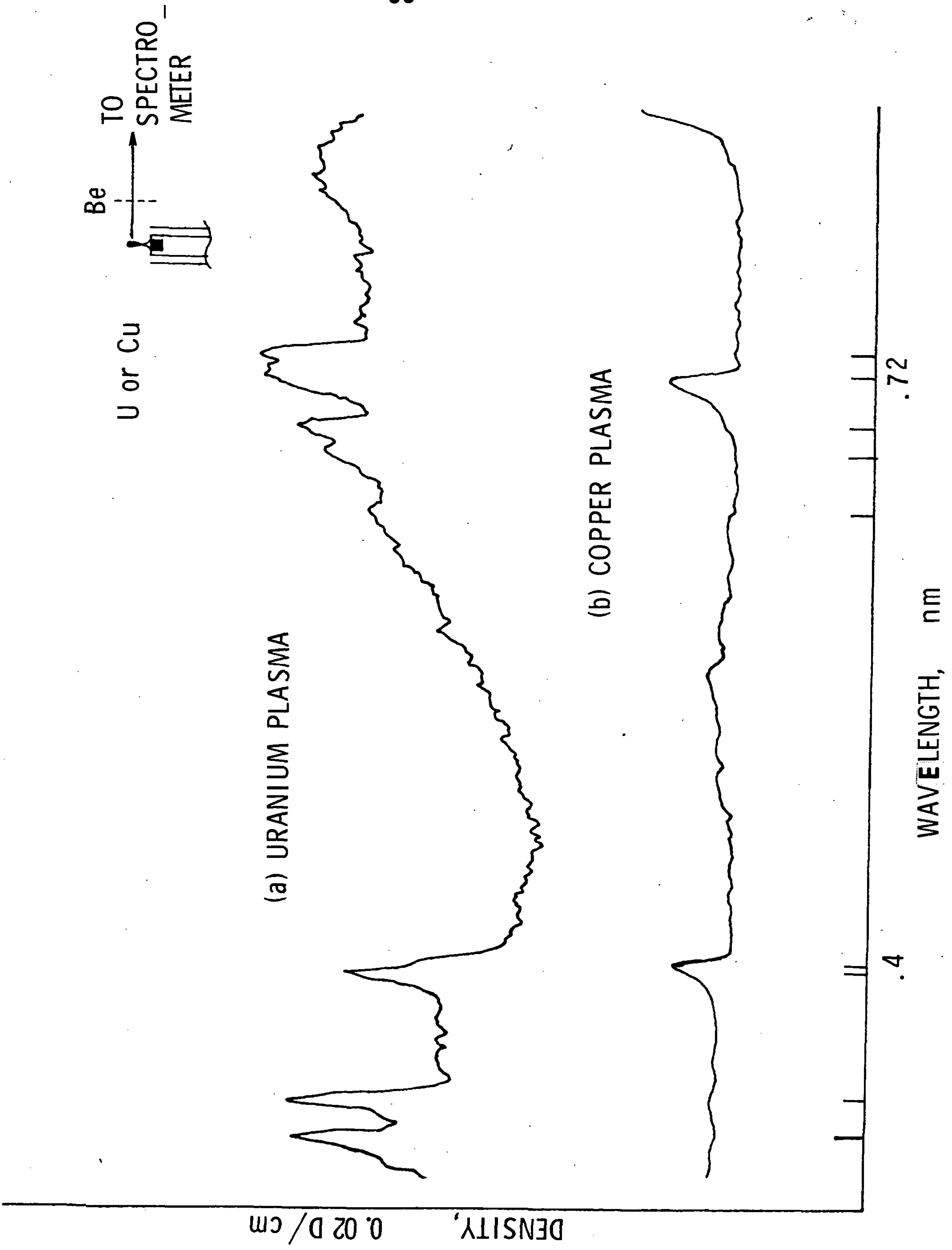

Figure 15.- Soft x-ray spectra of a uranium plasma (a) and a copper plasma (b) strong line emission below 4 Å and strong intensity of white spectrum clearly distinguish the uranium spectrum from the copper spectrum.

STATUS OF NUCLEAR FUSION RESEARCH

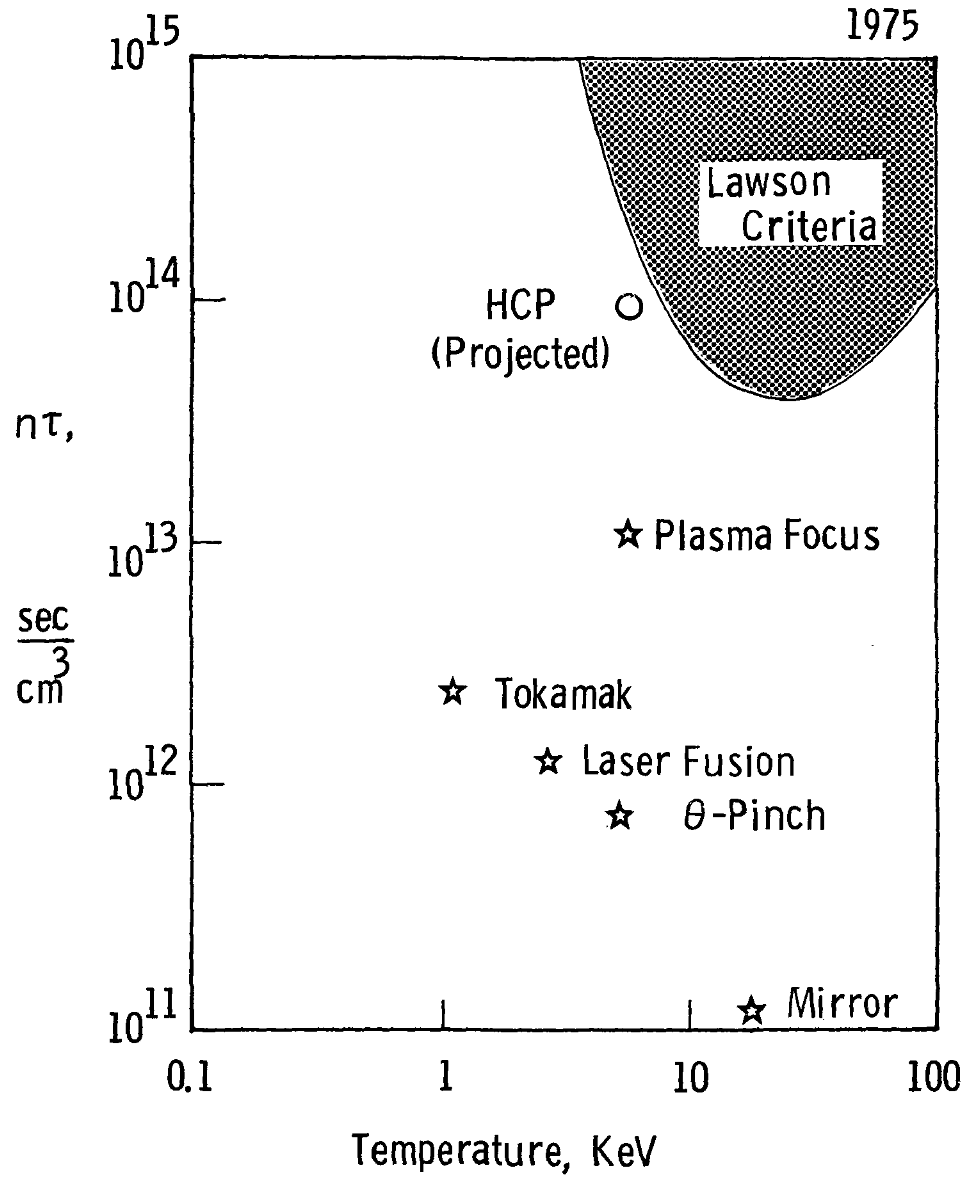

Figure 16.- Status of nuclear fusion research. The plasma focus apparatus is most successful in approaching Lawson's criterion.

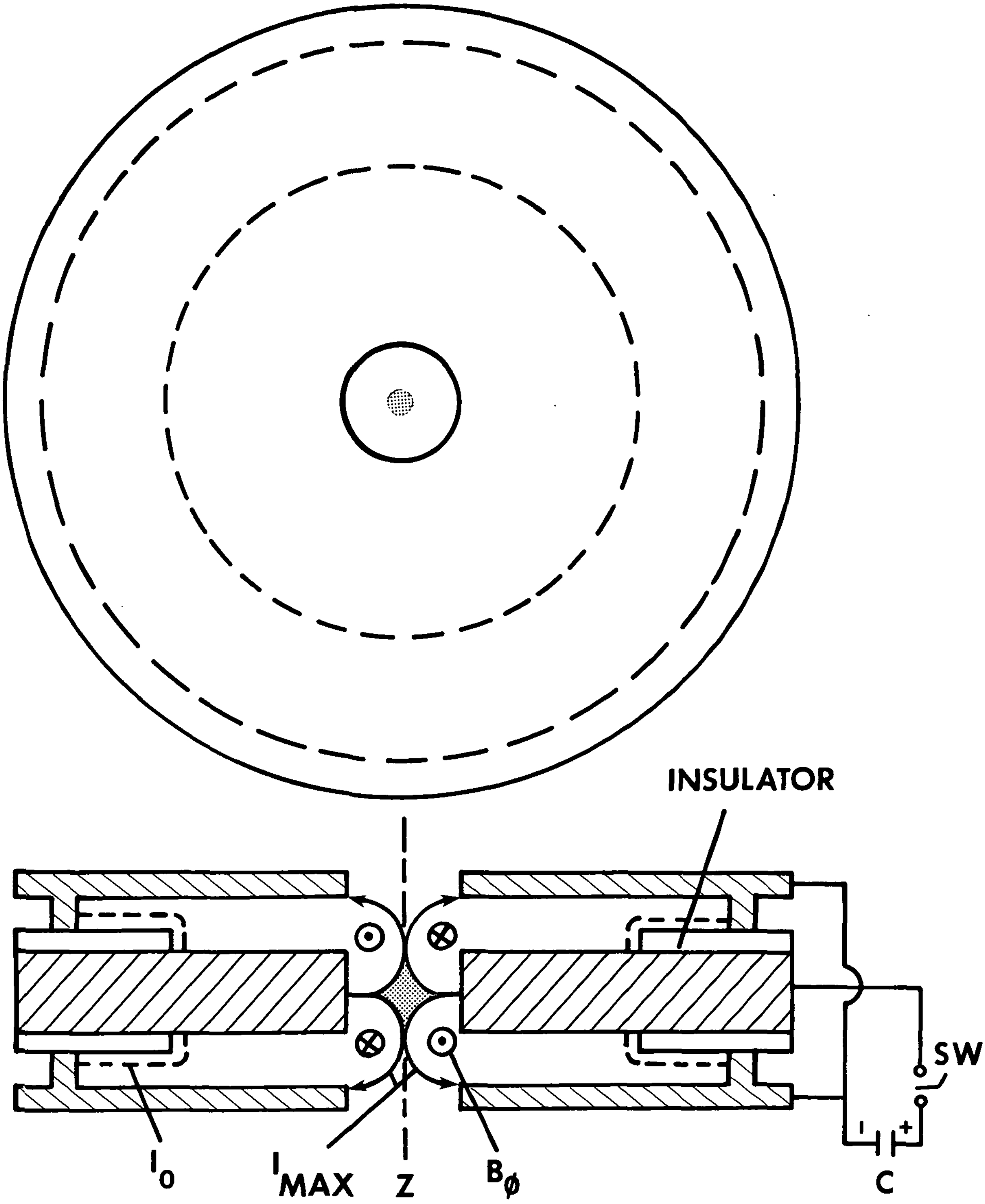

Figure 17.- The plan view and a cross section through a hypocycloidal-pinch apparatus.

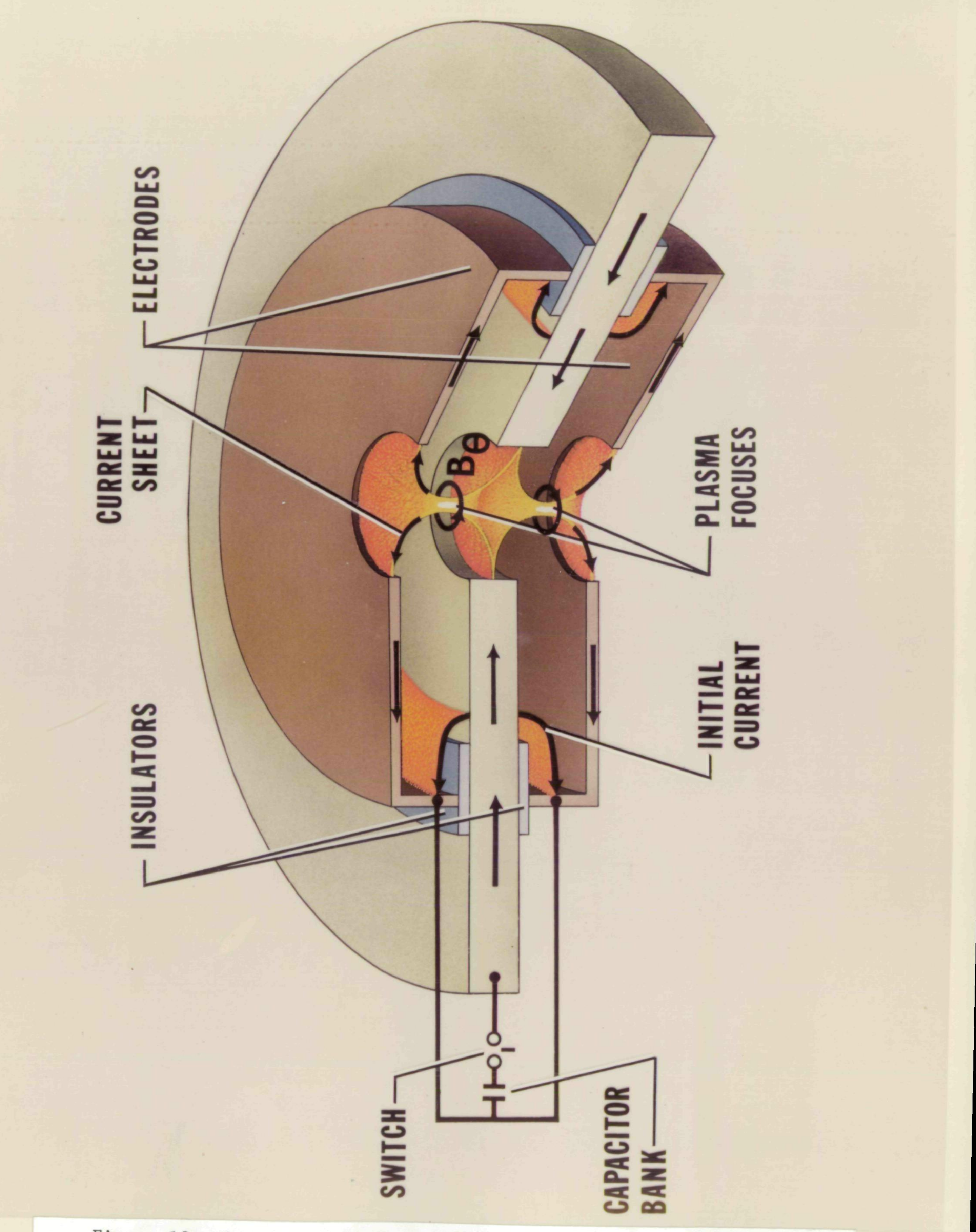

Figure 18.- A cut-out view of the hypocycloidal-pinch apparatus.

NASA
L-73-5867

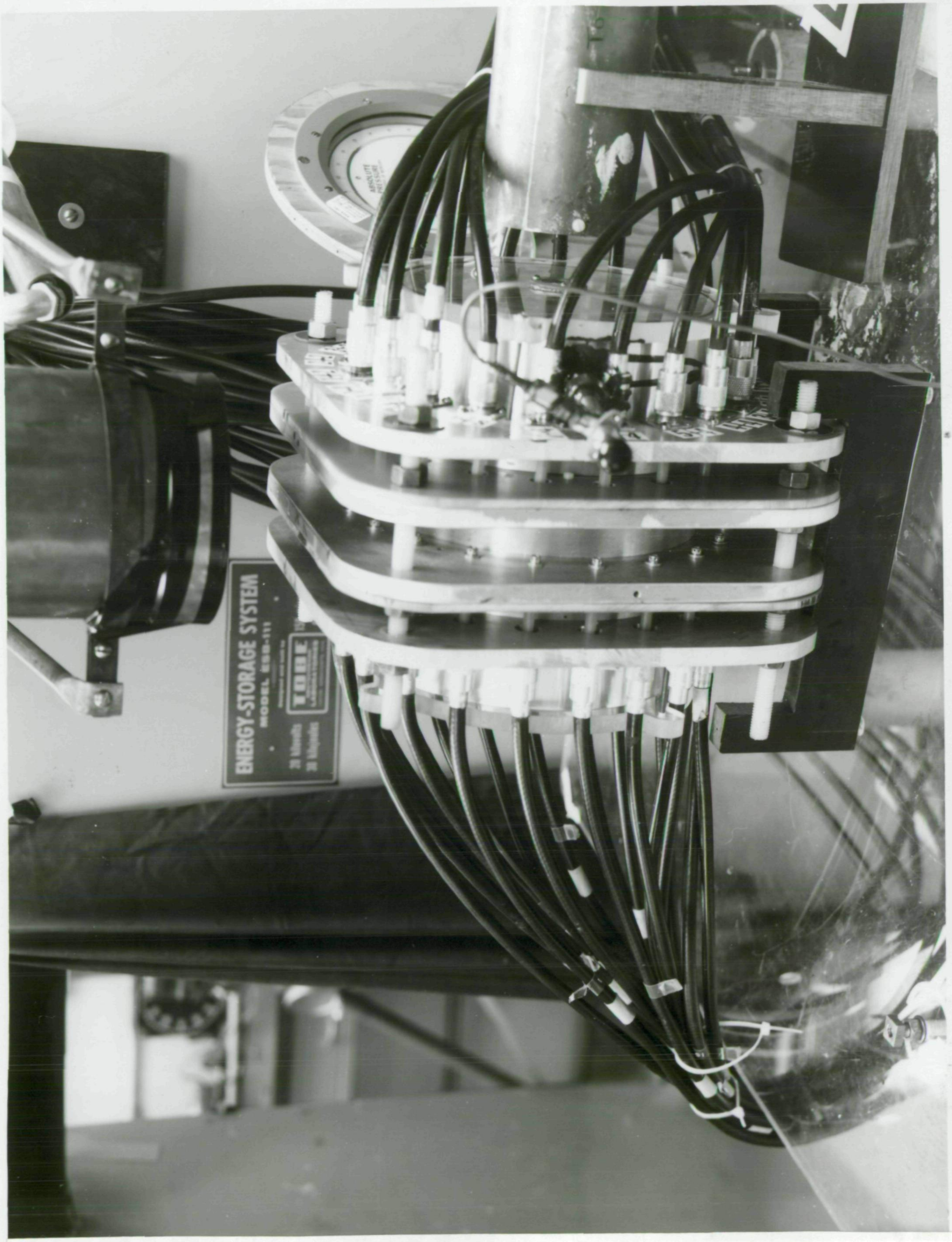

Figure 19.- Prototype HCPI installed in NASA Langley Research Center.

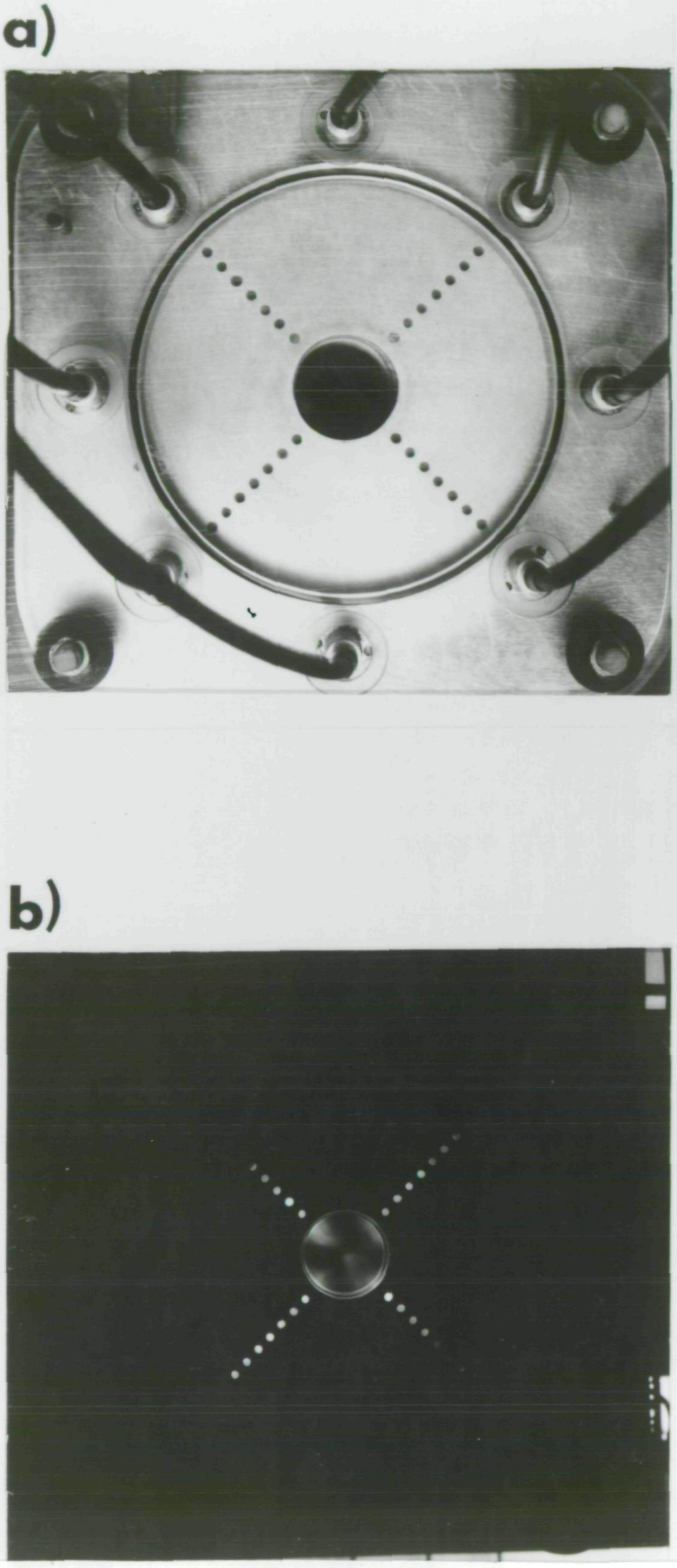

Figure 20.- Effect of perforation. (a) still reference photograph showing the lines of holes, (b) time integrated photograph during the apparatus is energized. The current fronts advance along the line of holes.

a)

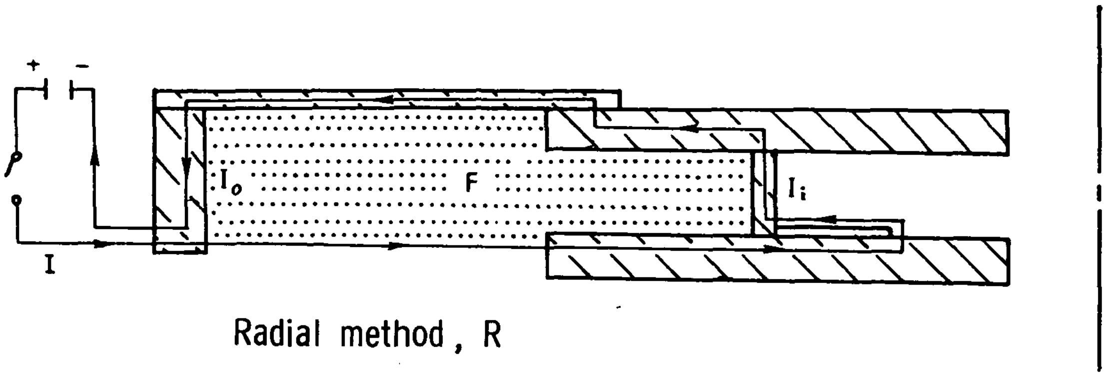

Radial method, R

b)

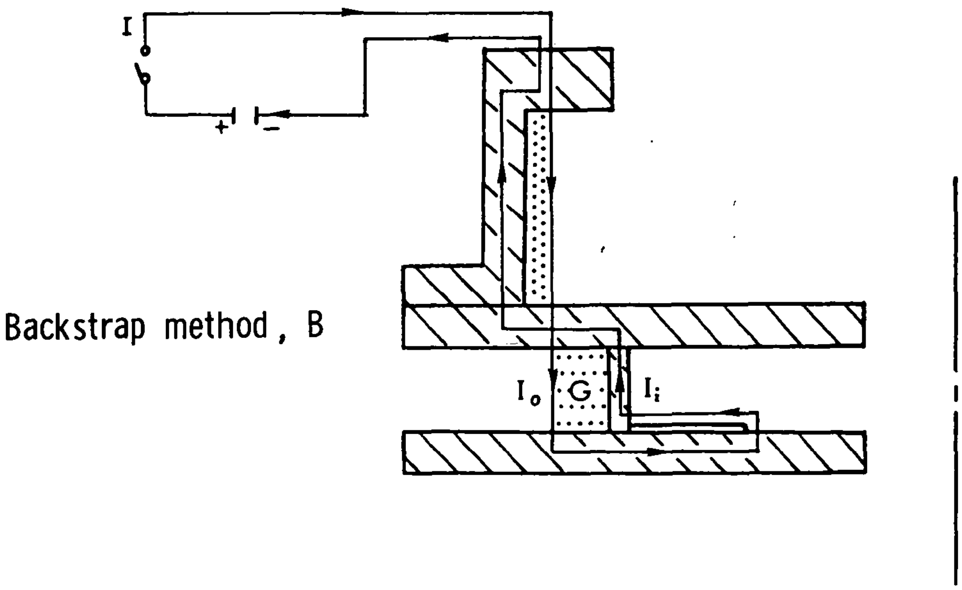

Backstrap method, B

Figure 21.- Two methods of cable connection; (a) radial method, (b) backstrap method.

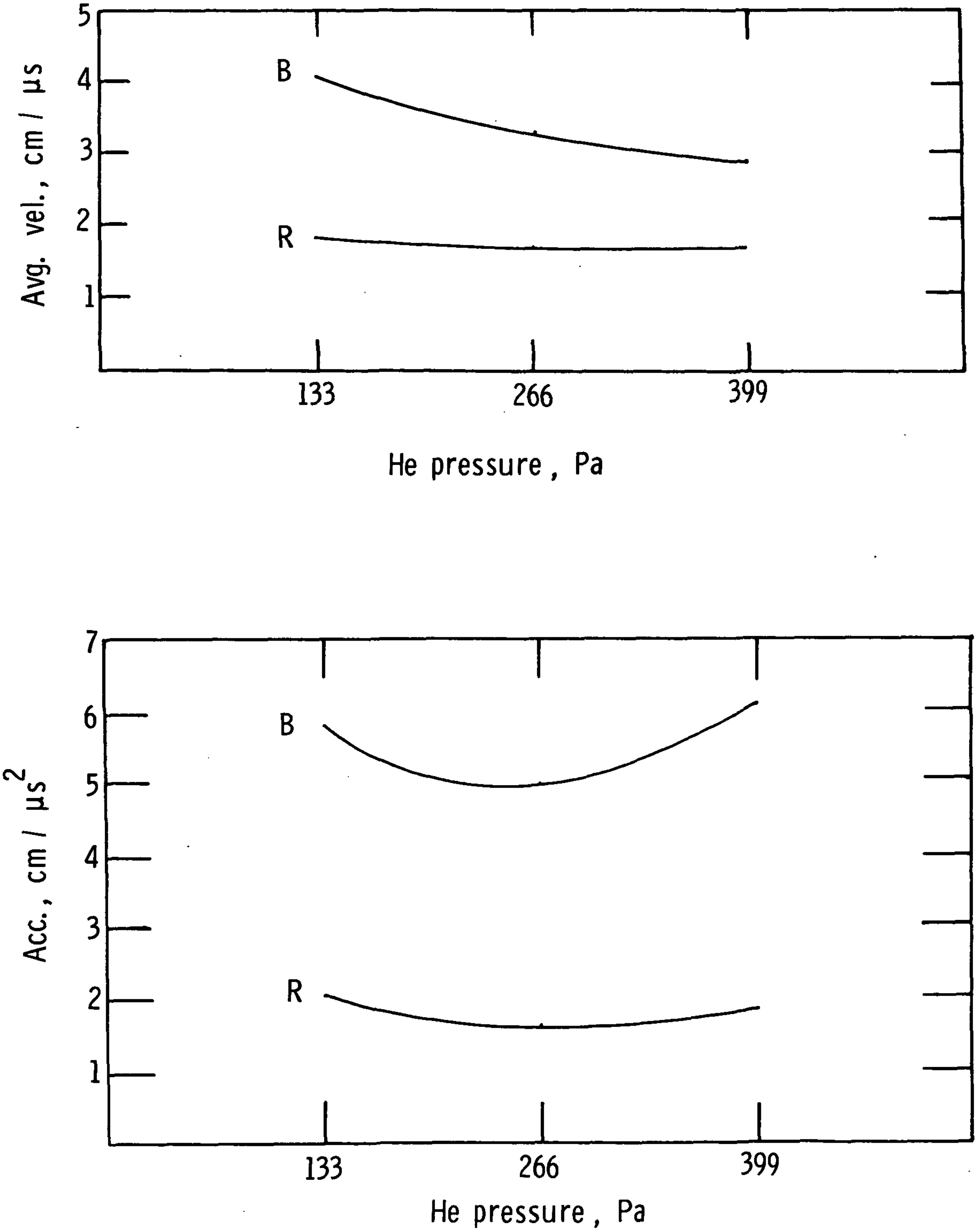

velocity changes between 41 mm and 31 mm from axis

Figure 22.- The average velocity and acceleration of the current sheet in the hypocycloidal apparatus. B- Backstrap method and R- Radial method.

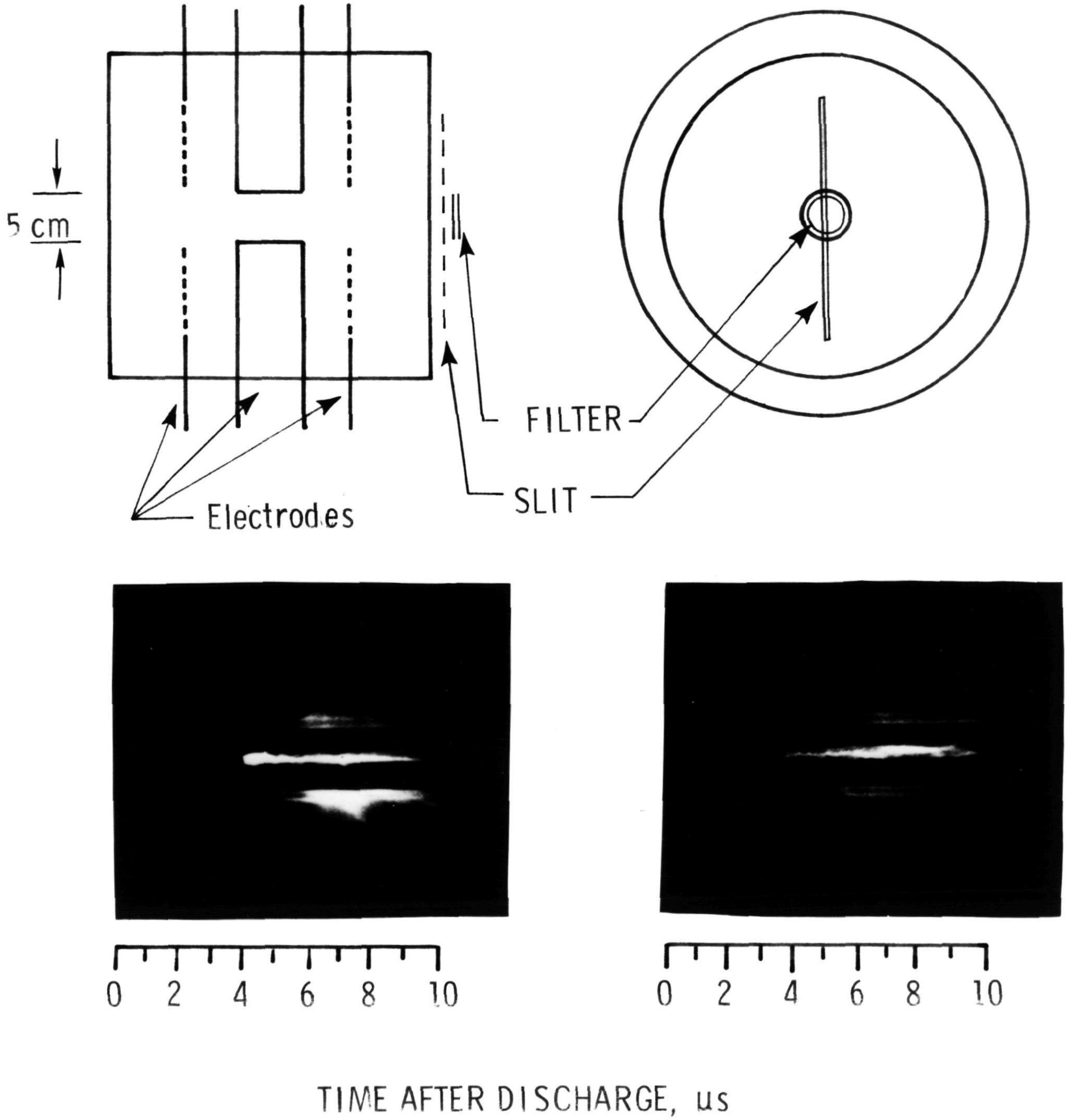

Figure 23.- Streak pictures taken through a slit placed across a diameter of the center hole. The pictures reveal production of a luminous plasma on the axis which has radial stability for ∿5 μs.

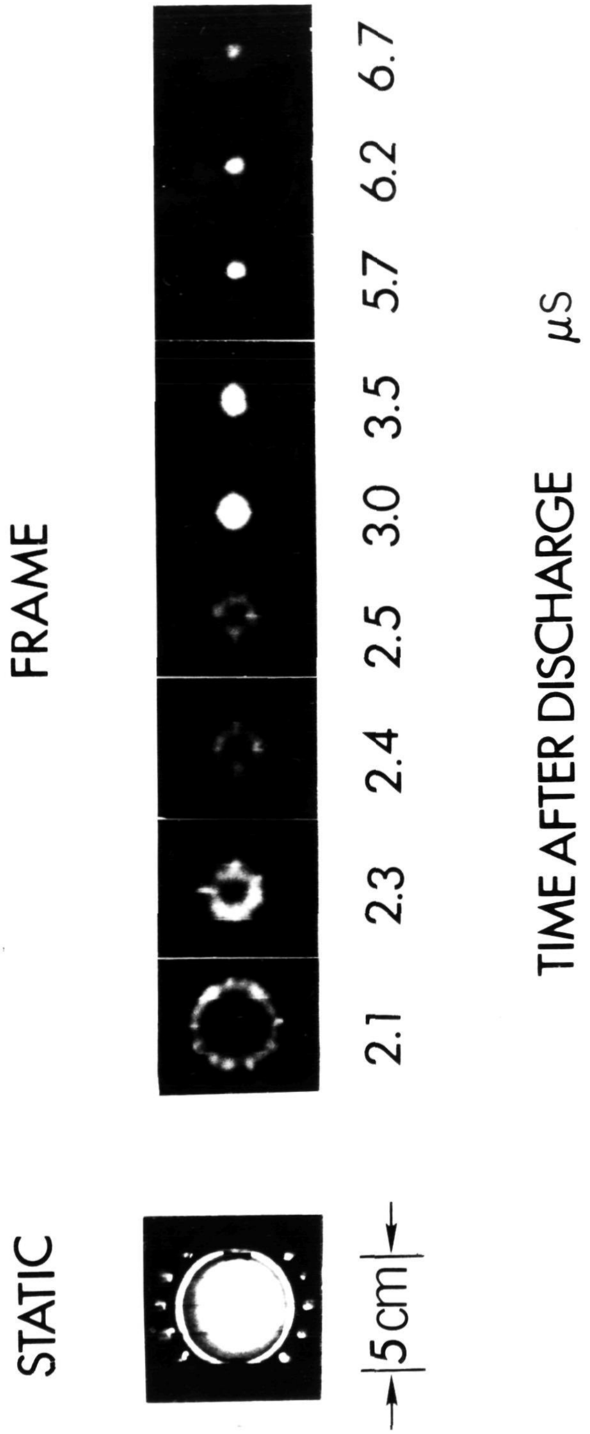

Figure 24.- Frame pictures of focused plasma in HCPI. A still reference picture is also shown. The progress of symmetrical compression is well illustrated.

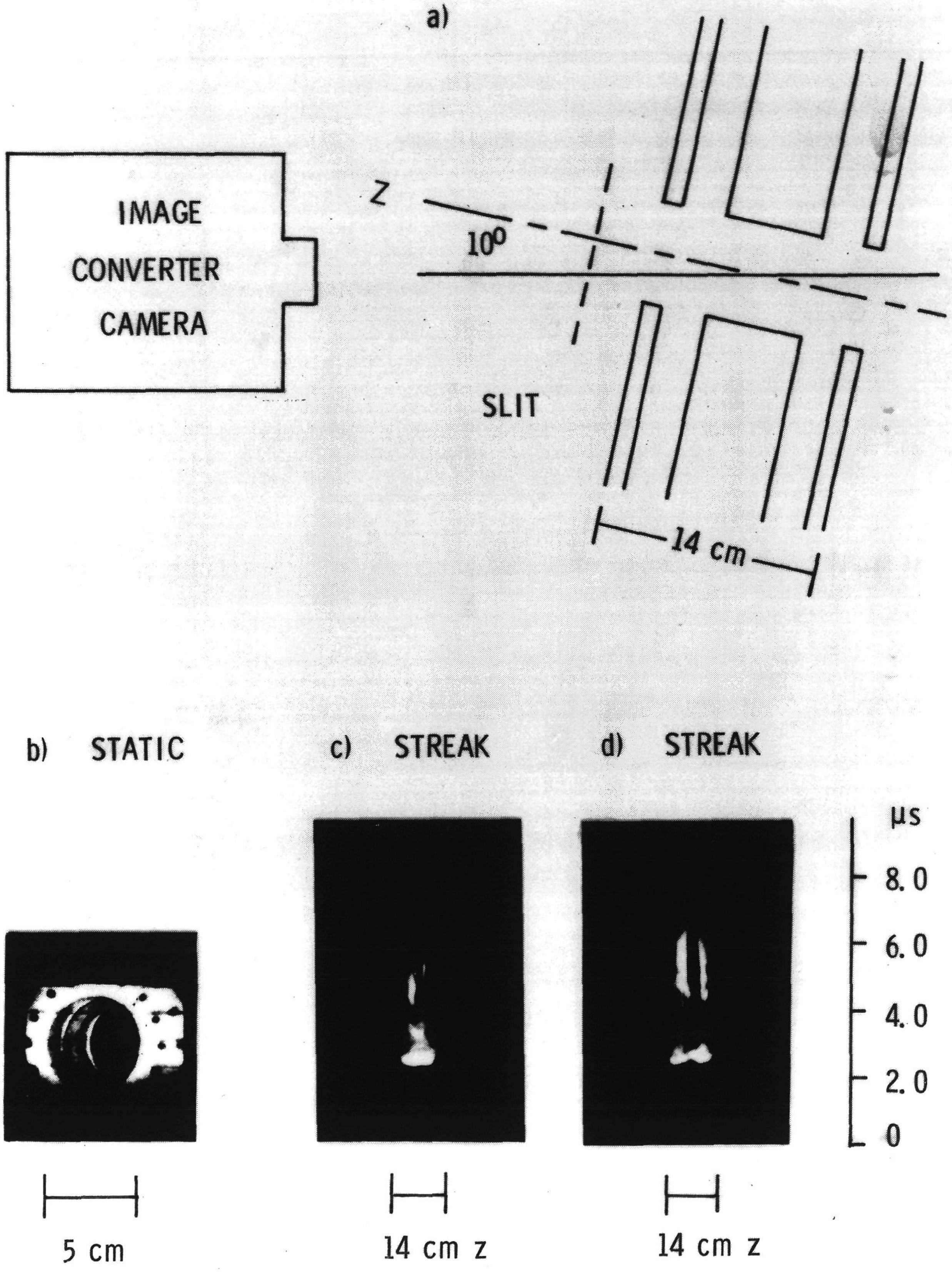

Figure 25.- The axial motion of the focused plasmas observed in a 10° angle with the axis of the apparatus as shown in (a) a still reference picture (b) shows the field of view of the camera and (c) shows that there are three stages in the axial motion.

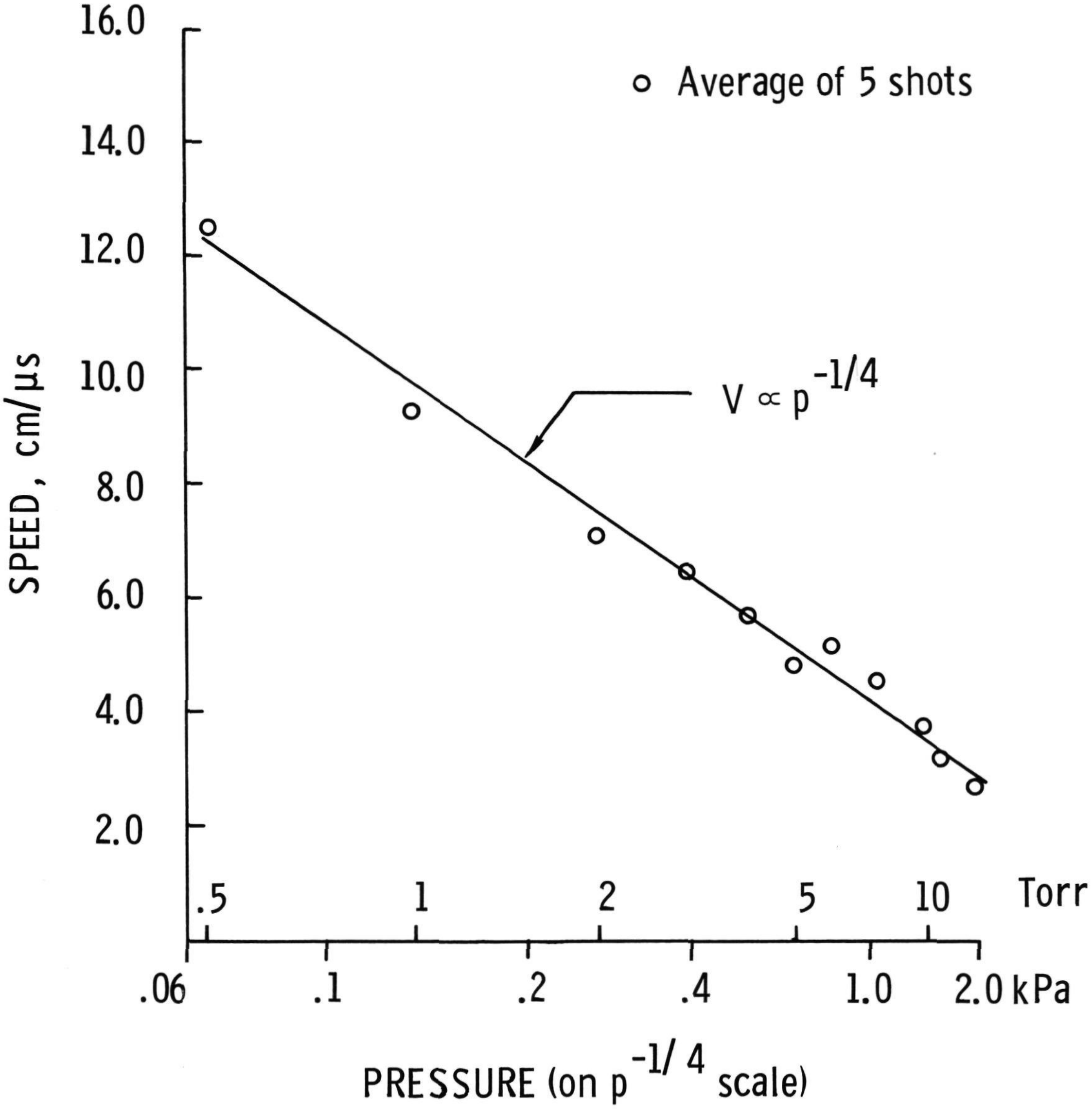

Figure 26.- Rundown speed of the current sheet as function of the filling pressure.

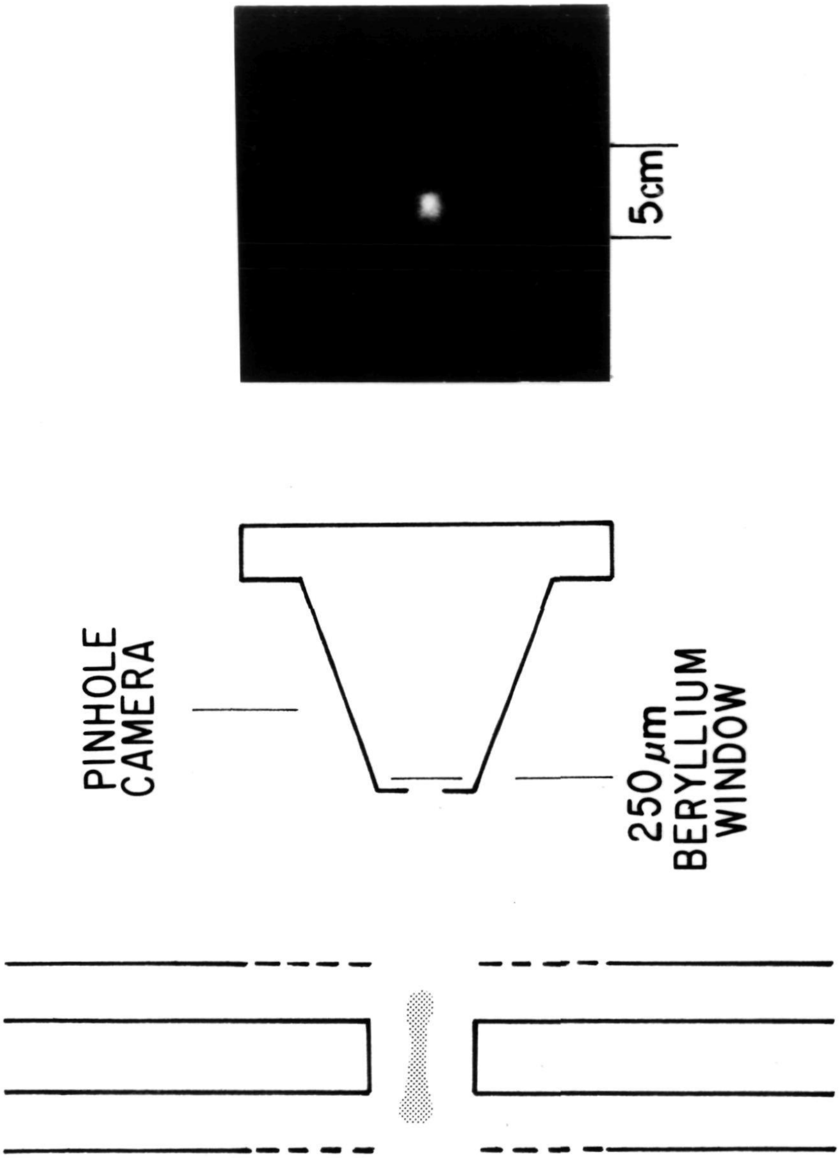

Figure 27.- Time integrated x-ray pinhole photograph of the focused plasma.

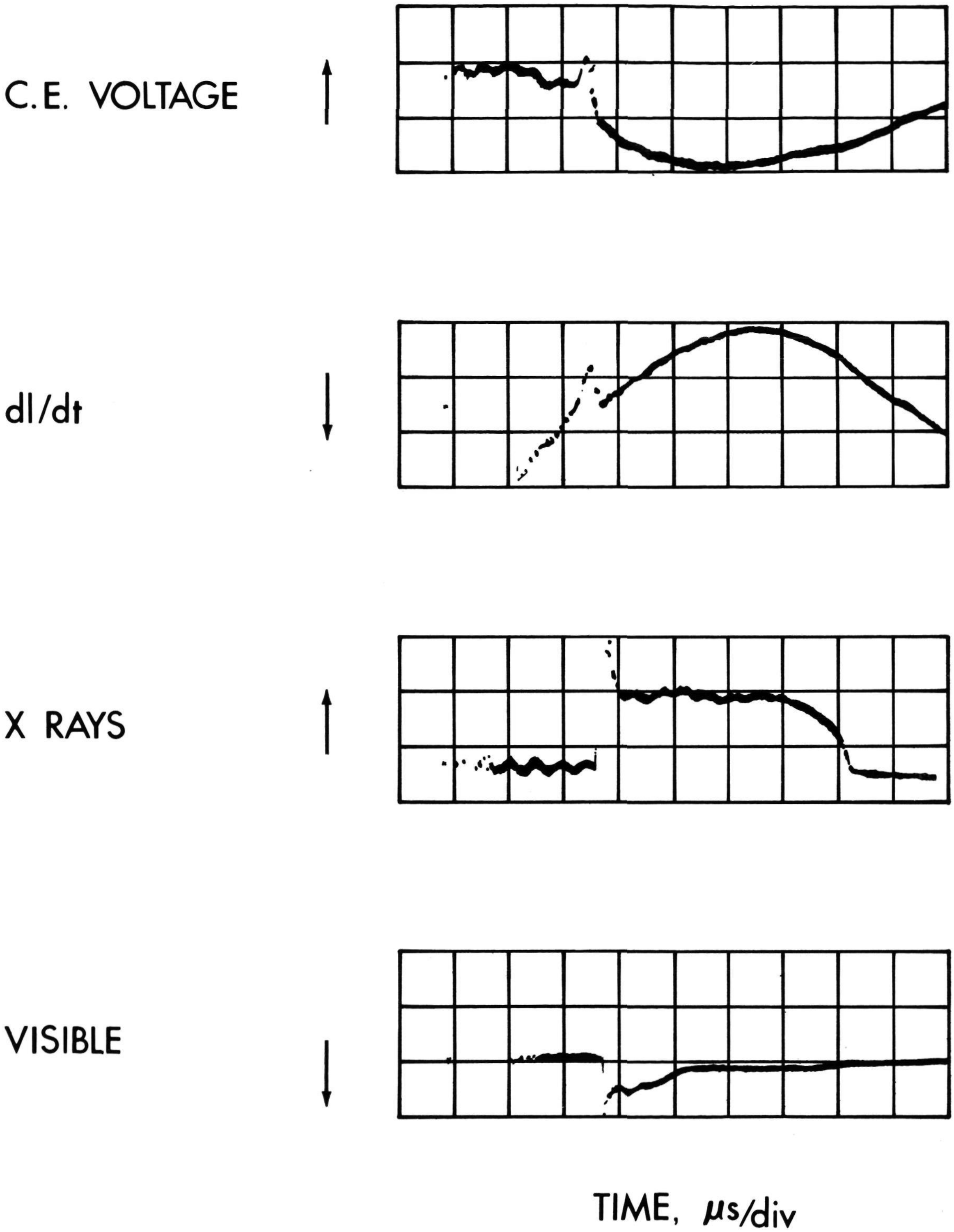

Figure 28.- Temporal evolution of the voltage and the dI/dt at the center electrode (C.E.), the x-ray emission detected by a fast scintillator-photomultiplier system, and the continuum emission in the visible.

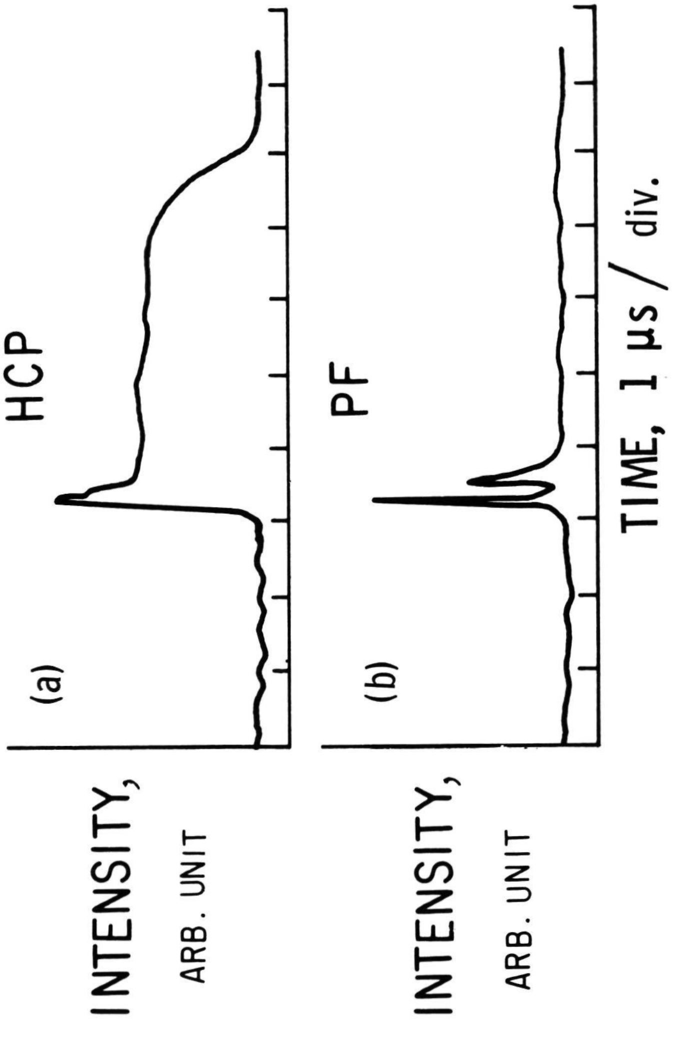

Figure 29.- Comparison of the periods of x-ray emission from the hypocycloidal-pinch and the coaxial plasma focus.

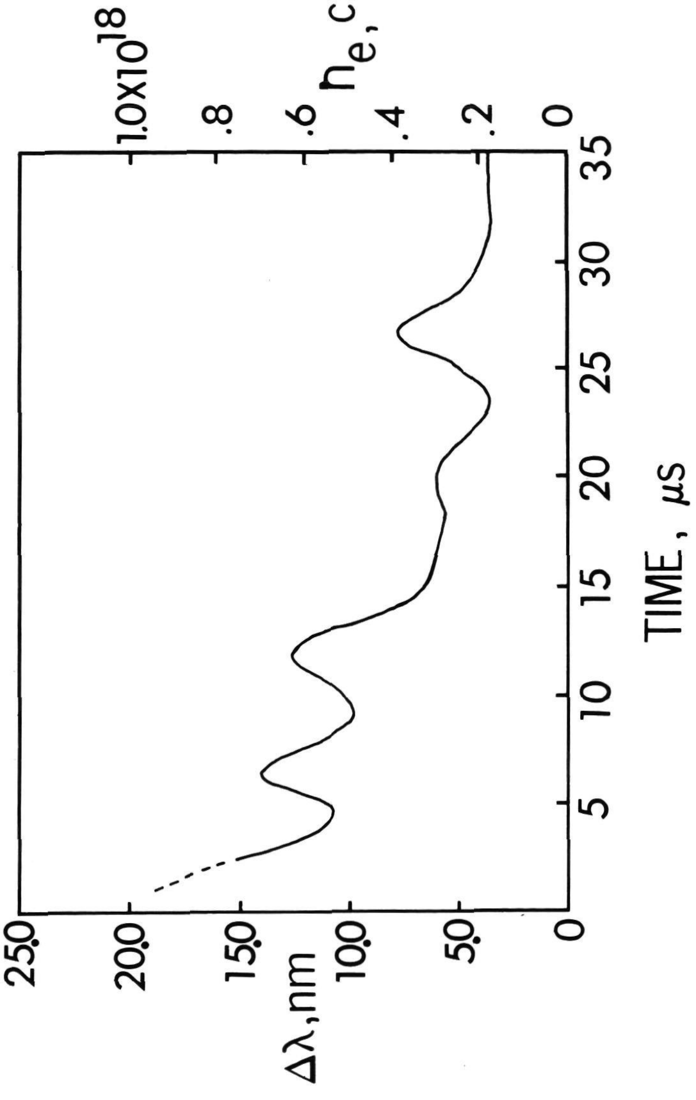

Figure 30.- Plasma density variation in time. The plasma density is obtained by the line broadening of D_α.

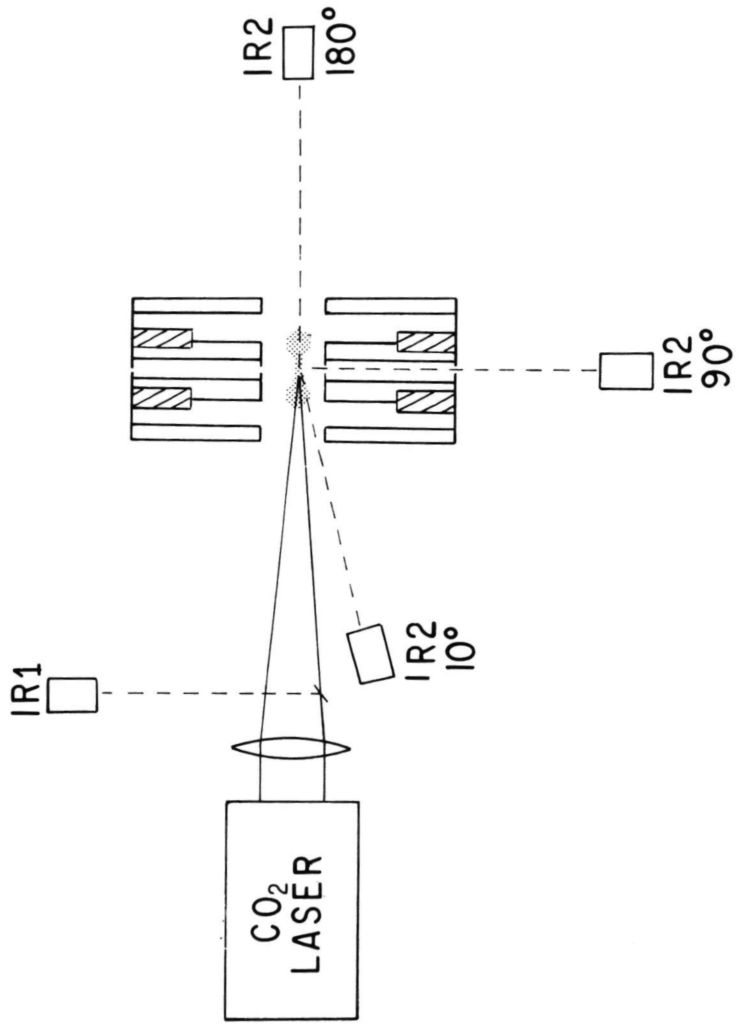

Figure 31.- Experimental setup for CO_2 laser transmission and scattering. Ir1 monitors the incident laser power and Ir2 measures the transmitted or scattered laser power.

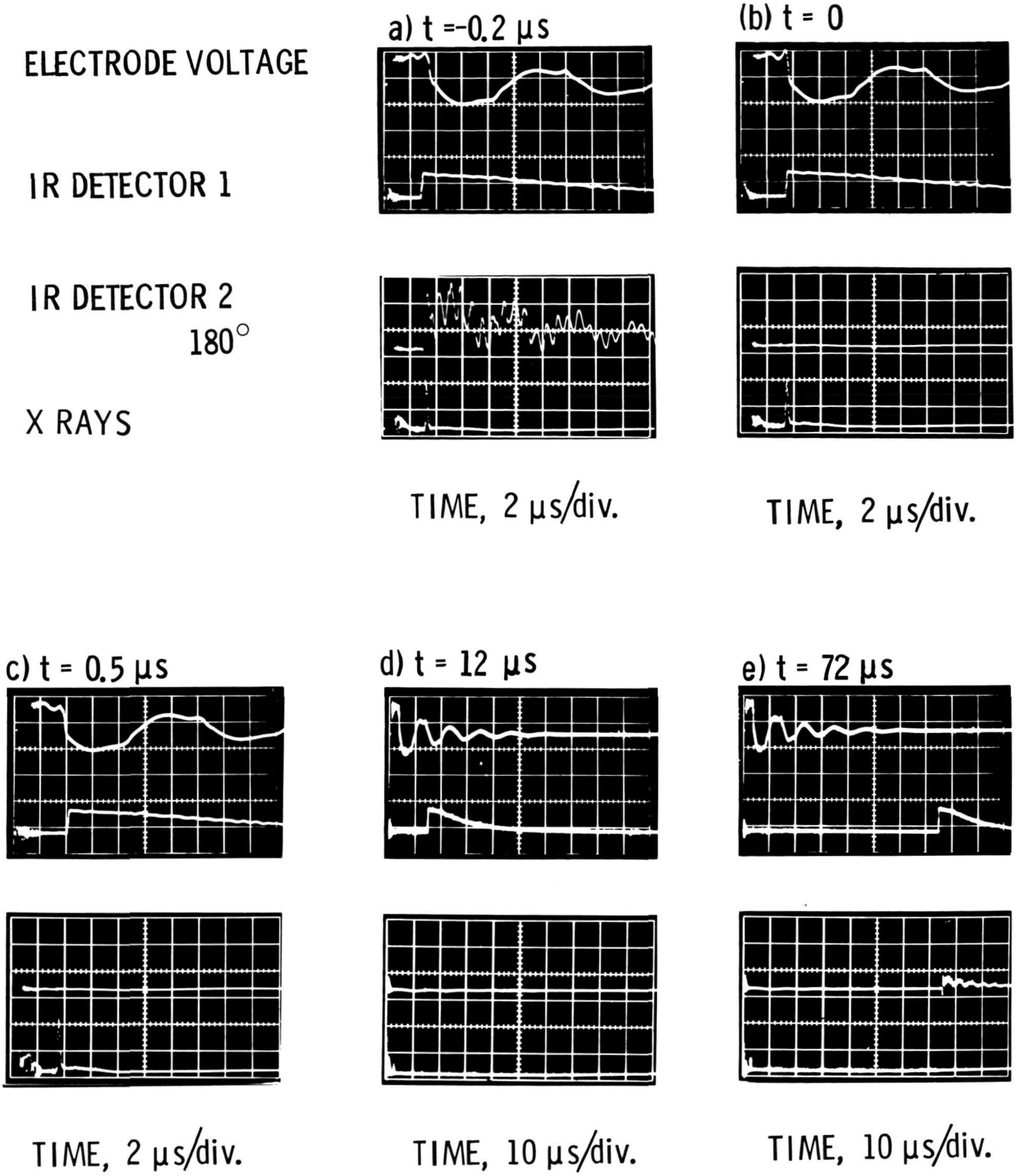

Figure 32.- Five sets of oscillograms for five different firing times of the CO_2 laser. The time t is measured from the onset of x-ray pulse. Little transmittance is recorded for $0 < t < 72$ μs.

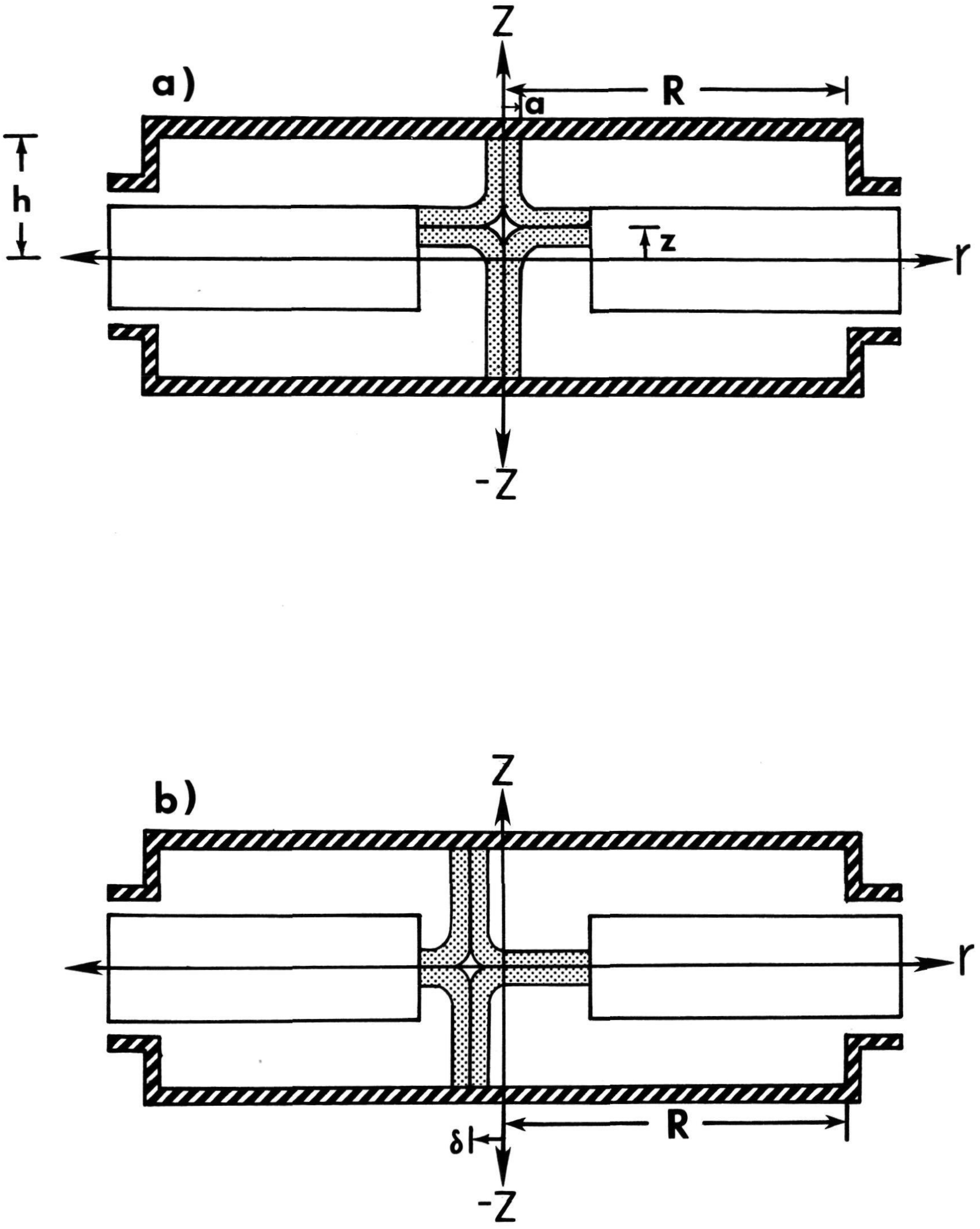

Figure 33.- Displacements from the equilibrium of the current; (a) axial displacement z, and (b) radial displacement δ. A restoring force results against these displacements.

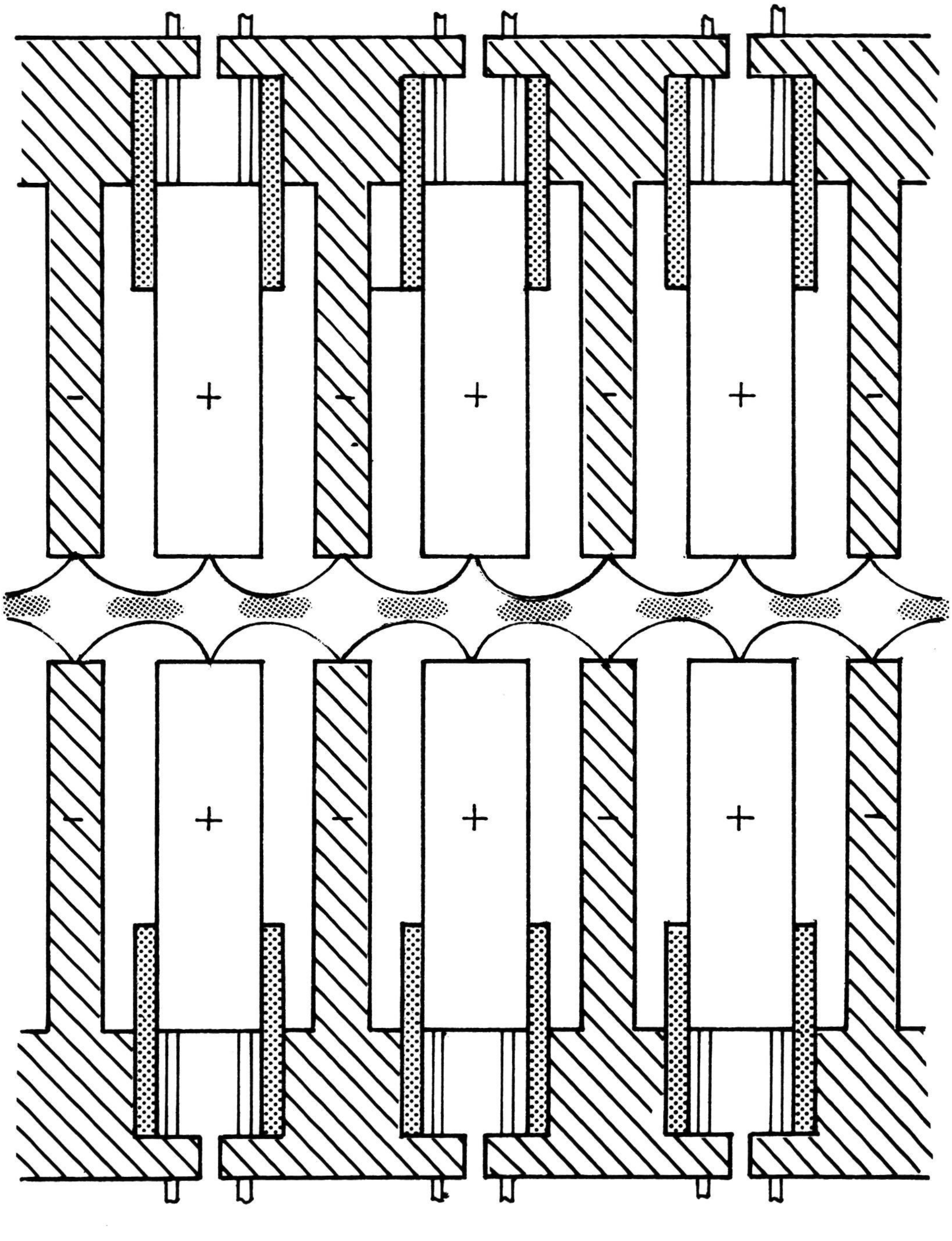

Figure 34.- A multiple array of hypocycloidal-pinches to form a linear system.

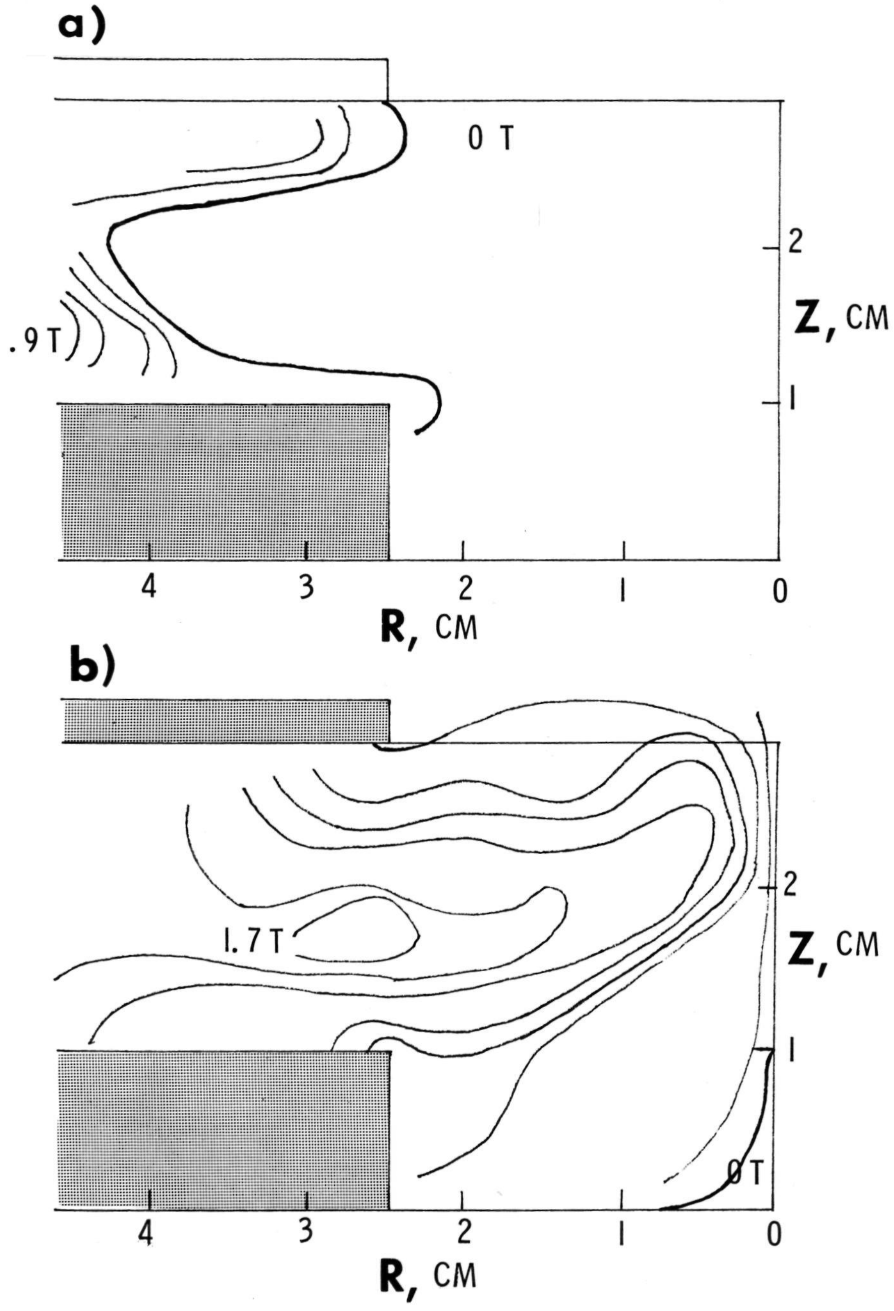

Figure 35.- Contours of the magnetic induction at (a) 1.4 μs and (b) 2.8 μs after the arc strike. Various features of the current sheet in the hypocycloidal-pinch apparatus are revealed.

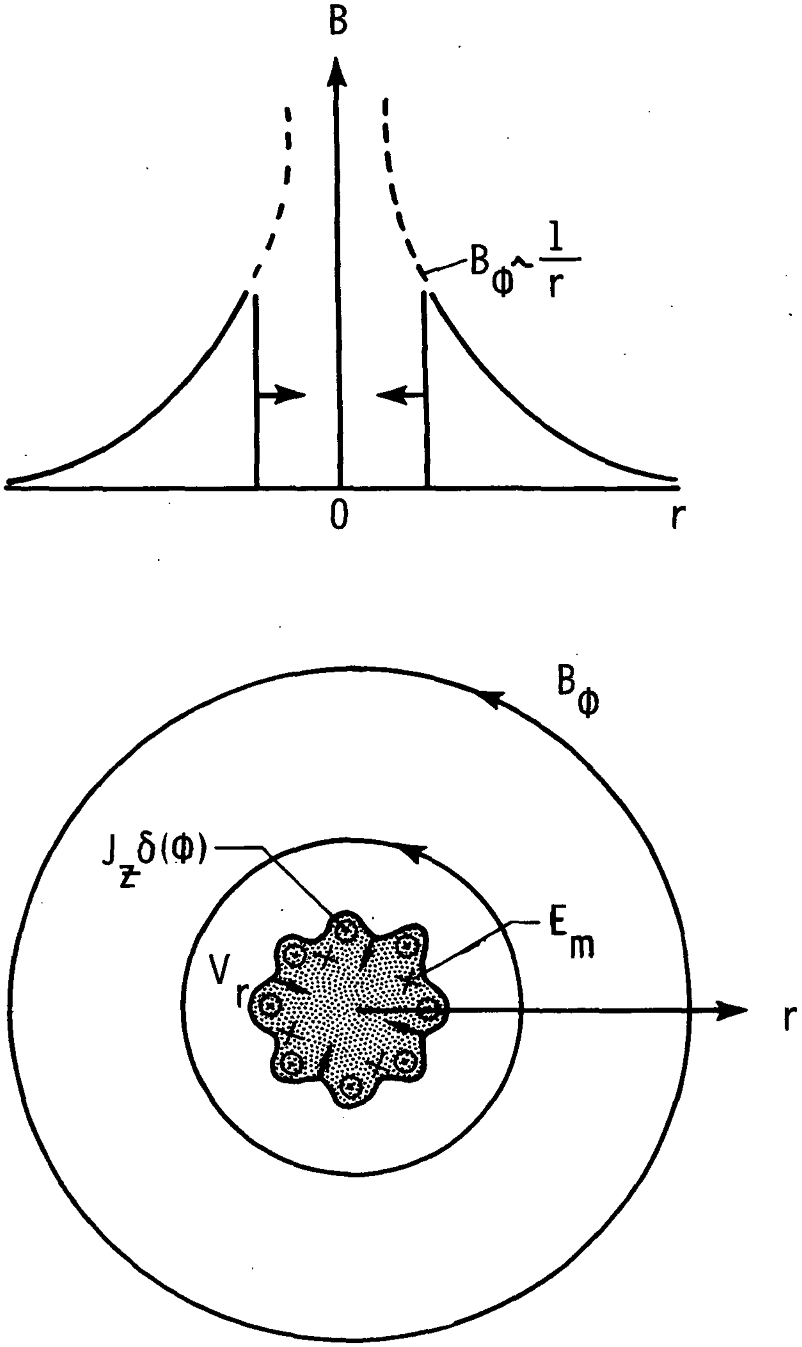

Figure 36.- The MHD relation with the motional emf Em generated in the shock-heated plasma ahead of the current sheet.

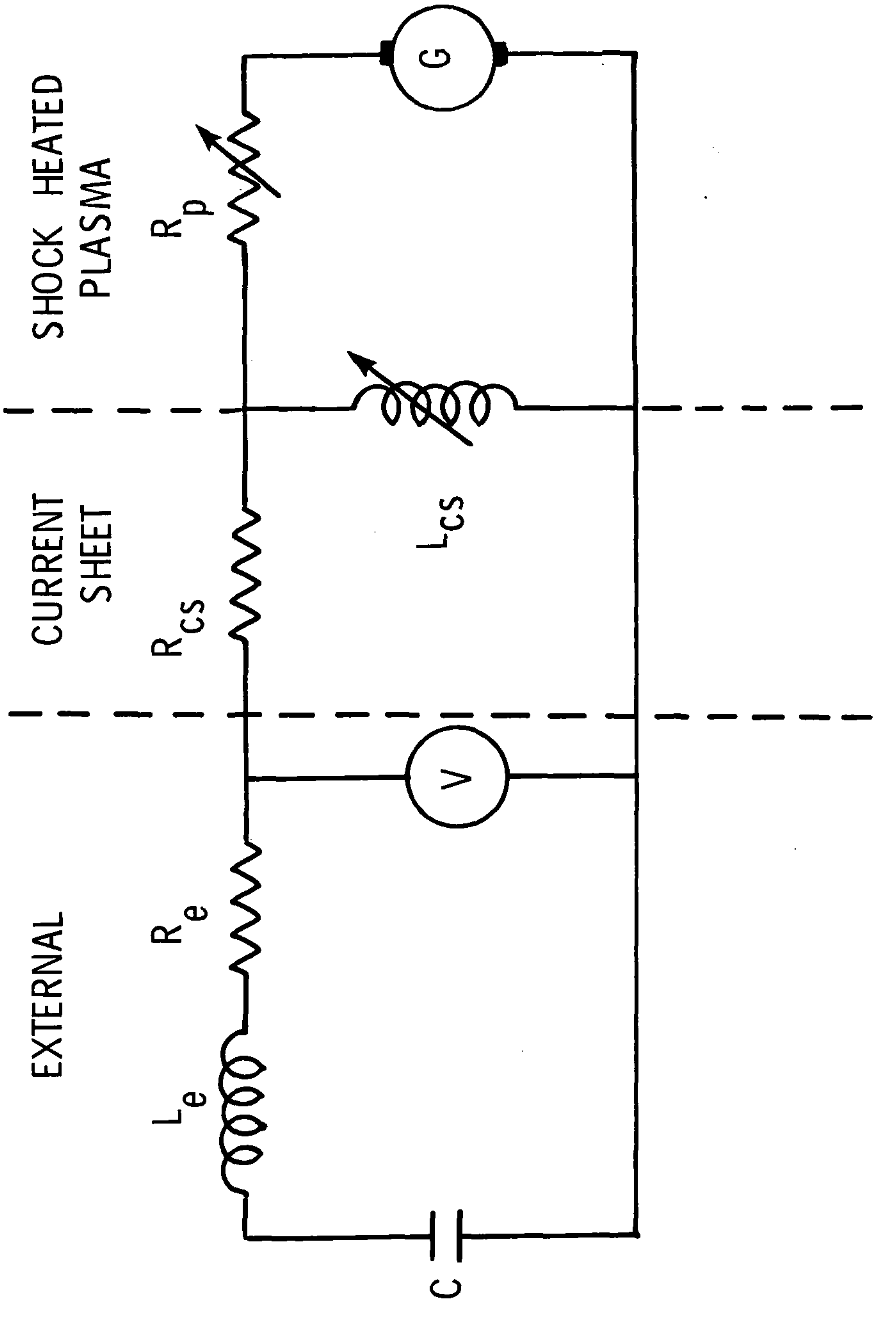

Figure 37.- An equivalent circuit for a plasma focus apparatus. The effect of the shock-heated plasma ahead of the current sheet is included as a variable resistance and a generator.

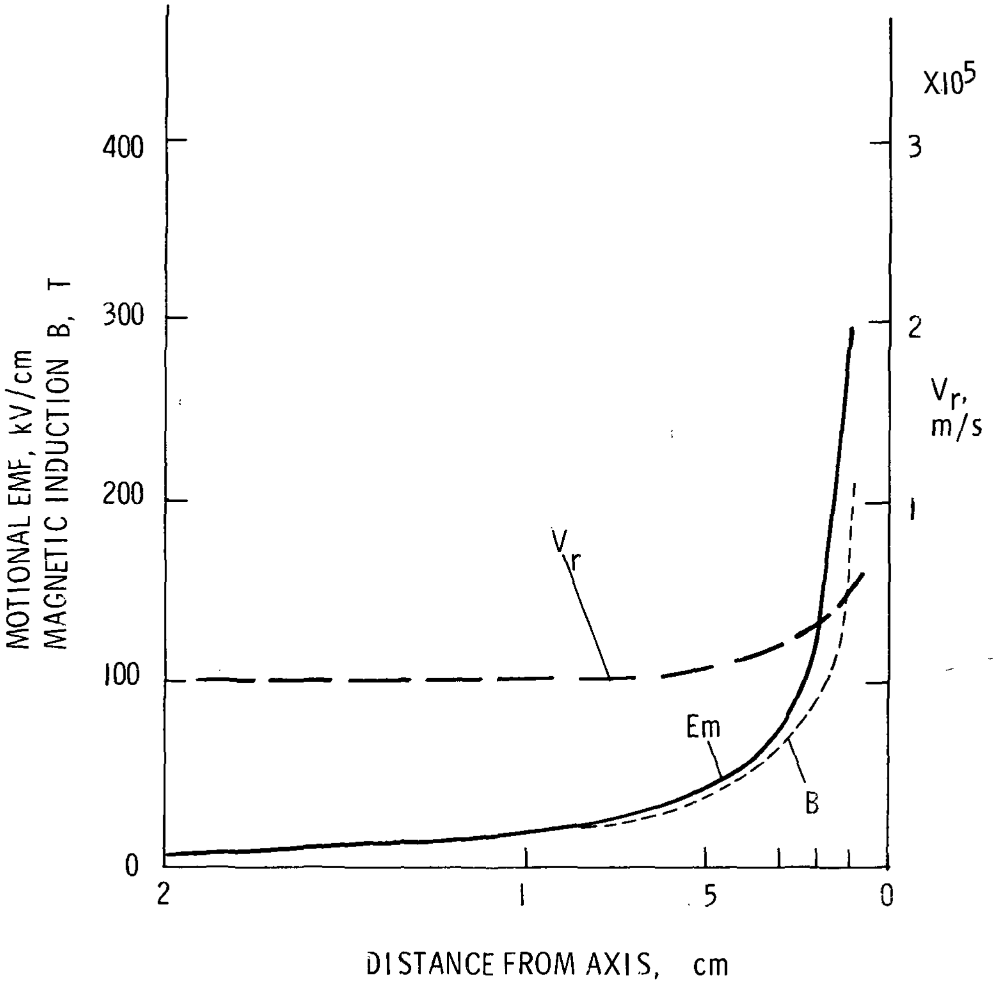

Figure 38.- The Em is steepened near the axis (r = o) by the slopes of Vr and B. 300 kV/cm is reached at r = 1 mm.

VII. LIST OF TABLES

TABLE I.

Measured Quantities	Moving Thermal Plasma Model	Axial Beam-Target Model	Converging Ion Model
	Ion Density = 5×10^{19} cm^{-3} Volume = 1×10^{-3} cm^{3}	Ion Density = 5×10^{19} cm^{-3} Volume = 1×10^{-3} cm^{3}	Ion Density = 5×10^{18} cm^{-3} Volume = 6×10^{-4} cm^{3}
Neutron Yield, Y_n			
$Y_n = 1.0 \times 10^{10}$	kT = 5 keV	E_d = 64 keV	E_d^{cm} = 80 keV
$Y_n = 2.4 \times 10^{9}$	kT = 3 keV	E_d = 41 keV	E_d^{cm} = 34 keV
Axial-to-Radial Neutron Fluence Ratio			
1.48 (@ $Y_n = 1.0 \times 10^{10}$)	$V_{cm} = 4.4 \times 10^{8}$ cm / sec	E_d = 29 keV	$V^*_{cm} = 4.4 \times 10^{8}$ cm/ sec
1.28 (@ $Y_n = 2.4 \times 10^{9}$)	$V_{cm} = 2.7 \times 10^{8}$ cm/sec	E_d = 16 keV	$V^*_{cm} = 2.7 \times 10^{8}$ cm/sec
Neutron Energy			
$\overline{E}_{z,gr}$ = 2.72 MeV	$V_{cm} = 1.1 \times 10^{8}$ cm/sec	E_d = 60 keV	
$\overline{E}_{r,gr}$ = 2.50 MeV			
$\overline{E}_{z,max}$ = 3.16 MeV		E_d = 417 keV	$V^*_{cm} = 2.7 \times 10^{8}$ cm/sec
$\overline{E}_{r,max}$ = 2.77 MeV			
Neutron Energy Spectra Half-width			
$\overline{\Delta E_z} = \overline{\Delta E_r}$		(Axial only $\overline{\Delta E}_r = 0$)	
Average 270 keV	kT = 11 keV	E_d = 15 to 136 keV	E_d^{cm} = 53 keV
Maximum 400 keV	kT = 24 keV	E_d = 4 to 183 keV	E_d^{cm} = 118 keV
Minimum 140 keV	kT = 3 keV	E_d = 33 to 96 keV	E_d^{cm} = 16 keV

NASA DISTRIBUTION LIST FOR FINAL CONTRACTOR REPORT

(NASA Grant NGR 43-002-031)

Addressee	No. of Copies
National Aeronautics and Space Administration Langley Research Center Hampton, Virginia 23665	
Attention: Dr. F. Hohl, Technical Officer Mail Stop 160	3
Attention: Mr. F. S. Kawalkiewicz, Grants Officer Mail Stop 126	1
Attention: Mr. John Samos, Officer of Technology Utilization and Applications Programs Mail Stop 139A	1
National Aeronautics and Space Administration Division of Research Washington, D.C. 20546	
Attention: Dr. Karlheinz Thom	1
NASA Scientific and Technical Information Facility Post Office Box 33 College Park, Maryland 20740	2 (including original)